X-612-65-180
NASA TMX-55258

A SUMMARY OF RESULTS FROM THE IMP-I MAGNETIC FIELD EXPERIMENT

BY
NORMAN F. NESS
CLELL S. SCEARCE
JOSEPH B. SEEK
JOHN M. WILCOX

MAY 1965

NASA

GODDARD SPACE FLIGHT CENTER
GREENBELT, MD.

Presented at Buenos Aires, Argentina, COSPAR (May 1965)
To be submitted to Space Research VI

X-612-65-180

A SUMMARY OF RESULTS FROM THE IMP-I MAGNETIC FIELD EXPERIMENT

by
Norman F. Ness
Clell S. Scearce
Joseph B. Seek
John M. Wilcox

May 1965

Presented at Buenos Aires, Argentina, COSPAR (May 1965)
To be submitted to Space Research VI

КРАТКОЕ ИЗЛОЖЕНИЕ РЕЗУЛЬТАТОВ, ПОЛУЧЕННЫХ ОТ МКС-I ПО ИССЛЕДОВАНИЮ МАГНИТНОГО ПОЛЯ

Норман Ф. Несс, Клел С. Скирс
Иосиф Б. Сик и Джон М. Вилкокс

РЕФЕРАТ

Первая междупланетная контрольная станция, МКС-I, была запущена 27-го ноября 1963 г. до апогея 31,7 R_e. Она сообщила первые точные измерения междупланетного магнитного поля, магнитосферной границы и несталкивающейся магнитогидродинамической ударной волны связанной со взаимодействием солнечного ветра с геомагнитным полем. Измерения были произведены с подсолнечной точки до ночного магнитного хвоста, включая съемку магнитного поля Земли в пределах магнитосферы. Экспериментальное обнаружения протяженного магнитного хвоста на ночной стороне Земли и магнитно огороженную нейтральную полосу является новейшим важным материалом о внешнем магнитном поле Земли. В этой работе дается краткое изложение результатов этих подробных измерений и экспериментальные данные, объясняющие эти различные явления. Прежные сообщения о первоначальных результатах пополняются дополнительными данными и обсуждением топологий магнитного поля, как в междупланетном пространстве, так и в пределах магнитосферы.

Среднее направление междупланетного поля приблизительно 140° восточнее линии Земля-Солнца, или же 60° к западу от Солнца. Вектор магнитного поля обыкновенно находится близко к плоскости эклиптике, а его статистическое расположение приблизительно 20° к югу от плоскости эклиптика. Общая Архимедова спиральная структура

междупланетного магнитного поля подтверждается междупланетными результатами. Это является прямым результатом радиального потока ионизированного газа от солнечной короны посредством сверх-Альфвеновского магнитогидродинамического расширения, как это было предсказано Паркером.

Взаимодействие сверх-Альфвеновского потока плазмы от Солнца с геомагнитным полем ведет к развитию обособленной головной ударной волны и турбулентной переходной области, в которой наблюдается переплетенные и быстро флюктуирующие магнитные поля. Переходная область граничится в точке застоя с несталкивающейся ударной волной у 13,4 R_e и магнитосферной границей у 10,2 R_e. Результаты указывают на значительную степень случайности направления магнитного поля около точки застоя и развитие упорядоченных магнитных полей, от 5 до 20 гамм, по сторонам магнитосферы. Последняя оказывается грубо-цилиндрической по форме, с диаметром равным 40 R_e, полусферической шапкой и радиусом кривизны равным приблизительно 14 R_e.

Подробное отображение земного магнитного поля на ночной стороне Земли выявило развитие значительного магнитного хвоста, не вращающегося вместе с Землей. Магнитные силовые линии ночной стороны Земли, соответствующие значениям L, приблизительно меньше 8, видимо вращаются вместе с Землей, а развитие большой полосообразной магнитно-нейтральной поверхности в пределах магнитного хвоста является результатом близости силовых линий противоположного направления. Предполагается, что они непосредственно связаны с областями полярной шапки. Значительные временные вариации магнитного поля в хвосте Земли противостоят главной фазе внезапных геомагнитных бурь. Итак, хвост повидимому играет преобладающую роль в различных земных явлениях. Нейтральная полоса заселена энергетическими электронами, которые могут быть источником излучения, приводящим к проявлениям северного сияния и поясу излучения Ван Аллена.

(КОНЕЦ)

Summary of Results from the IMP-I

Magnetic Field Experiment

Norman F. Ness
Clell S. Scearce
Joseph B. Seek
Space Sciences Division
NASA-Goddard Space Flight Center
Greenbelt, Maryland

and

John M. Wilcox
Space Sciences Laboratory
University of California
Berkeley, California

29810 over

Abstract: The first Interplanetary Monitoring Platform, IMP-I, was launched on November 27, 1963 with an apogee of 31.7 R_e. It has provided the first accurate measurements of the interplanetary magnetic field, the magnetosphere boundary and the collisionless magnetohydrodynamic shock wave associated with the solar wind interaction with the geomagnetic field. Measurements were made from the subsolar point to the nighttime magnetic tail and included a mapping of the Earth's magnetic field within the magnetosphere. The experimental detection of an extended magnetic tail on the nighttime side of the Earth and the enclosed magnetically neutral sheet represents the most recent important result with respect to the Earth's outer magnetic field. This paper presents a summary of the results of these detailed measurements and the experimental data yielding the interpretation

of these various phenomenon. Previous reports on the initial results of the magnetic field are expanded upon and the magnetic field topologies both in interplanetary space and within the magnetosphere are discussed.

The average direction of the interplanetary field is approximately 140^{o} east of the Earth-Sun line or 60^{o} west of the Sun. The magnetic field vector generally lies close to the plane of the ecliptic but with a statistical distribution approximately 20^{o} southward from the ecliptic plane. The interplanetary results confirm the general Archimedean spiral structure of the interplanetary magnetic field. This is a direct result of the radial flux of ionized gas from the solar corona by super-Alfvénic magnetohydrodynamic expansion as predicted by Parker.

The interaction of the super-Alfvénic plasma flow from the Sun with the geomagnetic field leads to the development of a detached bow shock wave and a turbulent transition region in which tangled and rapidly fluctuating magnetic fields are observed. The transition region is bounded at the stagnation point by the collisionless shock wave at 13.4 R_e and by the magnetosphere boundary at 10.2 R_e. The results indicate a significant randomization of the magnetic field direction near the stagnation point and a development of ordered magnetic fields of approximately 5 to 20 gammas on the flanks of the magnetosphere. The shape of the magnetosphere is found to be

roughly cylindrical in shape, diameter = 44 R_e, with a hemispherical cap with a radius of curvature of approximately 14 R_e.

Detailed mapping of the Earth's magnetic field on the nighttime side of the Earth has revealed the development of a significant magnetic tail which does not co-rotate with the Earth. The magnetic lines of force on the nighttime side of the Earth corresponding to L values of less than approximately 8 appear to co-rotate with the Earth while the development within the magnetic tail of a large sheet-like magnetically neutral surface is a result of the proximity of lines of force oppositely directed. These are inferred to be directly connected to the polar cap regions. Significant time variations of the magnetic field in the tail of the Earth are in opposition with the solar phase of the geomagnetic sudden commencenent storms. Thus the tail appears to play a dominate role in various terrestrial phenomenon. The neutral sheet is populated with energetic electrons which may be the source of radiation leading to auroral displays and the Van Allen radiation belts.

CONTENTS

1.0 Introduction

The Interplanetary Monitoring Platform IMP-I, the first in a series of satellites monitoring the interplanetary medium in cislunar space, was launched on Nov. 27, 1963. The satellite carried instruments to perform detailed measurements of magnetic fields, plasmas, energetic particles and solar and galactic cosmic rays. A number of publications on the initial results of the magnetic field experiment have already appeared (Ness et.al., 1964; Ness and Wilcox, 1964; Ness, 1965a, 1965b; Ness and Wilcox, 1965a, 1965b). In addition publications presenting the results of other experiments carried onboard the satellite have also appeared in the literature (Anderson et.al., 1965; Balasubrahmanyan et.al., 1965; Bridge et.al., 1965; Fan et. al., 1964; McDonald and Ludwig, 1964; Serbu, 1965). It is the purpose of this paper to briefly summarize and review the significant results of the magnetic field experiment and to present certain new aspects of the experimental measurements and their interpretation. This introductory section will review pertinent characteristics of the IMP-I satellite orbit as a function of time and present a brief summary of the initial results to set the framework within which the remainder of the paper shall be presented.

The initial apogee of the satellite was on the sunlit side of the Earth at an Earth-Sun angle of approximately 33^{o}

West of the Sun at a geocentric distance of 197,616 kilometers = 31.7 R_e (R_e = Earth Radius) and an initial perigee of 192 kilometers. The period of this highly eccentric orbit is 93.5 hours. Interpretation of the results from the IMP-I satellite was initially performed by transforming all data obtained into a solar ecliptic coordinate system. This is because the interaction of the solar wind with the geomagnetic field shows a strong day-night asymmetry with apparent cylindrical symmetry about the Earth-Sun line. The geocentric solar ecliptic coordinate system is defined by an X-axis directed from the Earth to the Sun, the Y-axis in the plane of the ecliptic and the Z-axis pointing towards the north ecliptic pole. In this coordinate system, the apparent motion of the satellite apogee is one of westward precession of 4^{o}/orbit as the Earth moves about the Sun.

In figure 1 is shown the variation of the apogee of the satellite in solar ecliptic coordinates. The angle θ_a is defined as the solar ecliptic latitude and the angle ϕ_a as the solar ecliptic longitude of satellite apogee. The measurements of the magnetic field in space will also be presented in the solar ecliptic coordinate system with θ and ϕ defining the direction of the field with magnitude $\bar{F}$. As shown in Figure 1 the useful lifetime of the satellite

extended over a period of approximately 6 months while satellite apogee varied from a solar ecliptic longitude of 335^{o} to 155^{o}. This permitted mapping of the boundary of the geomagnetic field formed by the interaction with the solar wind from the subsolar point through the sunrise terminator and far into the nighttime region of the Earth.

As shown in Figure 2, apogee was sufficiently high so that during the first 21 orbits of the satellite direct measurements of the interplanetary medium were possible which were not affected by the presence of the Earth and its magnetic field in the supersonic flow of the solar wind. Following orbit 21 measurements in cislunar space were limited to that portion associated with the interaction of the solar wind with the geomagnetic field. Finally subsequent to orbit 31 the measurements were performed while the satellite was completely enclosed within the distorted geomagnetic field. As seen in Figure 2 the space surrounding the Earth is divided into three characteristic physical regions:

1. The interplanetary medium, •
2. the turbulent transition region and
3. the magnetosphere or distorted geomagnetic field of the Earth.

These three regions are separated from each other by two characteristic boundaries:

1. The collisionless magnetohydrodynamic shock wave (Axford, 1962; Harrison, 1962; and Kellogg, 1962) and
2. the magnetosphere boundary or magnetopause.

Repeated traversals of these two boundaries by IMP-I have yielded extensive measurements defining their physical properties and have permitted the geometrical description and physical separation of cislunar space into these three characteristic regions.

The interplanetary medium is characterized by a weak magnetic field of approximately 5.1 gammas average magnitude embedded within a radial plasma flux emitted from the surface of the Sun which is referred to as the solar wind (Parker, 1958). At the Earth's distance of 1 A.U. (Astronomical Unit) the plasma shows flow velocities between 300 to 700 kilometers/sec and densities between 2 to 20 protons/cubic centimeter. The direction of the magnetic field is variable but the magnitude is impressively constant over long periods of time so that $\delta\bar{F}/\bar{F} \leq 0.1$. A general Archimedean spiral structure has been observed in the interplanetary field which can be correlated with the rotational period of the Sun and hence corotates with the Sun and is suggested to be of solar origin.

The transition region is observed to be a turbulent thermalized and magnetized plasma with field strengths varying

between 5 and 20 gammas and fluctuations over short time scales of 10 to 20 gammas. No periodic wave forms are readily discernible in the data and the fields are thus described as tangled or randomly oriented. A thermalized plasma is observed near the stagnation point of the solar wind flow in which the spectrum is considerably broadened and the density increases by a factor of approximately 8 (Bridge et.al., 1965). The solar wind is found to resume a supersonic flow condition around the flanks of the magnetosphere.

The measurements of the distorted geomagnetic field on the night side of the Earth reveal the extension of the geomagnetic field far behind the Earth forming a magnetic tail. Embedded within this magnetic tail has been discovered a magnetically neutral surface separating regions of oppositely directed fields over a thin planar region of space. This is referred to as a neutral sheet and can be correlated with increased particle fluxes illustrating a balance between field and particle pressures.

This paper is organized to present first a summary of the results obtained while the satellite was in interplanetary space beyond the shock wave during orbits 1 through 21. This represents the time interval November 27, 1963 through February 17, 1964 and corresponds approximately to three solar rotations, 1784 through 1786. In general solar

activity has remained at a low level throughout the entire lifetime of the satellite. This paper will not present a discussion of any storm time variations, either of the interplanetary magnetic field or the Earth's magnetic tail field, Subsequent publications shall deal with these transient phenomenon in as comprehensive a treatment as possible.

2.0 Interplanetary Magnetic Field Results

Subsequent to the early suggestions by Biermann (1951) that the Sun must be a continual source of a low energy corpuscular flux or solar plasma, Parker (1960) developed the theory of the solar wind. This described the expansion of the solar coronal gases into interplanetary space at super Alfvénic velocity. A particular distinguishing result of Parker's model is the twisting of solar photospheric magnetic fields into an Archimedean spiral in the ecliptic plane as a result of the uniform radial flux of coronal gases and the rotation of the Sun. This is illustrated in Figure 3 for solar wind velocities as typically measured in the interplanetary medium from 300 to 900 kilometers/sec. (Snyder and Neugebauer, 1964; Bridge et.al., 1965) It is seen that the angle ϕ or ϕ' is approximately 135° or 315° respectively. Thus the direction of the field is approximately 45° with respect to the Earth-Sun line. This is a direct result of the approximate equality of radial velocity of solar plasma with

the tangential velocity of a radius vector fixed to the Sun and rotating with a synodic period of 27.3 days.

The measurement of the magnetic field on IMP-I was performed for 4.8 seconds every 20.4 seconds repeatedly within a telemetry format for a consecutive total of 12 such data points. These were distributed over a time interval of 5.46 minutes in the transmission of information from the satellite. These measurements yielded 12 vector samples of the interplanetary magnetic field. Individual orthogonal components of the vector field were averaged and used to construct an average vector magnetic field for the time interval of 5.46 minutes. The statistical distribution of the direction of the interplanetary magnetic field observed by the IMP-I satellite, when beyond the shock wave, is shown in Figure 4. A broad but nonetheless distinct peak in the direction of the field is observed at approximately the angle predicted by Parker's uniform coronal expansion model. The left-hand side of Figure 4 shows the direction of the interplanetary field projected into the plane of the ecliptic. The right-hand side of the figure shows the direction of the field as projected normal to the plane of the ecliptic and without regard to the direction of the field in the plane of the ecliptic. Accompanying Figure 4 is the magnitude distribution of the interplantary magnetic field as shown in Figure 5. It should be noted that extremely

stringent requirements were placed upon the satellite experiment hardware to minimize their magnetic properties. In addition the satellite was constructed with long booms which supported the magnetometer sensors at remote distances. These procedures yielded measurements of fields accurate to $\pm$ 1/4 gamma, the most accurate in space yet performed.

Individual measurements averaged over 5.46 minutes have been component averaged over a time interval of 1 hour. The statistical distribution of the direction of the interplanetary magnetic field on such a time scale is shown in Figure 6 in the same format as used in Figure 4. The average direction closely parallels that proposed by Parker, as clearly evidenced by the closer and more peaked distribution about the theoretical angles. Accompanying Figure 6 is Figure 7 which shows the interplanetary magnetic field magnitude constructed from the hourly component averages. The average magnitude is seen to be 4.5 gammas, approximately 1/2 gamma less than that for the individual values. This indicates that the magnetic field fluctuates in direction and magnitude about the average spiral direction such that the average field magnitude decreases as averages extend over longer time intervals.

Additional statistical characteristics of the interplanetary magnetic field are presented in Figures 8, 9, and 10. These show respectively, the directional distribution

of the 3 hour component averages of the interplanetary magnetic field, the average magnetic field magnitude over 3 hour intervals and finally a magnitude averaged interplanetary magnetic field over the 3 hour time interval. Figure 10 illustrates the differences of averaging the magnetic field components or magnitudes over different time intervals by comparison with Figure 9. The description of a vector field which is time variable in both direction and magnitude is a complex task since simple component averages may represent an average vector field which does not correspond to one which the "real" field ever showed. Thus in the analysis of the time changes of the magnetic field direction which follows in section 3.0 recourse was always made to the original 5.46 minute averages. Directional histograms were then constructed for time intervals of 3, 6, 12, and 24 hours yielding characteristic directions for the field rather than to directly average the components of the magnetic field separately and thence to construct an average field direction.

The measurement of 5.1 gamma average magnitude field roughly in the plane of the ecliptic, but with a slight southward component of the field, and directed approximately parallel to the angle predicted by Parker for the field, dramatically confirm the uniform coronal expansion model proposed by him, at least during the years of the quiet Sun. It strongly suggests the Sun as the origin of the interplanetary

magnetic field and indeed in the next section this argument will be developed further to illustrate the continuity of field lines from the Sun out to 1 A.U.

3.0 Correlation with the Photospheric Magnetic field

As shown in Figures 4, 6 and 8 the direction of the field can be assigned as either positive or negative depending upon whether or not the field appears to be directed away from the Sun or to be directed back towards the Sun along the streaming angle. Using the range of ϕ indicated in Figure 4 as positive or negative, it is possible to assign a +1 or -1 to each 3 hour interval covered by the interplantary data on IMP-I. This time series of alternating values shows the changes in direction of the field as measured at 1 A.U. by IMP-I. Construction of the auto-correlation function will reveal any basic recurrence tendencies within this time series. Figure 11 presents the normalized auto-correlation of the direction of the inter-planetary magnetic field and the results show a statistically significant peak at a time interval of approximately 27 days. Since this corresponds to the solar synodic rotation period, it is strongly suggestive of a direct connection of the interplanetary magnetic field with magnetic fields originating on the Sun.

It is possible to directly compare the interplanetary and solar fields by utilizing data obtained with the solar

magnetograph at the Mount Wilson Observatory in California (Babcock, 1953). Figure 12 illustrates the result from the solar magnetograph during the IMP-I lifetime which presents a mapping of the photospheric magnetic field as observed at central meridian passage (CMP) on each day. The magnitude of the line-of-sight component of the photospheric magnetic field is measured by the longitudinal Zeeman effect on one of the F_e lines in the solar spectrum. Consecutive daily measurements at CMP are combined to produce a contour map which shows large areas on the surface of the Sun with magnetic fields in the photosphere which are directed either out-of or into the Sun.

In a process similar to that for the interplanetary data, a time series was constructed for individual latitude bands of 10^{o} width across the Sun, by determining the direction of the field within the surface area of the solar disk corresponding to a 12 hour longitude interval, equivalent to 6.7^{o} heliographic longitude. With a time series covering the same interval as IMP-I in interplanetary space, it is possible to construct a cross-correlation function between the directions of the interplanetary magnetic field and the photospheric magnetic field. This result is shown in Figure 13 in which a statistically significant and coherent peak is shown for three separate latitude bands across the solar disk. The time lag of 4.5 days is evidenced which

corresponds to a transport velocity of lines of flux by the solar wind to 1 A.U. of approximately 385 kilometers/sec. The uncertainty in the time lag corresponds to the smallest unit of time available, $\pm$ 12 hours so that the average solar wind velocity from the magnetic field measurements is inferred to be 385 $\pm$ 45 Km/sec. The lower limit of this velocity, 340 Km/sec is very close to the direct measurement of the solar wind velocity by the MIT plasma probe which yielded an average of 320 kilometers/sec. (Bridge et.al., 1965).

In addition to investigating the solar origin of the interplanetary magnetic field by the previous method of analysis, it is also possible to superpose the time variations in magnetic field direction in a circular epoch graph as shown in Figure 14. It is seen that the direction of the interplanetary magnetic field is repetitive on a time scale of 27 days in a very dramatic fashion which reveals the existence of 4 distinct sectors or filaments. Within each sector the magnetic field is directed either away-from or towards the Sun within the entire sector. Three of the sectors have a time interval of approximately 7.6 days, while the third sector shows a time interval corresponding to 3.8 days at 1 A.U.

This superposed epoch chart also illustrates the characteristic geometrical configuration of the field lines

within the interplanetary medium during three solar rotations of the quiet Sun. As the Sun rotates, this sector structure sweeps past the Earth and changes associated with spatial variations within each sector can be associated with changes on the surface of the Earth in magnetic field activity and cosmic ray variations. Shown in Figure 15 is the variation of the planetary magnetic index K_p within the 2/7 sectors of the interplanetary magnetic field. It is seen that high K_p follows shortly after a sector boundary passes and that low K_p values are reached towards the end of each sector. There appears to be no significant difference between + and - sectors, at least at the present time.

It should be noted out that there is a close correspondence of the orbital period (3.9 days) with the time scale of the sector structure (1/7 sector = 3.8 days). The analyses have been critically reviewed to verify that the sector results are not an artifact generated in the analysis.

In summary these results show that during the three solar rotations near the minimum of the solar cycle, the photospheric field is dragged out by the solar wind to form the nearby interplanetary magnetic field and that a semi-permanent sector structure exists. These conclusions are consistent with the model suggested by Ahluwalia and Dessler (1962) in which the sense of the field in the sectors is

related to the sense of photospheric magnetic field regions.

In the interpretation of the solar wind interaction with the geomagnetic field, it is necessary to have average values of the interplanetary medium available from direct measurements to justify a comparison between supersonic gas dynamics and the flow of solar wind. Figure 16 summarizes the average values of pertinent physical parameters in the interplanetary medium deduced from the magnetic field experiment on IMP-I. The average magnitude of the magnetic field is 5.1 gammas and the directional changes indicate a solar wind velocity of 385 kilometers/sec. which yield a proton cyclotron radius of 820 kilometers. It has been suggested by Axford (1962) and Kellogg (1962) that this represents the appropriate physical scale unit to utilize in considering the characteristics of the interaction of the solar plasma flow with the geomagnetic field. Since the magnetosphere as shown in Figure 2 is approximately 44 R_e in diameter, clearly the plasma flow can be considered as a fluid since the proton cyclotron radius is much smaller than the size of the magnetosphere.

4.0 Magnetosphere and Boundary Layer Results

Magnetic field measurements by the IMP-I satellite, in comparison with plasma measurements, have shown a unique and coherent picture of the termination of the geomagnetic

field and the transition to the interplanetary medium. The first traversal of the magnetosphere and shock wave boundaries by IMP-I is shown in Figure 17 for the magnetic field experiment. The magnitude, $\bar{F}$, and the two angles θ and ϕ describe the vector magnetic field over the 5.46 minute time interval. The root-mean-square deviation of the individual solar ecliptic components is also shown as δX, δY and δZ. It is seen that the transition region is one in which both the direction and magnitude of the field vary on short and long time scales. Within the interplanetary medium, magnetic field fluctuations are less than the quantization errors of the telemetry system and correspond to a few tenths of a gamma. Thus for the interplanetary medium the characteristic fluctuations $\delta\bar{F}/\bar{F}$ are seen to be less than 0.1 while within the transition region $\delta\bar{F}/\bar{F}$ varies generally between 0.5 and 2.

An enlarged time scale presentation of the traversal of the shock wave boundary is shown in Figure 18. Individual measurements at 20.4 second intervals are illustrated for the three orthogonal components. The motion of the satellite between successive 20.4 second samples corresponds to approximately 40 kilometers in space. The identification of the shock wave boundary as an abrupt change from a stable weak ordered field to a turbulent stronger field is clear and indicated by the dashed line in the figure.

On an expanded scale Figure 19 shows the characteristic raw telemetry signals corresponding to individual samples of the magnetic field as sampled by the fluxgate magnetometers at time intervals of 0.160 seconds. The individual spin modulated segments of the telemetry signal are presented on an enlarged scale but in time sequence. Again the identification of the boundary is evidenced as a transition from a uniform stable field to a turbulent and rapidly fluctuating magnetic field. This characteristic thinness of the shock wave boundary, separating stable and turbulent fields, was not anticipated and is one unique aspect of the magnetic field measurements by IMP-I.

Corresponding to the magnetic field measurements on outbound orbit # 1, Figure 20 shows the pertinent plasma measurements from the MIT plasma Faraday Cup (Bridge et.al., 1965). The diagram shows the maximum and minimum flux values during each spin period as measured in the channel corresponding to protons with energies between 220 and 660 electron volts. A measurement of the extreme fluxes during each satellite spin is an indirect measurement of the anistropy of the plasma flow. Within the transition region, which corresponds perfectly with that defined by the magnetometer measurements, the plasma flow is seen to be generally isotropic and other energy channels not shown would indicate a similar response characteristic. The MIT plasma measurements have revealed a broad region of turbulent, thermalized

plasma flow immediately behind the shock wave and enclosing the magnetosphere. The remainder of orbits 2 through 21, which permit sampling of the interplanetary medium, show excellent agreement between plasma and magnetic field measurements with respect to the positions of the characteristic shock wave and magnetosphere boundaries in cislunar space.

Figure 21 presents the inbound orbit # 1 magnetic field measurements illustrating the character of the magnetosphere boundary near the stagnation point. The magnetic field interior to the boundary is seen to be increased by approximately a factor of 2 above that theoretically predicted by extrapolation from the Earth's surface using spherical harmonics. This corresponds to the compression of the geomagnetic field by an infinitely conducting plasma and the factor of two is in agreement with theoretical prediction (Beard, 1964). The direction of the field is seen to be only slightly distorted interior to the magnetosphere boundary. Beyond this a turbulent magnetic field is seen both in direction and magnitude as shown previously in Figure 17. Accompanying Figure 21 are the energetic particle results for inbound orbit # 1 showing electrons with energies greater than 45 KeV as detected by the gieger counter experiment of Anderson et.al. (1965). An intense flux of particles is observed interior to the

magnetosphere boundary to the trapped particles in the outer radiation belts. The termination of the trapping region is seen to be coincident with the boundary of the magnetosphere as observed first by Freeman et.al. (1963) on Explorer XII. This is a characteristic feature of orbital data obtained near the stagnation point, that is, within 45^{o} of the Earth-Sun line. Magnetic fields interior to the magnetosphere boundary in this region of space are connected in a distorted but approximately continuous dipole topology which supports trapped particle motion.

Figure 6 illustrates magnetic field measurements obtained on orbit # 6 inbound previously reported by Ness et. al. (1964). For this orbit, original determination of the boundary was based upon magnitude measurements and showed a boundary at 10.3 R_e. Subsequent re-evaluation of the data has indicated that the termination of the magnetosphere boundary must be determined by the topology of the field: as to whether or not the field is connected to the Earth or to interplanetary space. On the assumption that the change in direction of the field is the pertinent parameter determining such connection, the boundary of the magnetosphere is identified at a distance of 8.1 R_e. That the magnetic field magnitude is continuous across the boundary is an interesting aspect which cannot be expanded upon in this brief summary of results.

Accompanying Figure 23 is Figure 24 showing the flux of electrons with energy greater than 45 KeV. Again the termination of the trapping region is seen to be exactly coincident with the boundary of the magnetosphere even though it has moved in to a distance of 8.1 R_e in this particular orbit. No important solar event or associated terrestrial event has been associated with a boundary in as close as this. The only other unique event associated with orbit # 6 which possibly might be physically related to it is that during orbit # 5 the magnetohydrodynamic wake of the moon was detected by the IMP-I satellite while in interplanetary space (Ness, 1965a). Whether or not it is possible for the wake of the moon to disturb the characteristics in the transition region and thereby effect the position of the magnetosphere boundary is presently unknown but currently under investigation.

Continuing in orbital coverage around to the Sunrise terminator, Figure 25 shows magnetic field measurements from outbound orbit # 11. The boundary of the magnetosphere is discernible as an abrupt change in the direction of the field and in this case again accompanied by a change in the magnitude of the field. Beyond this boundary the turbulent and tangled magnetic field is observed until the shock wave boundary is detected at 19.7 R_e. Accompanying Figure 25 is Figure 26 showing the flux of energetic electrons greater than 45 KeV energy for the same orbit. Here it is seen that

the boundary of the trapping region occurs close to the Earth at approximately 4 or 5 R_e and hence not coincident with the boundary of the magnetosphere.

This is a characteristic feature of the results from the IMP-I satellite. The boundary of the trapping region and the magnetosphere boundary are coincident near the stagnation point but gradually separate towards the Sun-rise terminator to an appreciable distance on the night side of the Earth. This implies that the magnetic field topology within the magnetosphere is such that durably trapped particle motions are possible for field lines which are approximately dipolar and connected from one hemisphere to the other. However, particles are not capable of stably drifting in longitude which correspond to field lines beyond approximately 8 R_e on the night side of the Earth. Although beyond this region of space intense transient fluxes are observed on field lines which originate at the surface of the Earth, the field lines do not appear to be directly connected to the other hemisphere. Additional discussion of the field topology within the magnetosphere will be presented in Section 5.0.

The last orbit on which interplanetary magnetic field measurements were performed was orbit # 21. Outbound orbit # 21 is illustrated in Figure 27 showing the magnetopause at a distance of 18.7 R_e. Again the magnetosphere boundary

is identified by an abrupt change in the direction of the field. The magnitude of the field is many times larger than that theoretically predicted. The simple model which explains the factor of two increase in magnitude at the stagnation point is no longer applicable on the flanks of the magnetosphere. The remainder of outbound orbit # 21 is shown in Figure 28 where the transition region is seen to consist of intervals in which the field strengths are high when compared to the interplanetary region and directions reasonably stable which alternate with regions of fluctuating and weak magnetic fields. This is a feature reminiscent of the Explorer 10 results near the Sunset terminator side of the magnetosphere (Heppner et.al, 1963; Bonetti et.al., 1963). Detailed correlations of these data with the plasma measurements will be necessary to determine whether or not the boundary of the magnetosphere has been traversed more than once on this particular orbit. The motion of the boundary of the magnetosphere was first deduced in the Explorer X results in 1961 (Ness, 1965c).

A summary of the positions of the magnetosphere boundary and the shock wave are shown in Figure 29. Each dot represents either the inner-most or outer-most position of the boundary as observed on each orbit. The terminations of the boundary on successive orbits are connected by solid lines if no data is missing or no boundary was unambiguously defined and

dashed if otherwise. In general it is seen that the magnetosphere is roughly hemispherical on the Sunlit side of the Earth with a radius of 13.9 R_e (Ness, 1965b) but broadens out to approximately a diameter of 44 R_e on the flanks of the magnetosphere. The shock wave boundary is separated from the magnetosphere by a distance of 3-4 R_e at the stagnation point and increases to 5-7 R_e on the flanks of the magnetosphere.

It is possible to consider a comparison of the supersonic gas dynamic analog of the solar wind flow with the magnetosphere, as studied initially by Spreiter and Jones (1962). It is important, however, in this interpretation to attempt to take into account the variable angle of attack which the Earth's magnetic dipole presents to the solar wind flow. This is associated with the obliquity to the ecliptic of 23.4° and the 11.7° tilt of the dipole axis of the geomagnetic field to the spin axis of the Earth. Figure 30 shows the variation in the angle of attack over the lifetime of the IMP-I satellite. This angle, χ_{ss}, has been used previously in attempts to rectify the positions of the boundary to the ideal position of impact of the solar wind flux normal to the axis of the Earth's magnetic dipole (Ness et.al., 1964). As the angle of attack increases it would normally be expected that the magnetosphere would increase in size since the magnitude of field at the

stagnation point increases. A first order correction using χ_{ss} yields the rectified positions of the magnetosphere boundary and shock wave as shown in Figure 31. The inner solid line correspond to the theoretical predictions by Spreiter and Jones (1962) of the shape of the magnetosphere boundary and assuming an individual particle model with specular reflections. A gas dynamic shock analog has been used to compute the shock wave position and shape using this theoretical magnetosphere. In general the shape comparison is excellent for the shock indicating substantial agreement in the physical model. This is to be expected since in any physical model of a shock, mass, momentum and energy must be conserved. It should be noted that the shape of the boundary on the flanks of the magnetosphere does not appear to correspond well with that predicted. The magnetosphere appears to be broader than anticipated and indeed is suggested to have a radius of 22 R_e. Also the position of the shock has been adjusted slightly to yield the comparison shown (Ness et.al., 1964).

This section summarized briefly the results of the mapping of the magnetosphere boundary and shock wave by the IMP-I satellite. Detailed discussions of the individual experiment results can be found in the original papers by the appropriate authors. The confining of the

geomagnetic field permanently by a continual flux of plasma from the Sun is a very new aspect in the understanding of the Earth's environment in space when compared to earlier work on a transient Chapman-Ferraro cavity as reviewed by Chapman (1963). Equally important are the results obtained on the night side of the Earth from IMP-I which shall be discussed in the following section.

5.0 Tail of the Magnetosphere

Detailed measurements of the distorted geomagnetic field on the night side of the Earth were performed by the IMP-I satellite on orbits # 31 through 47 (Ness, 1965b). A conspicuous and dominant feature of the measurements on these orbits was the direction and strength of the magnetic field when the satellite was beyond approximately 10 to 15 R_e from the Earth. The direction of the field was observed mainly to parallel the Earth-Sun line with magnitudes of 10 to 20 gammas. A representative orbit has been chosen to illustrate these characteristics. In Figure 32 the outbound portion of orbit # 41 shows the direction of the field paralleling the Earth-Sun line within a few degrees and with magnitudes many times larger than predicted as shown by the dashed curve. These data extend out to satellite apogee, which corresponds approximately

halfway to the distance of the Moon.

Accompanying Figure 32 is the inbound portion of orbit # 41 shown in Figure 33. In this a continuation of the characteristic direction of the field is indicated with magnitudes again between 10 and 20 gammas. However, at a distance of 16 R_e the magnitude of the field is observed to decrease rapidly while the direction of the field abruptly changes from being directed away from the Sun to being directed towards the Sun. This change in direction of the field is interpreted to be associated with the magnetic neutral surface in the Earth's magnetic tail (Axford et.al., 1965). This surface separates regions of space in which the direction of the distorted geomagnetic field is either away from or towards the Sun.

That the direction of the field parallels the Earth-Sun line appears to be associated with the mechanism for the formation of the tail. Although this is not yet understood in detail it is clearly associated with the interaction of the solar wind with the magnetic field of the Earth. Since this parallels the Earth-Sun line, neglecting the 3^o-5^o aberration effect, then the direction of the tail and indeed the field direction within the tail can be expected to parallel the Earth-Sun line. The discovery of the neutral sheet in the Earth's magnetic tail by IMP-I is one of the very significant results of the experiment.

Theoretical treatment of the formation of a magnetic tail of the Earth by Piddington (1959, 1960) was on the basis of storm theory and more recently by Dessler and and Juday (1965) and Axford et.al., (1965) on the basis of limited satellite experimental data (Heppner, 1963; Cahill, 1964). This extended magnetic tail represents a change in the concept of the Earth's magnetospheric cavity shape.

A summary of the hourly average components projected on the X-Y plane within the magnetosphere is shown in Figures 34 and 35. The measurements are shown for even hours only for clarity of presentation. The formation of the extended magnetic tail of the Earth is dramatically evidenced in this presentation. The crosses correspond to traversal of the magnetosphere boundary by the satellite and individual orbits are distinguished by a continuous pattern of vectors which can be discerned in these figures. Figure 34 shows the X-Y component of the magnetic field corresponding to positions of the satellite when below the plane corresponding to $Z_{se} = -2.5\ R_e$ while Figure 35 corresponds to $Z_{sat} > -2.5\ R_e$. In this figure the reversal of direction of the field across the neutral sheet is readily evidenced. In some instances the direction of the field does not change by exactly 180^o and the field topology across the neutral sheet is not exactly anti-parallel but rather crossed. The thickness of the neutral sheet can

be inferred but not accurately determined since it is not known if the neutral sheet is in motion at the time of traversal by the satellite. Assuming that the satellite motion is the only pertinent relative velocity then it is possible to estimate the thickness of the neutral sheet as a fraction of an Earth radius over the 14 orbits in which it has been observed. This indicates a very thin magnetically-neutral sheet (on the scale of the magnetosphere) embedded within the Earth's magnetic tail.

Figure 36 through 39 show the hourly average components of the magnetic tail field projected on X-Z planes. An attempt has been made to present a three dimensional view of the tail field in these 4 figures. They are separated according to Z_{sat} being below the plane of the ecliptic for Figures 36 and 37 while the satellite is above the plane of the ecliptic in Figures 38 and 39. In the pair of Figures 36-37 and 38-39 the position of the satellite is separated according to whether or not Y_{sat} is greater than or less than -3.0 R_e respectively. Finally the projection of the vector on planes separated by intervals of 2 R_e are shown offset in an isometric projection. Careful inspection of Figures 36 through 39 and also Figures 34 and 35 yields the details of the physical existence and directional characteristics of the magnetic tail of the Earth.

The measurements of the magnetic tail extend over a time interval of approximately 4 months. Thus the Earth's

magnetic tail appears to be as permanent a feature of the Earth's environment as was previously deduced about the confinement of the geomagnetic field by the flow of solar plasma. The original suggestion by Piddington (1959) was for the temporary existence of a magnetic tail of the Earth. The characteristics of the neutral sheet are an important aspect of the Earth's tail and shall be discussed in the following section.

A schematic summary of the cislunar space environment is shown in Figure 40. This shows the projection of the interplanetary field lines on the plane of the ecliptic as well as the shock wave and magnetosphere boundary. The magnetosphere tail is shown to be filled with lines of force which originate from the southern polar cap region. An estimate of the total magnetic flux in the Earth's magnetic tail can be obtained by integrating over an assumed cylindrical surface. Equating this total flux to that through a polar cap region of colatitude = θ should yield equivalence if the total flux in the cap is dragged behind the Earth to form the Earth's magnetic tail. Figure 41 illustrates this relationship and inspection of the chart shows that for observed field strengths of 20 gammas and a tail radius of 22 R_e the colatitude predicted for the polar cap region is approximately 16^{o}. This is in remarkable agreement with the positions of the auroral zones as directly measured and substantiates the general qualitative model

of the Earth's tail which is formed by the distortion of the geomagnetic field by the solar wind. Recent low altitude measurements of particle fluxes on the night side of the Earth at high latitudes above the trapping regions support the field topology proposed (McDiarmid and Burrows, 1965).

6.0 Neutral Sheet Characteristics

Observations of the magnetic neutral sheet in the Earth's tail have been performed on 14 of orbits # 31 through # 47. These have ranged over geocentric distances of 9.9 R_e to 28 R_e. In general the early orbits possessed neutral sheet traversals closer to the Earth than later orbits. Analyses have been performed to deduce the orientation of the neutral sheet in the Earth's magnetic tail. Indeed, that the neutral surface separating fields of opposite direction is more or less a flat planar feature, as suggested by the word sheet is one result of this particular investigation. The latitude of the positions of crossing of the neutral surface in the Earth's magnetic tail has been examined in three coordinate systems:

1. Solar ecliptic,
2. Geomagnetic
3. Solar magnetospheric

The last system is a recent addition to those coordinates used in interpretation of magnetospheric phenomena.

It incorporates the Earth-Sun line as the X-axis but unlike solar ecliptic includes a dependence upon the position of the geomagnetic axis rather than the ecliptic plane. The coordinate system is illustrated in Figure 42 showing the XZ plane as including the magnetic axis of the Earth. This implies that the Y axis in the new coordinate system is always normal to both the Earth-Sun line and the Earth's magnetic dipole axis.

Previous research workers in the field of magnetosphere physics have suggested that such a coordinate system might be appropriate in the analysis of magnetospheric phenomenona (Dessler and Juday, 1965) but until these IMP-I data were available there appeared to be no appropriate need for its consideration. The variation and position of the neutral sheet in the three coordinate systems discussed has been investigated. The best fit to the equatorial plane in the three coordinate systems occurred in the solar magnetospheric coordinate system. This is shown in Figure 43 in which it is seen that the position of the neutral surface crossing is always within 5^{o} or 10^{o} of the solar magnetospheric equatorial plane. Thus it is suggested by these results that the neutral sheet in the Earth's magnetic tail is roughly parallel to the solar magnetospheric equatorial plane and indeed is approximately equivalent to it. The variation in the tilt of the neutral

sheet to the ecliptic plane is an important parameter in comparing these results with previous and future satellite measurements. Figure 44 shows the annual variation of the tilt of the neutral sheet with respect to the ecliptic plane when viewed along the Earth-Sun line. The maximum inclination is $\pm$ 35.4^{o} with an annual seasonal variation.

Measurements by Anderson et.al., (1965) Frank and Van Allen (1964), Freeman (1964), Gringauz et.al.(1960), Montgomery et.al. (1965), Singer et.al., (1965) and Anderson et.al., (1965) have shown enhanced particle fluxes on the night side of the Earth. Some of these are probably related to the magnetic neutral sheet. Previous measurements by Frank (1964) are particularly pertinent in this respect since they revealed the formation of an electron "tail" of the magnetosphere on the night side of the Earth with the Explorer 14 satellite. As noted by Axford et.al.(1965) in order that a magnetic neutral sheet exist in the Earth's magnetic tail it is necessary that the sheet be filled with an increased plasma flux which balances the opposing field configurations. Figure 45 predicts the minimum particle flux necessary to balance a magnetic field in the Earth's tail and superimposes experimental evidence of the neutral sheet. These measurements were not originally interpreted to be indicative of the neutral sheet but with the magnetic field topology of the Earth's tail as measured by the IMP-I satellite, it is

possible to place these measurements in a proper perspective As noted by Van Allen (1963) the measurements by Gringauz (1960) do not necessarily indicate a third radiation belt. They now can be reasonably interpreted in terms of the neutral sheet in the Earth's magnetic tail.

In Figure 46 correlated particle and field measurements performed on IMP-I in the Earth's magnetic tail are shown. Precipitious increases in particle fluxes are observed coincident with rapid decreases in magnetic field intensity. The interpretation of these time variations is that the total flux of the electrons in the Earth's tail at this time is sufficiently large that the diamagnetic moment of the particles cancels the magnetic field in the Earth's tail, at least locally. Thus the Earth's magnetic tail, at times, may form a third regime in cislunar space quite unlike that of the interplanetary medium in which plasma energy completely dominates magnetic field energy nor the radiation belts in which the reverse situation is true. Rather there is an intimate coupling of the magnetosphere plasma and field and in which the β value is close to unity.

The principal problem related to the tail is whether or not it is the source of auroral particles which are accelerated from low energies to high energies by a mechanism acting only in the Earth's tail. Ness (1965b) has previously suggested that this mechanism may be related to instabilities

of the neutral sheet similar to well known sheet pinch instabilities studied in the plasma fusion program (Furth et.al.,1963). A schematic summary of the geomagnetic field topology and its interaction with the solar wind in the noon"midnight meridian plane is shown in Figure 47. A strong day-night asymmetry is indicated in the trapped radiation belts and the neutral sheet is shown as including the Earth-Sun line. A sample orbit of IMP is shown in the Earth's tail to illustrate the region of space in which magnetic field measurements were performed which reveal the formation of this extended magnetic tail of the Earth. Polar regions of the Earth are as yet unmapped at great distances. The indentations shown on the boundary of the magnetosphere are associated with theoretically suggested neutral points of the Earth's magnetic field in the geomagnetic cavity (Beard, 1964).

7.0 Summary

The continual flux of solar plasma confines the geomagnetic field to a region of space surrounding the Earth but extending on the night side to a distance as yet unknown. It appears certain that the Earth's magnetic tail extends beyond the orbit of the Moon and thus the Moon must traverse the Earth's magnetic tail once every 29.5 days. The presence of the neutral sheet in the Earth's magnetic tail implies an enhanced particle flux within it to balance the field pressure.

It is possible that the Earth can be viewed as a magnetic comet if the Earth is considered as a nucleus, the radiation belts as a coma and the Earth's magnetic tail as a cometary tail with characteristic Type-I cometary tail rays represented by the Earth's neutral sheet. Certain aspects of this analog are currently being investigated and will be reported upon in future publications. At the present time investigation of the Earth's magnetic tail and its association with auroral and radiation belt phenomena present distinct challenges to futhure space experiments and theory.

Acknowledgements

We gratefully appreciate the outstanding efforts of the IMP project staff and personnel at GSFC who so ably assisted us in our efforts to achieve a "magnetically-clean" satellite. Without their support, cooperation and that of our co-experimenters this work could not have been completed. One of us (J.M.W.) thanks the director of the Mt. Wilson Observatory for guest investigator privileges extended him.

References

Ahluwahlia, H.S., and A.J. Dessler, Diurnal Variation of Cosmic Radiation Intensity Produced by a Solar Wind Planet. Space Sci. 9, 195-210, 1962.

Anderson, K.A., H.K. Harris, and R.J. Paoli, Energetic Electron Fluxes in and beyond the Earth's Outer Magnetosphere, J. Geophys. Res., 70,1039-1050, 1965.

Axford, W. I., The interaction between the solar wind and the Earth's magnetosphere, J. Geophys. Res., 67, 3791-3796, 1962.

Axford, W. I., H. E. Petschek and G. L. Siscoe, The Tail of the Magnetosphere, J. Geophys. Res., 70, 1231-1236, 1965.

Babcock, H.W., The Solar Magnetograph, Astrophys. J., 118, 387-396, 1953.

Balasubramanyan, V. K., G. H. Ludwig, F.B. McDonald, and R.A.R. Palmeira, Results from the IMP-I GM Counter Telescope Experiment, GSFC preprint X-611-65-49, 1965.

Beard, D. B., The Solar Wind Geomagnetic Field Boundary, Rev. Geophys., 2, 335-365, 1964.

Biermann, L., Kometenschweife and Solare Korpuscular Korpuscular Strahlung, Z. Astrophys. 29, 274-286, 1951.

Bonetti, A., H.S. Bridge, A. J. Lazarus, B. Rossi and F. Scherb, Explorer 10 plasma measurements, J. Geophys. Res., 68, 4017-4063, 1963.

Bridge, H., A. Egidi, A. Lazarus, E. Lyon and L. Jacobson, Preliminary results of plasma measurements on IMP-A, in Space Research V, North-Holland Publ. Co. (1965), presented at COSPAR, Florence, Italy, 1964.

Cahill, L.J. and P.G. Amazeen, The boundary of the geomagnetic field, J. Geophys. Res., 68, 1835-1844, 1963

Cahill, L.J., Preliminary Results of Magnetic Field Measurements in the tail of the Geomagnetic cavity, IGY Bulletin 79, Trans. Am. Geophys. Union, 45, 231-235, 1964.

Chapman, S., Solar plasma, geomagnetism and aurora in geophysics: The Earth's Environment, Les Houches 1962 Lectures, ed. by C. DeWitt et.al., 371-502, Gordon and Breach, New York 1963.

Dessler, A.J., and R.D. Juday, Configuration of Auroral Radiation in Space, Planet. Space Sci. 13,63-72, 1965.

Fan, C.Y., G. Gloecker, and J.A. Simpson, Evidence for >30 KeV electrons accelerated in the shock transition region beyond the Earth's magnetospheric boundary, Phys. Rev. letters, 13, 149-153, 1964.

Frank, L.A., A Survey of electrons beyond 5 R_e with Explorer XIV, J.Geophys. Res., 70, 1593-1626, 1965.

Frank, L.A. and J.A. Van Allen, A Survey of Magnetospheric Boundary Phenomena, in Research in Geophysics, Vol. 1 pp. 161-187, MIT Press, Cambridge, Mass. 1964.

Freeman, J.W., Electron distribution in the outer radiation zone, J. Geophys. Res., 69, 1691-1724, 1964.

Freeman, J.W., J.A. Van Allen and L.J. Cahill, Explorer XII observations of the magnetosphere boundary and the associated solar plasma on September, 13, 1961, J. Geophys. Res., 68, 2121-2130, 1963

Furth, H.P., J. Killeen and M.N. Rosenbluth, Finite-Resistivity Instabilities of a Sheet Pinch, Phys. of Fluids, 6, 459-484, 1963.

Gringauz, K.I., Kurt, V.G., Moroz, V.I. and Shklovsky, I.S., Results of observations of charged particles observed out to 100,000 Km with the aid of charged particle traps on Soviet Space Probes, Astron. Zhur. 37-4, 716-735, 1960.

Harrison, E.R., The Earth's Distant Magnetic Field, Geophys. J. 6, 479-492, 1962.

Heppner, J.P., N.F. Ness, T.L. Skillman and C.S. Scearce, Explorer X magnetic field measurements, J. Geophys. Res., 68, 1-46, 1963.

Kellogg, P.J., Flow of Plasma around the Earth, J.Geophys. Res., 67, 3805-3811, 1962.

McDiarmid, I.B., and J.R. Burrows, Electron fluxes at 1000 Km. Associated with the Tail of the Magnetosphere, J. Geophys. Res., 70, to appear, 1965.

McDonald, F.B., and G.H. Ludwig, Measurement of Low-Energy Primary Cosmic-Ray Protons on IMP-I Satellite, Phys. Rev. letters, 13, 783-786, 1964.

Montgomery, M.D., S. Singer, J.P. Conner and E.E. Stogsdill, Spatial Distribution, Energy Spectra and Time Variations of Energetic Electrons (E> 50 Kev) at 17.7 Earth Radii, Phys. Rev letters, 14, 209-213, 1965.

Ness, N.F., C.S. Scearce and J.B. Seek, Initial results of the IMP-I Magnetic Field Experiment, J. Geophys. Res., 69, 3531-3570, 1964.

Ness, N.F. and J.M. Wilcox, The solar origin of the Interplanetary Magnetic Field, Phys. Rev. letters, 13 (15), 461-464 1964.

Ness, Norman F., The Magnetohydrodynamic Wake of the Moon, J. Geophys. Res., 70, 517-534, 1965a.

Ness, Norman F., The Earth's Magnetic Tail, J. Geophys. Res. 70 (13), to appear, 1965b.

Ness, Norman F., Observations of the Geomagnetic Cavity Boundaries, C.U. Symposium on Plasmas in Space (1963), North-Holland Publ. Co., Amsterdam, 1965c.

Ness, N.F., and J.M. Wilcox, Extension of the Photospheric Magnetic Field into Interplanetary Space ,GSFC preprint X-612-65-79, submitted to Astrophys. J., 1965a.

Ness, N.F. and J.M. Wilcox, Sector Structure of the Interplanetary Magnetic Field, GSFC preprint X-612-65-157, submitted to Science, 1965b.

Parker, E.N., Dynamics of the interplanetary gas and magnetic field, Astrophys. J., 128, 664-676, 1958.

Parker, E.N., The hydrodynamic theory of solar corpuscular radiation and stellar winds, Astrophys. J, 132, 821-866, 1960.

Piddington, J.H., The transmission of geomagnetic disturbances through the atmosphere and interplanetary space, Geophys. J., 2,173-189, 1959.

Piddington, J.H., Geomagnetic storm theory, J. Geophys, Res., 65, 93-105, 1960.

Serbu, G.P., Results from the IMP-I Retarding Potential Analyzer, Space Research V, North Holland Publ, Co., (1965), presented at COSPAR Florence, Italy; May, 1964.

Singer, S., J.P. Conner, W.D. Evans, M.D. Montgomery and E.E. Stogsdill, Plasma Observations at 10^5m, in Space Research V, North-Holland Publ. Co. (1965), presented at COSPAR Florence, Italy, May, 1964.

Snyder, C. and M. Neugebauer, Interplanetary solar wind measurements by Mariner 2, Space Research IV, edited by P. Muller, pp. 89-113, North-Holland Publ. Co., Amsterdam, 1964.

Spreiter, J.R. and W. P. Jones, On the effect of a weak interplanetary magnetic field, J. Geophys. Res., 68, 3555-3565, 1963.

Van Allen, James A., Remarks on Accompanying Letter by K.I. Gringauz, J. Geophys. Res., 69, 1011-1013, 1964.

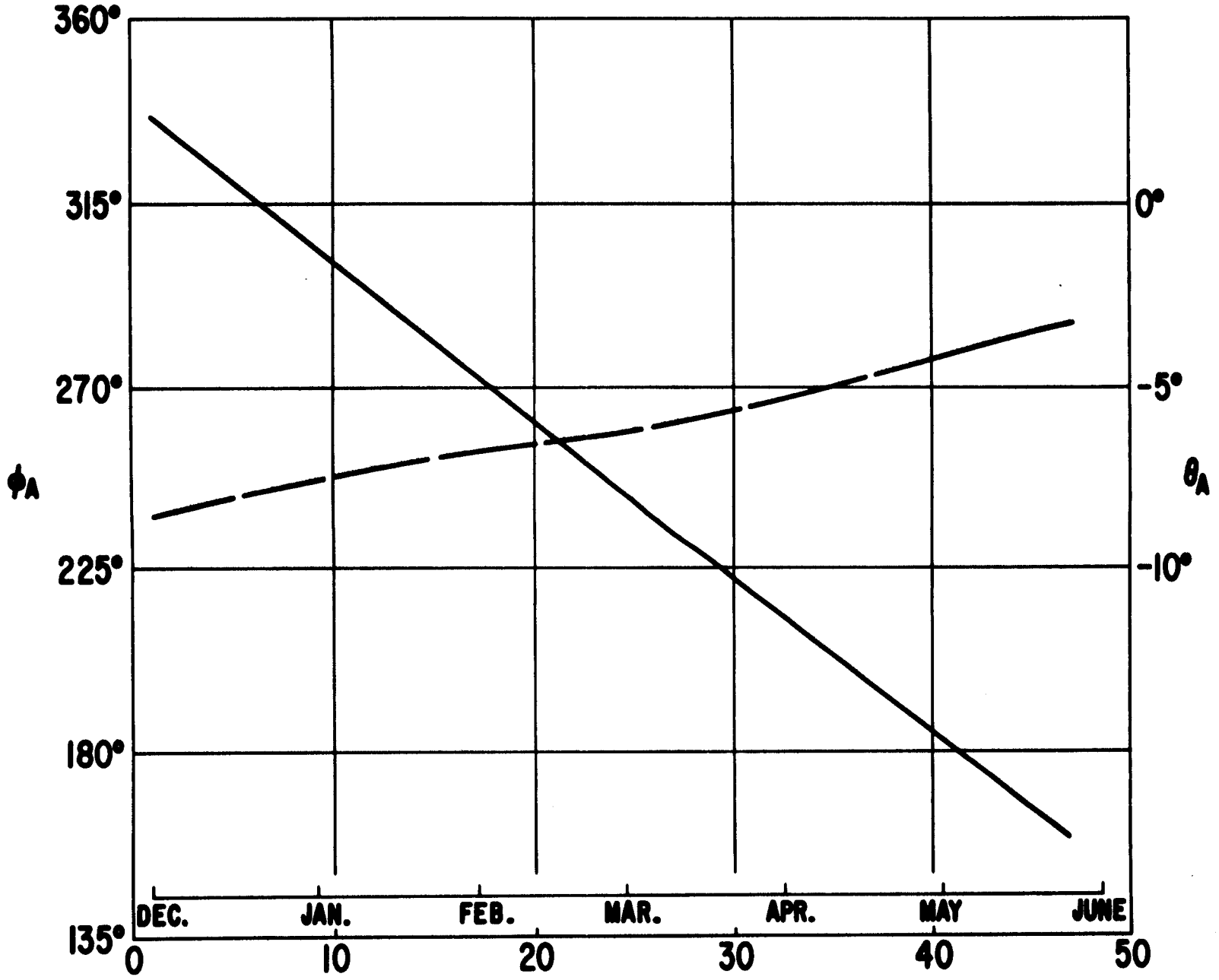

Figure 1. Variation of the apogee (31.7 R_e geocentric) of the IMP-I satellite for orbits # 1-47 during the time interval Nov. 27, 1963, through May 27, 1964. The two angles θ_a and ϕ_a represent, respectively, the latitude and longitude of the apogee of the satellite in solar-ecliptic coordinates.

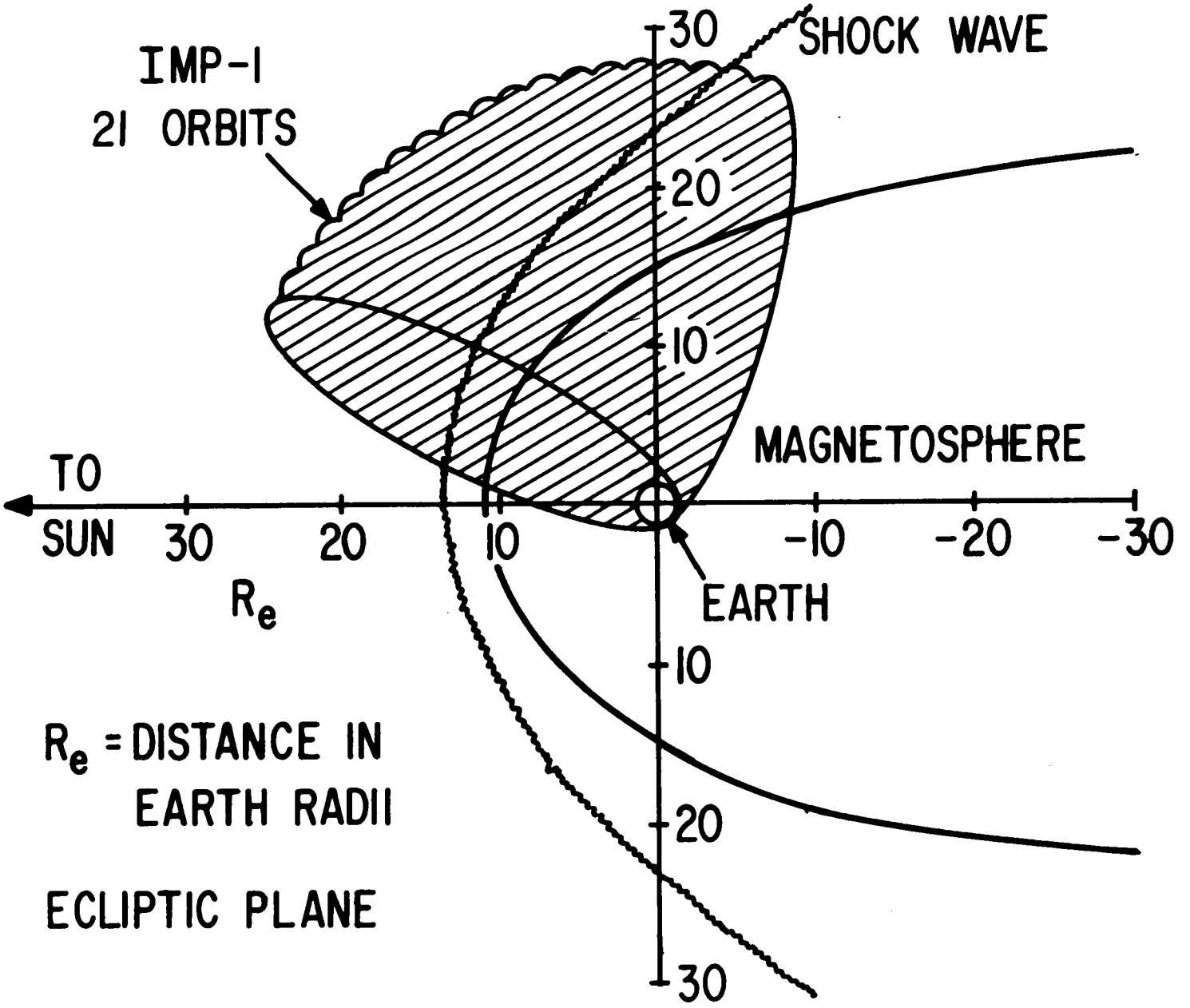

Figure 2. Simplified summary of results of mapping the terrestrial magnetosphere boundary with the interplanetary medium. Illustrated on the plane of the ecliptic are the positions of the magnetosphere boundary and the collisionless magnetohydrodynamic shock wave. The shape and position of the detached bow shock wave closely parallel that observed in supersonic gas dynamics at Mach numbers corresponding to the ratio of the solar wind velocity to the Alfven velocity.

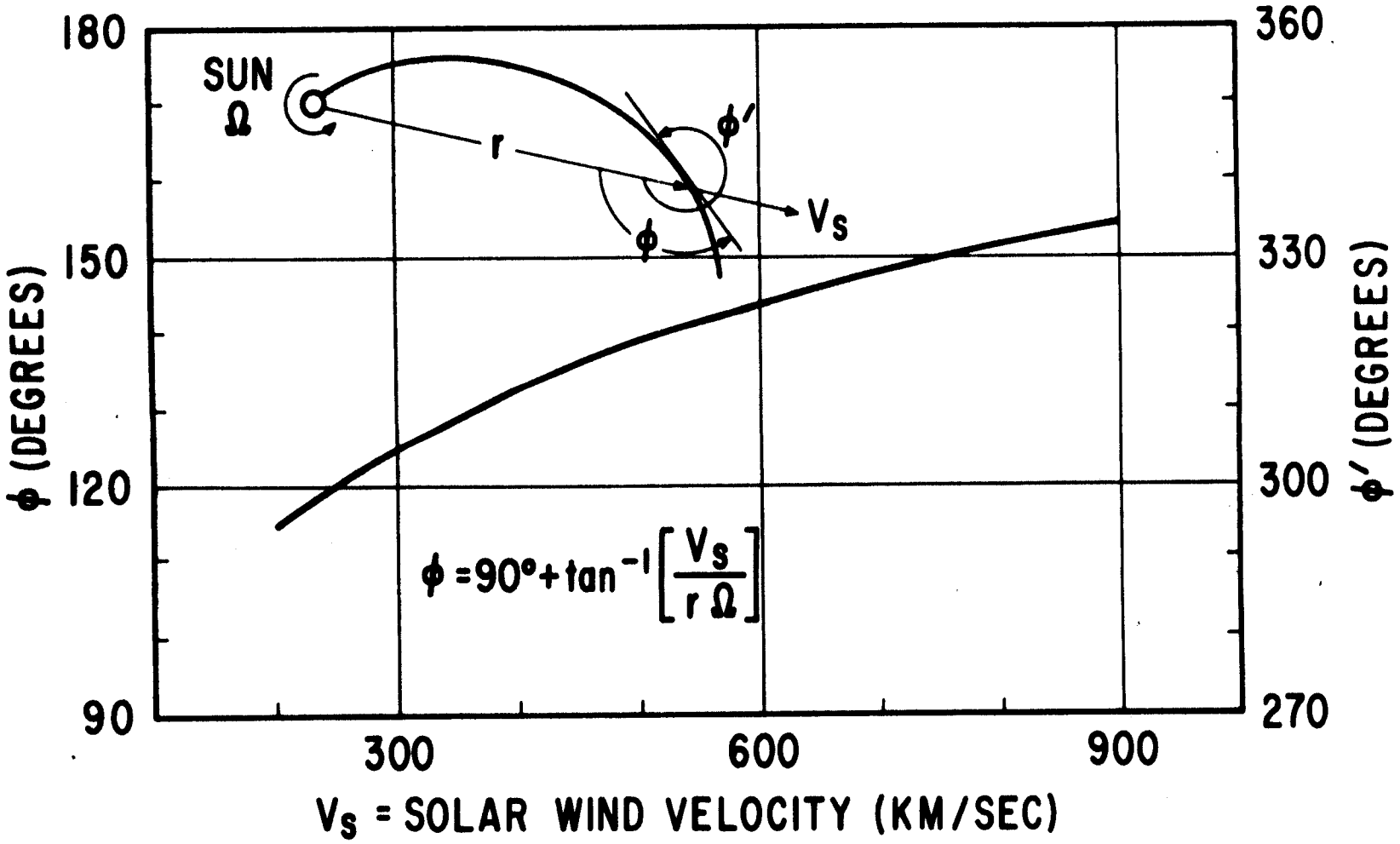

Figure 3. Theoretical direction of the interplanetary magnetic field, assumed to be of solar origin, twisted into an Archimedean spiral by the rotation of the Sun and the radial efflux of highly ionized gases. The two directions ϕ and ϕ' correspond to fields directed essentially away-from or back-towards the Sun along the characteristic streaming angle. Note the relative insensitivity of the direction to changes in typical solar wind velocities from 300 to 700 kilometers/sec.

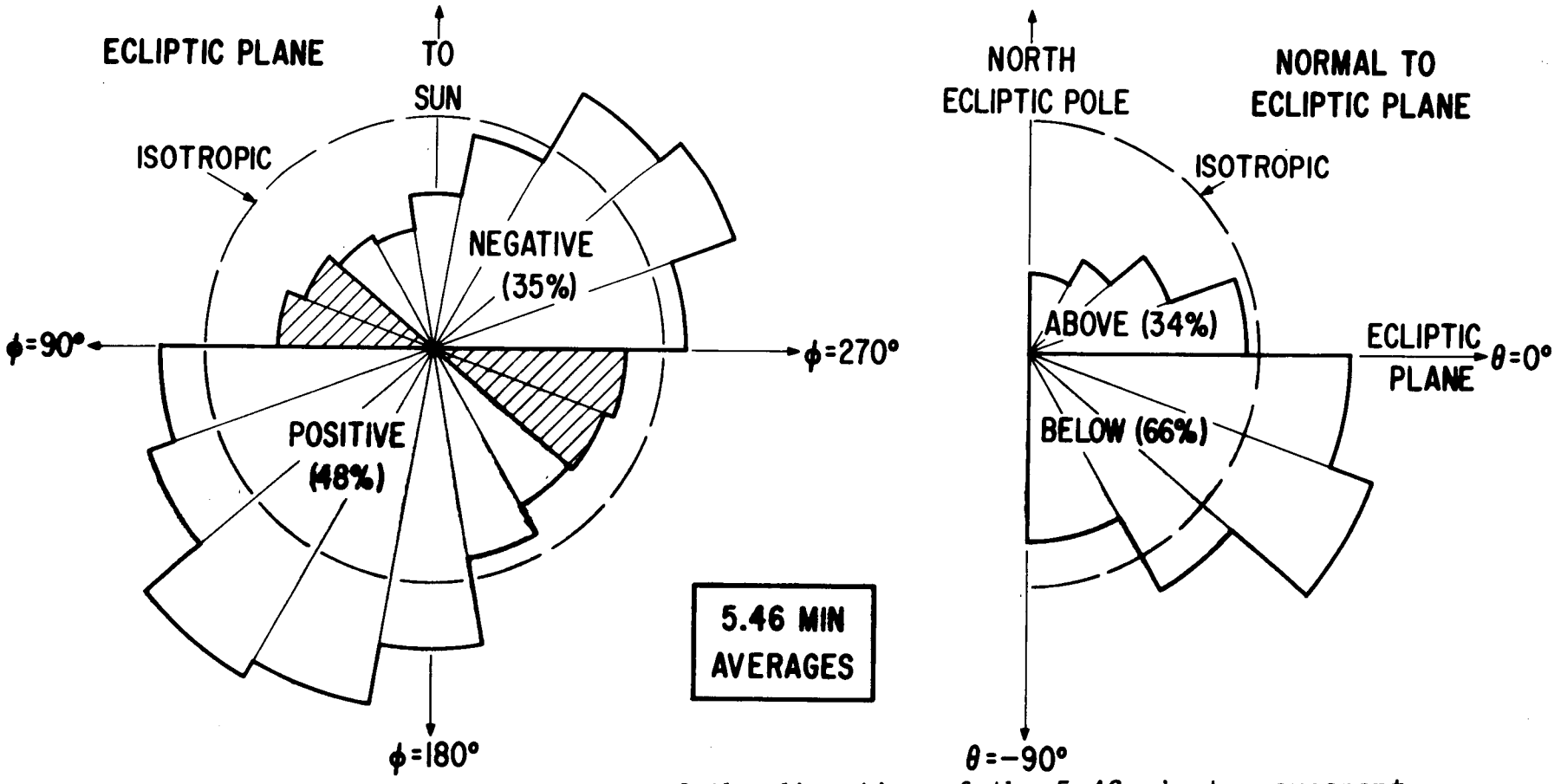

Figure 4. Statistical distribution of the direction of the 5.46 minute component averaged interplanetary magnetic field as observed on IMP-I during solar rotations 1784-1786. The distribution in the plane of the ecliptic indicates a close correspondence with the theoretical model of a continual uniform solar coronal expansion developed by Parker. The field distribution normal to the plane of the ecliptic indicates a small but distinct southward directed component.

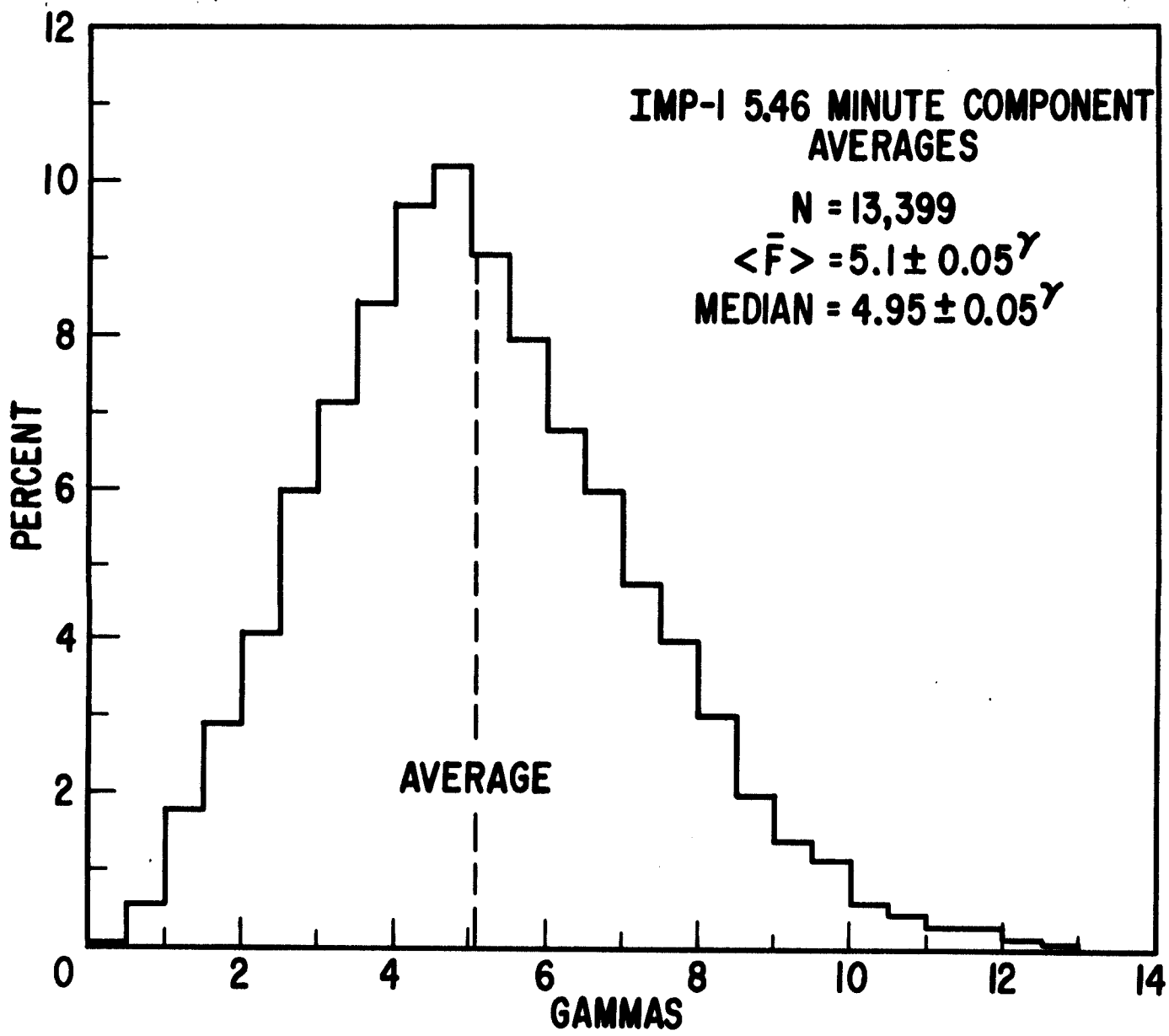

Figure 5. Statistical distribution of the interplanetary magnetic field magnitude for the same data corresponding to that shown in Figure 4. The uniformity of the distribution with an average value of 5.1 gammas is indicative of average photospheric fields of the Sun of a few gauss, according to Parker's model.

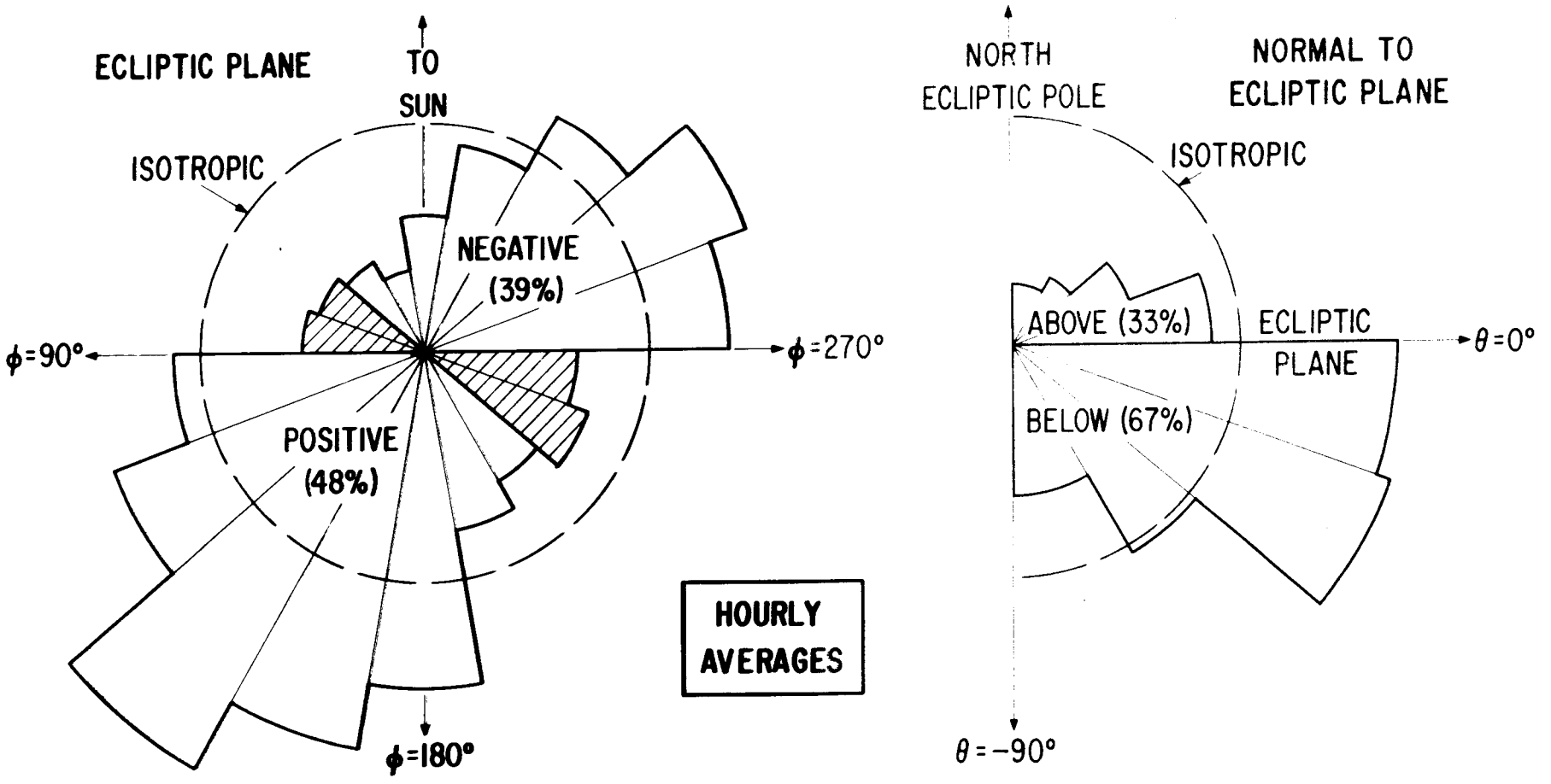

Figure 6. Statistical distribution of the direction of the 1 hour component averaged interplanetary magnetic field as observed on IMP-I during solar rotations 1784-1786. The distribution in the plane of the ecliptic indicates a closer correspondence with the theoretical model of a continual uniform solar coronal expansion than the 5.46 minute data as shown in Figure 4.

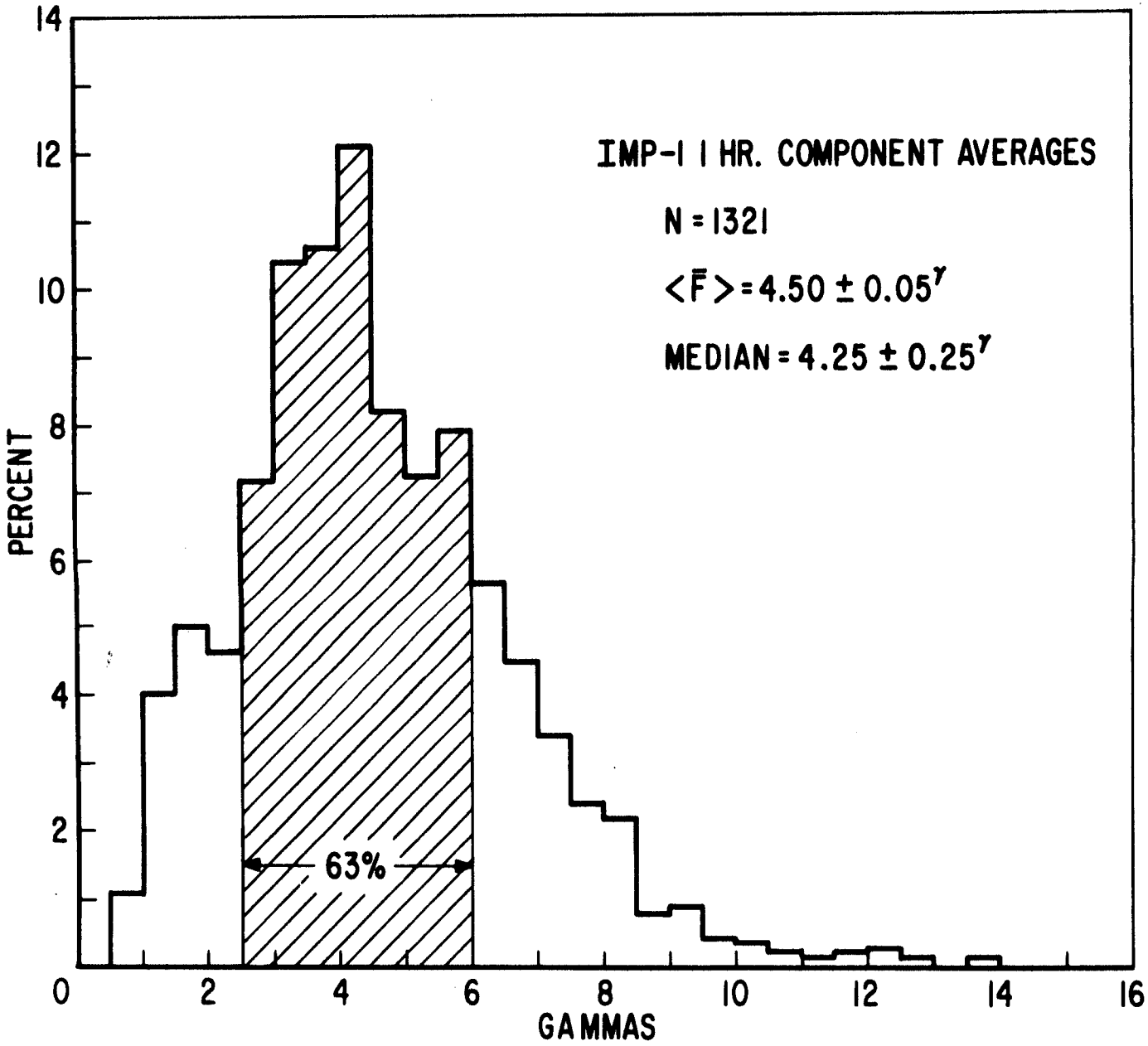

Figure 7. Statistical distribution of the interplanetary magnetic field magnitude for the same data corresponding to that shown in Figure 6. The uniformity of the distribution with an average value of 4.5 gammas is indicative of average photospheric fields of the Sun of a few gauss.

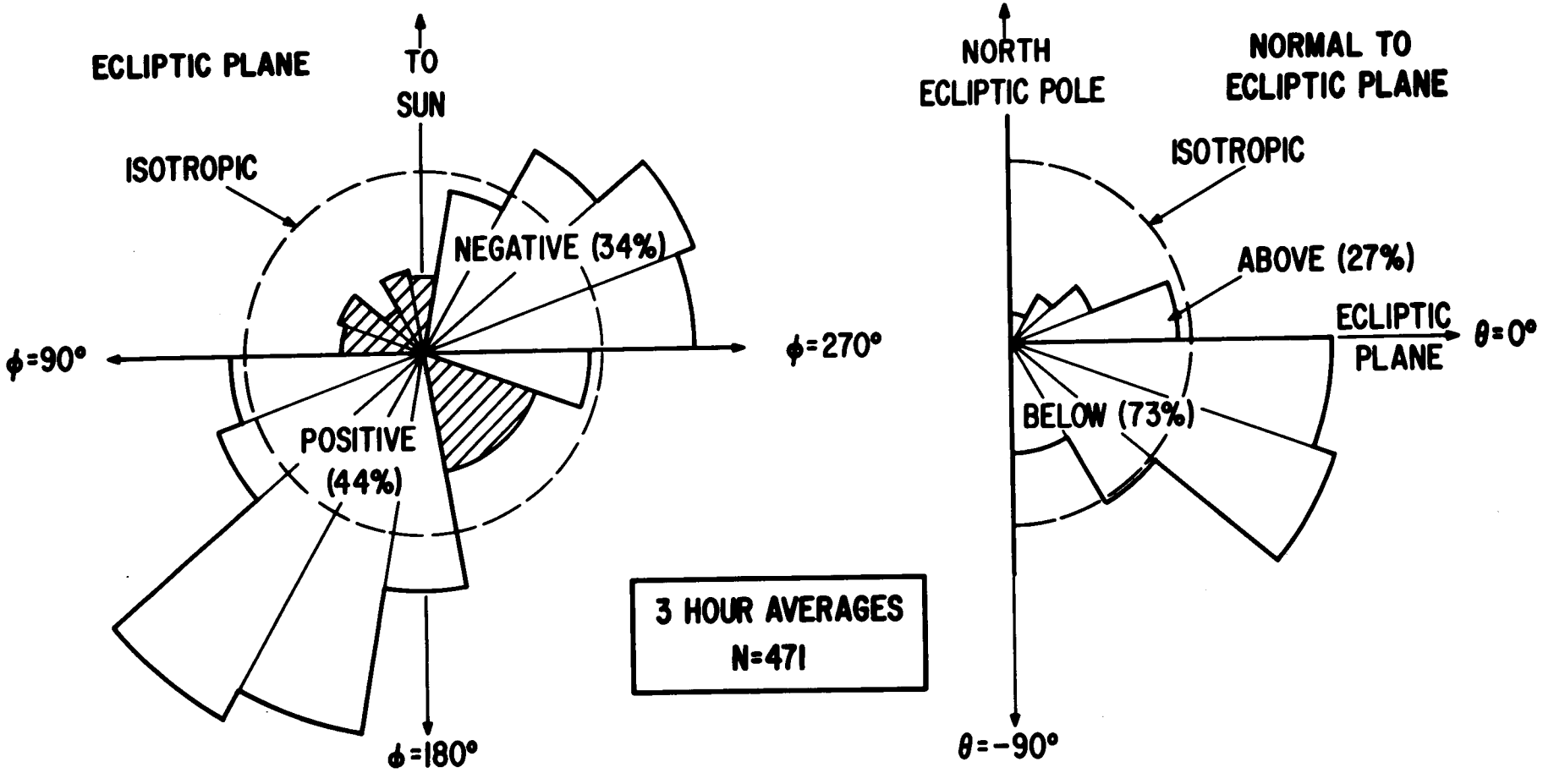

Figure 8. Statistical distribution of the direction of the 3 hour component averaged interplanetary magnetic field as observed on IMP-I during solar rotations 1784-1786. The distribution in the plane of the ecliptic indicates a still closer correspondence with the theoretical model than shown in Figures 4 and 6 although the lack of 180° symmetry is clearly evident.

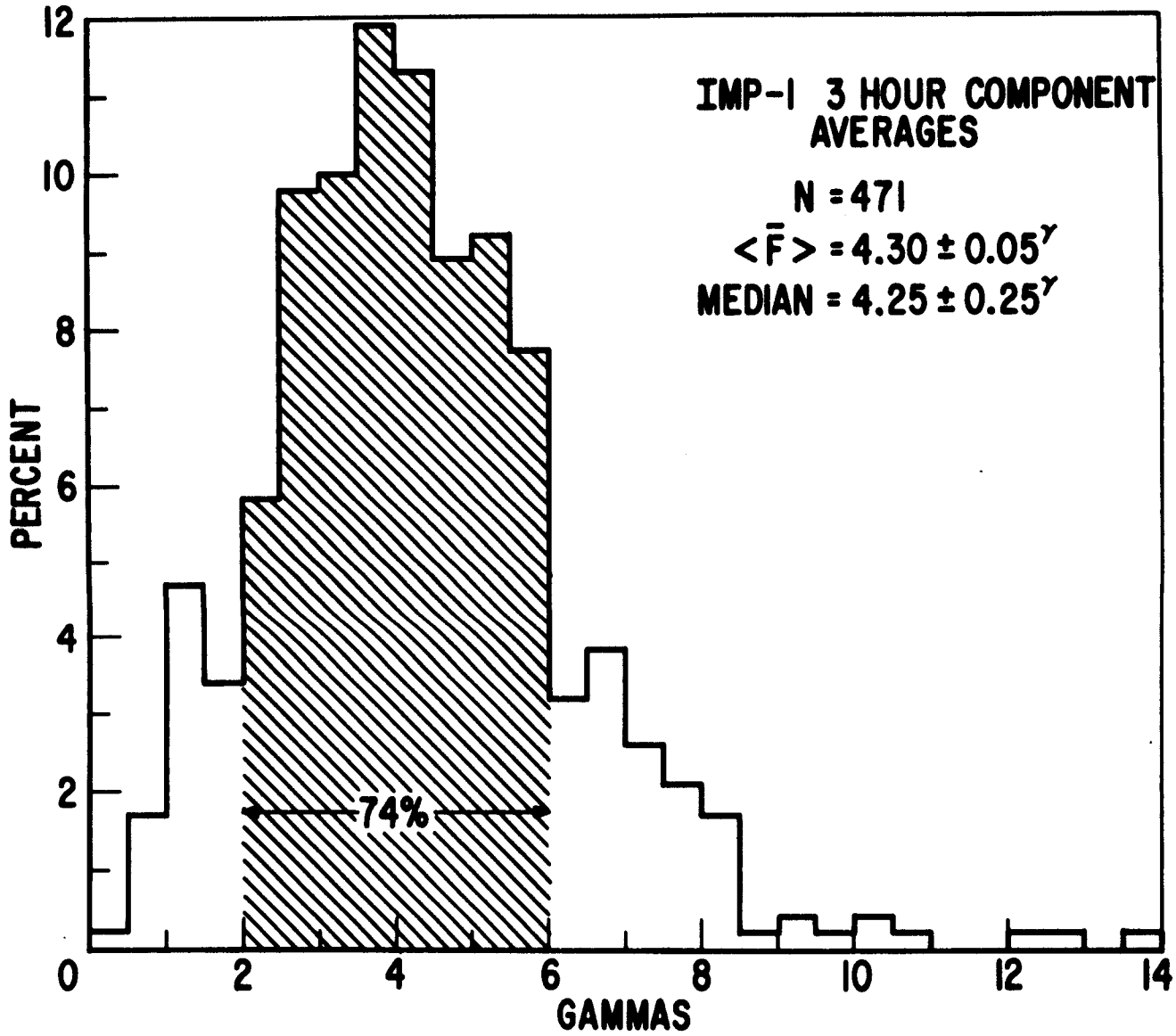

Figure 9. Statistical distribution of the interplanetary magnetic field magnitude for the same data corresponding to that shown in Figure 8. The uniformity of the distribution with an average value of 4.3 gammas is indicative of average photospheric fields of the Sun a few gauss according to Parker's model.

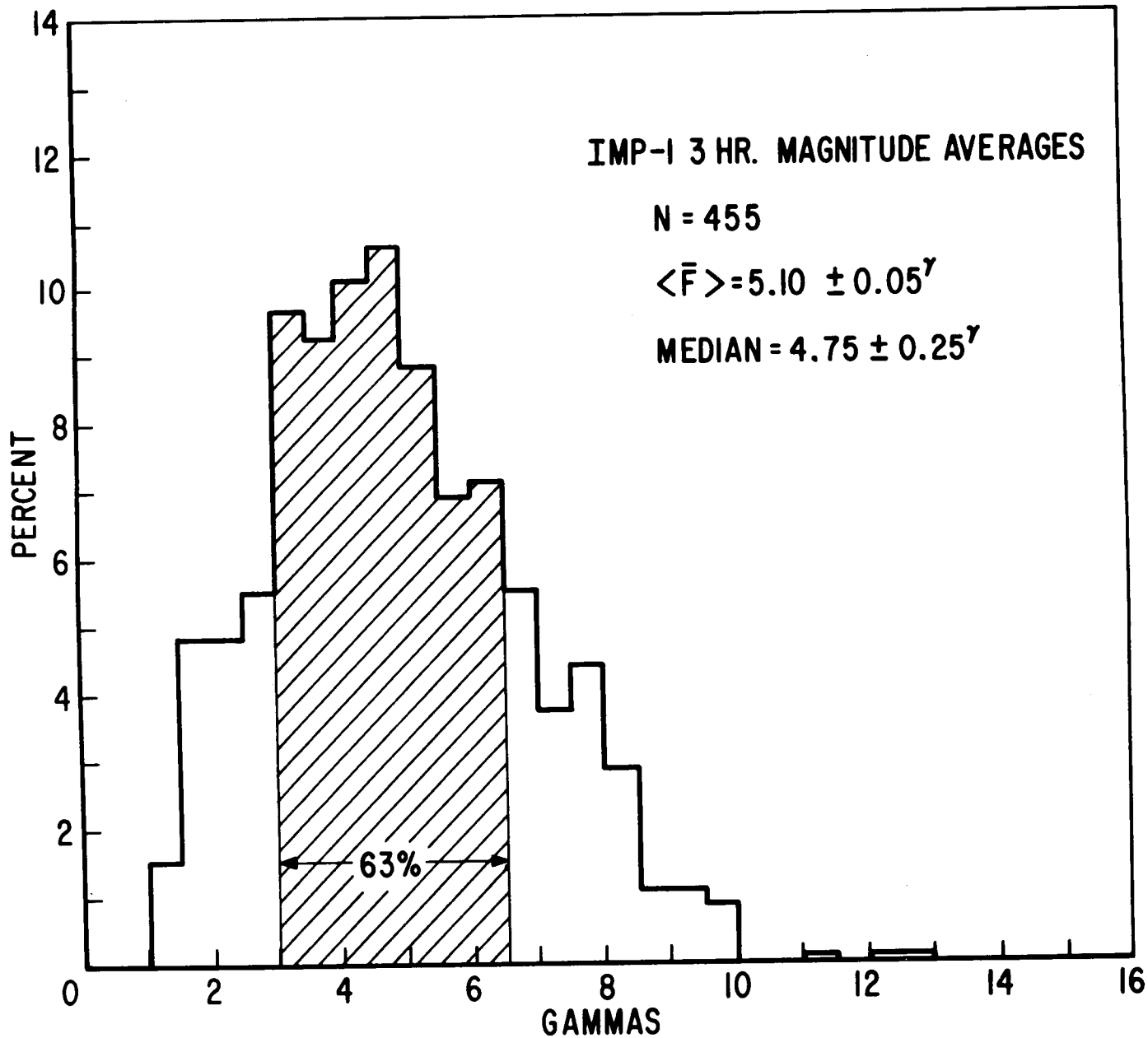

Figure 10. Statistical distribution of the averaged magnitudes of the interplanetary magnetic field over a 3 hour interval. This figure is to be distinguished from the preceding figure in which component averages were employed to construct a 3 hour magnitude average. The average value of 5.1 gammas is identical to Figure 5, as is to be expected.

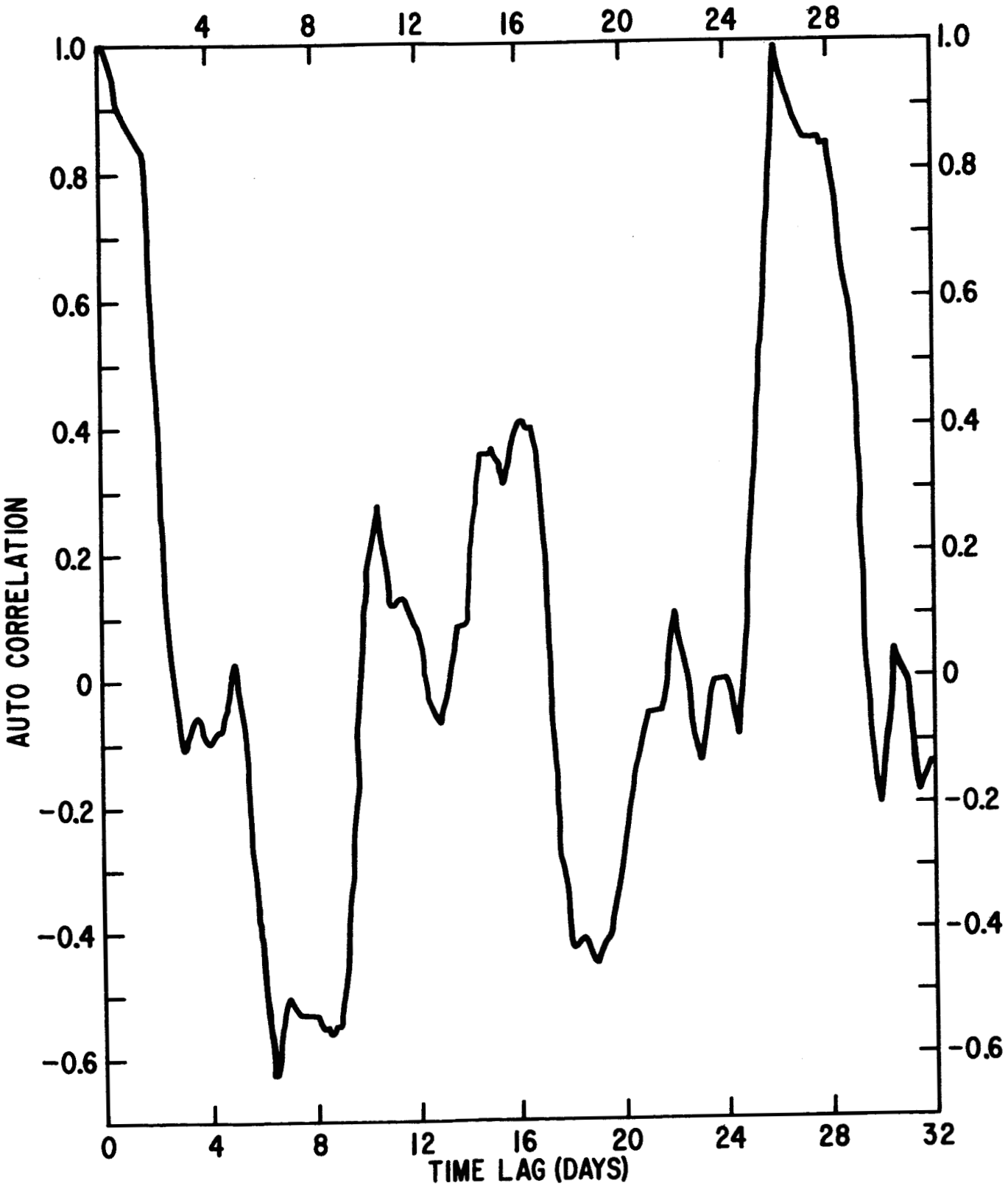

Figure 11. Auto correlation of the direction of the interplanetary magnetic field as observed by IMP-I. The direction of the field is defined to be either positive or negative according to Figure 4. The Auto correlation of this time series yields a significant peak at approximately 27 days. (See text).

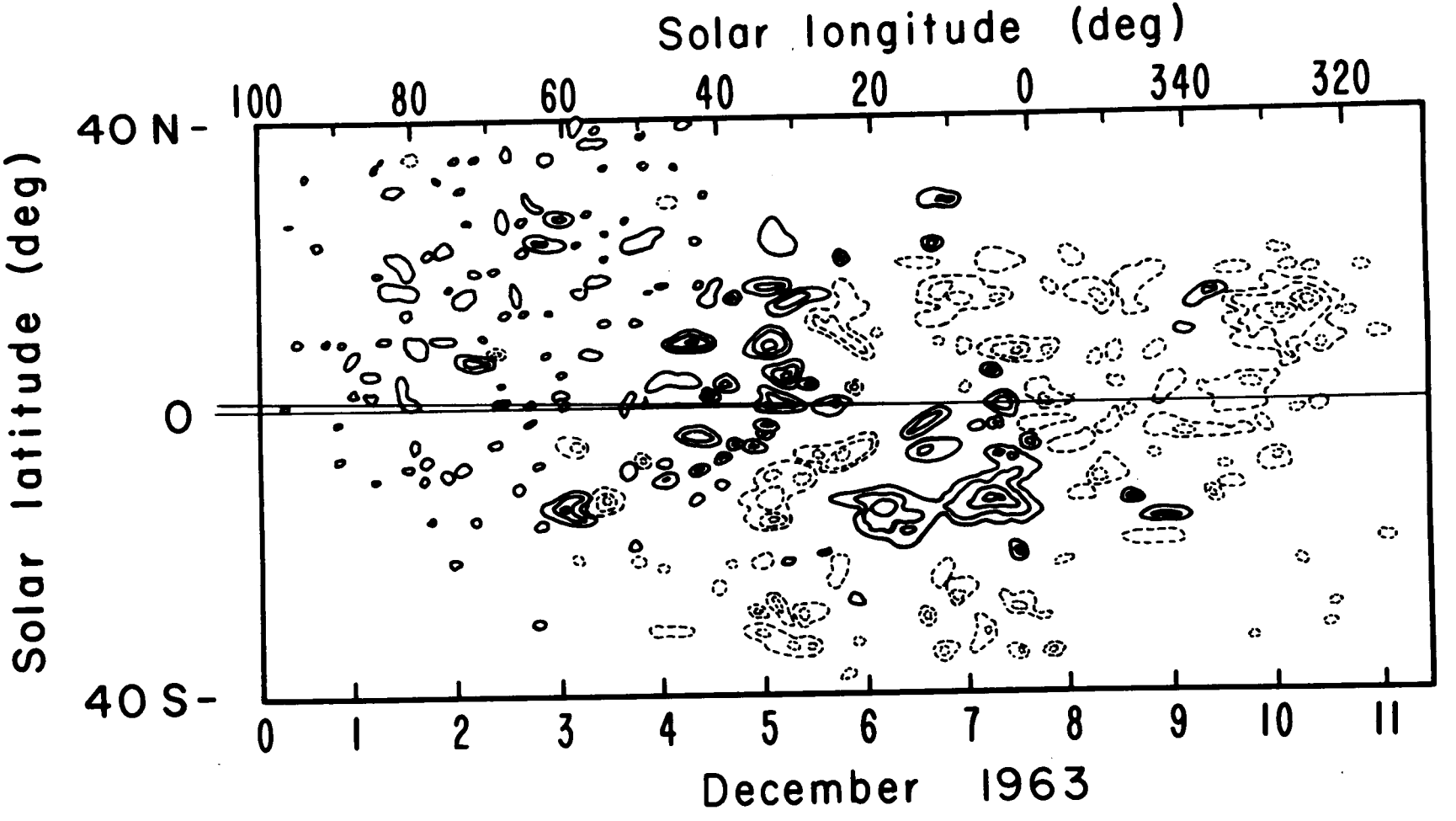

Figure 12. Representative solar magnetograph obtained from the Mount Wilson Observatory showing the magnitude and direction of the line-of-sight component of the photospheric magnetic field at CMP on date shown. The contour interval for these data are taken to be 2, 4, 8, 12 and 25 gauss. A solid line indicates fields directed out of the Sun while dashed lines indicate fields directed into the Sun.

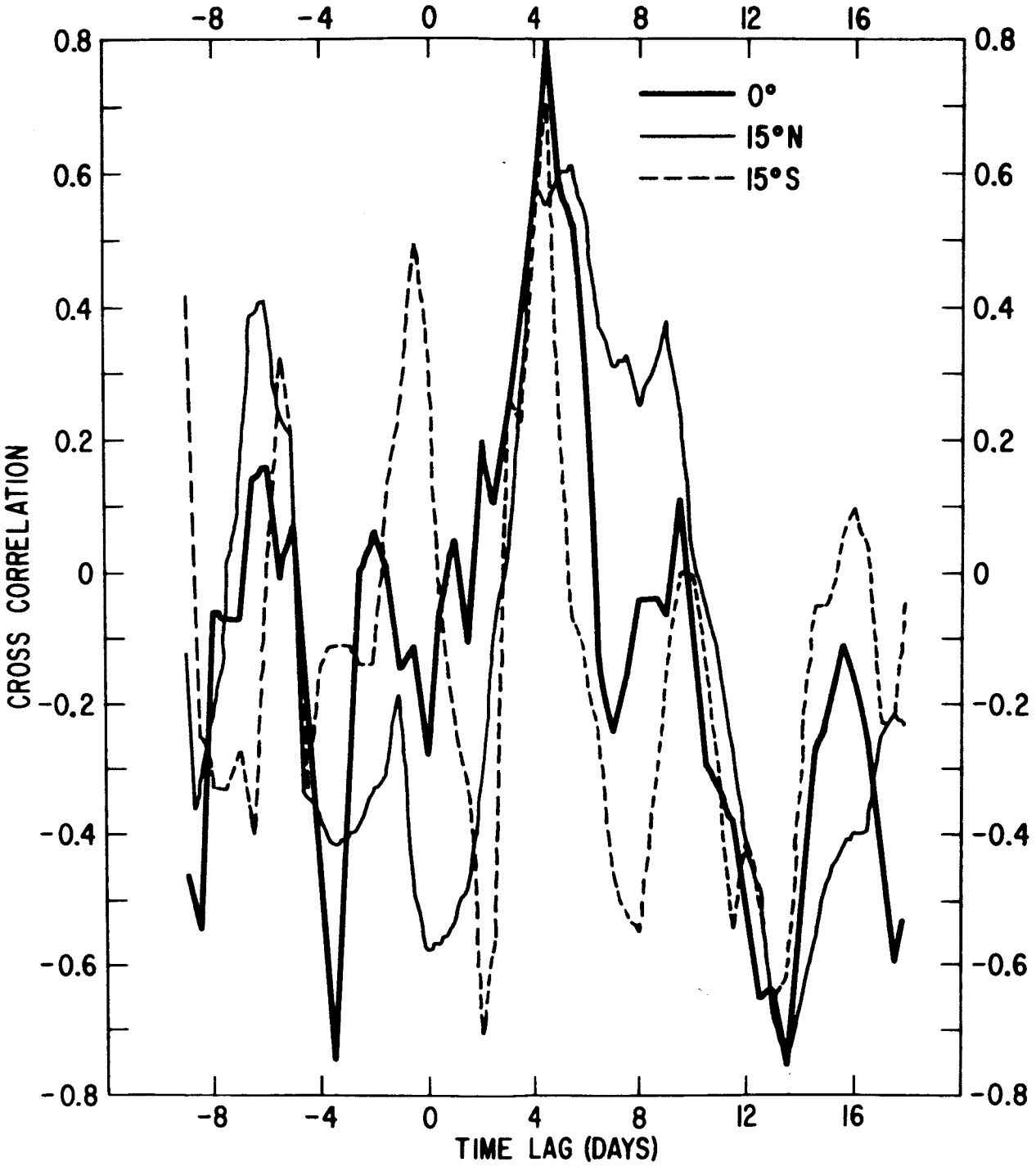

Figure 13. Cross correlation of the IMP-I interplanetary magnetic field data and the photospheric magnetic field for three latitudes illustrating the coherent and statistically significant peak at 4.5 days. This corresponds to a transport velocity of solar lines of flux to 1 AU of approximately 385 kilometers/sec.

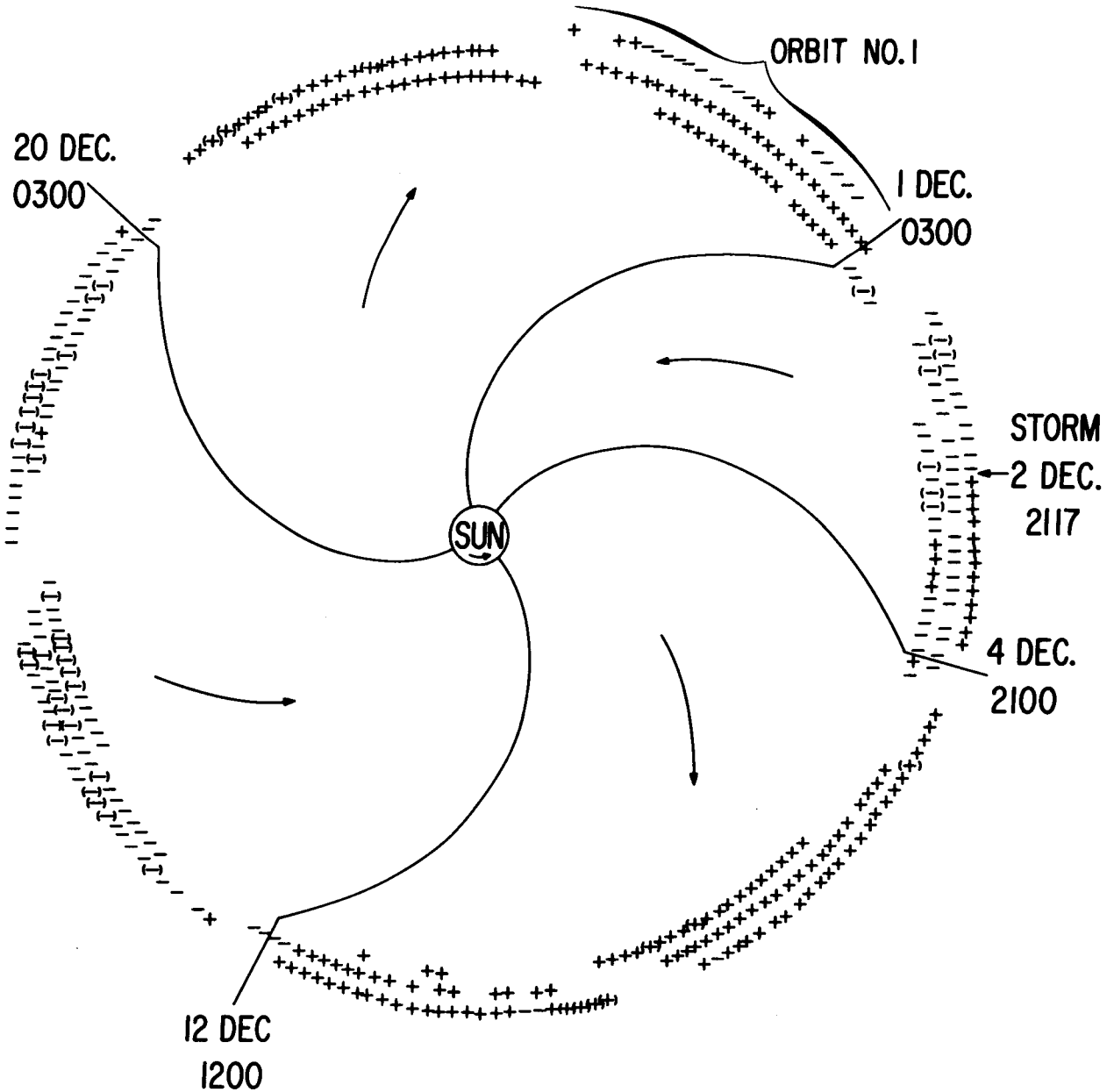

Figure 14. Superposed epoch structure of the interplanetary magnetic field direction for solar rotations 1784-1786. Immediately evident is the sectoring of the interplanetary field into four portions of which three are approximately equal in angular extent. This sector structure co-rotates with the Sun and hence observable effects associated with this structure should be detectable at periodic time intervals of approximately 27 days.

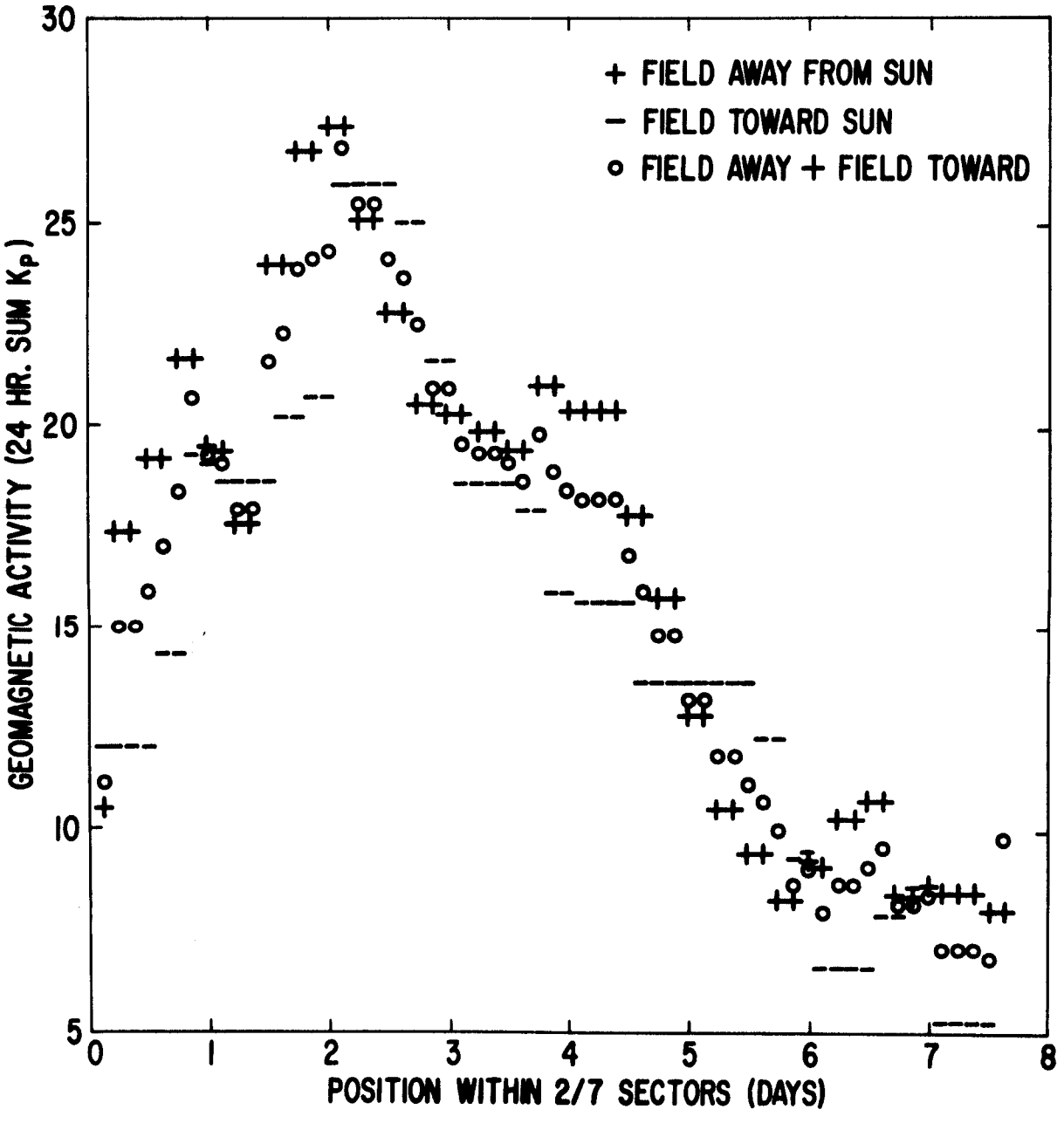

Figure 15. Characteristic variation of the K_p index as observed in the combined sectors illustrated in Figure 14. The high K_p index follows the change in sense of the directed flux tube from the Sun and K_p decreases to a minimum at the end of the sector. Implications regarding the recurrent M- region storms on the Sun are discussed in the text.

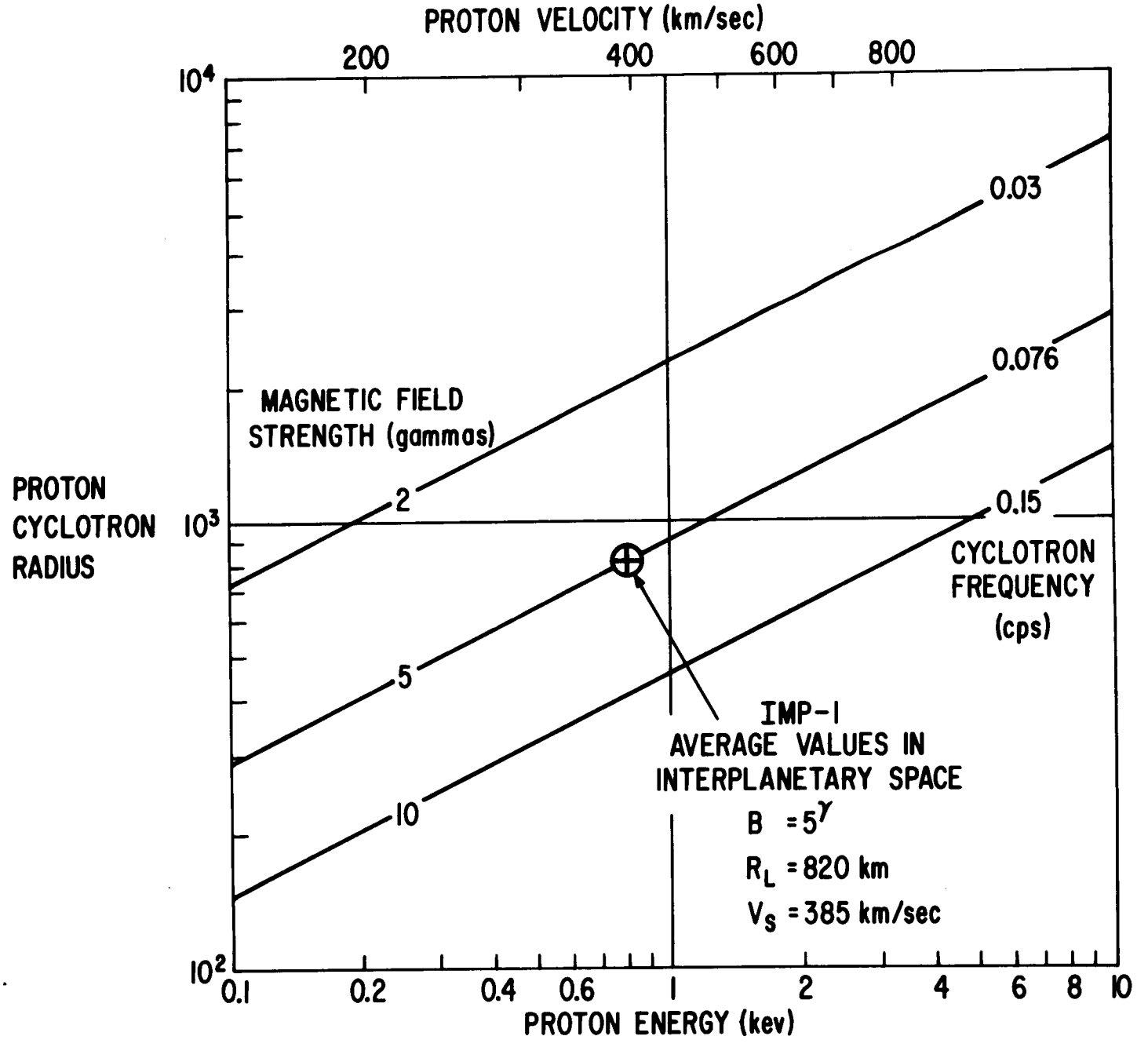

Figure 16. Representative values of the interplanetary medium during the quiet Sun as observed by IMP-I. The interplanetary magnetic field magnitude and velocity, as derived from directional considerations and cross correlation with the Sun, yield a characteristic proton cyclotron radius of 820 kilometers.

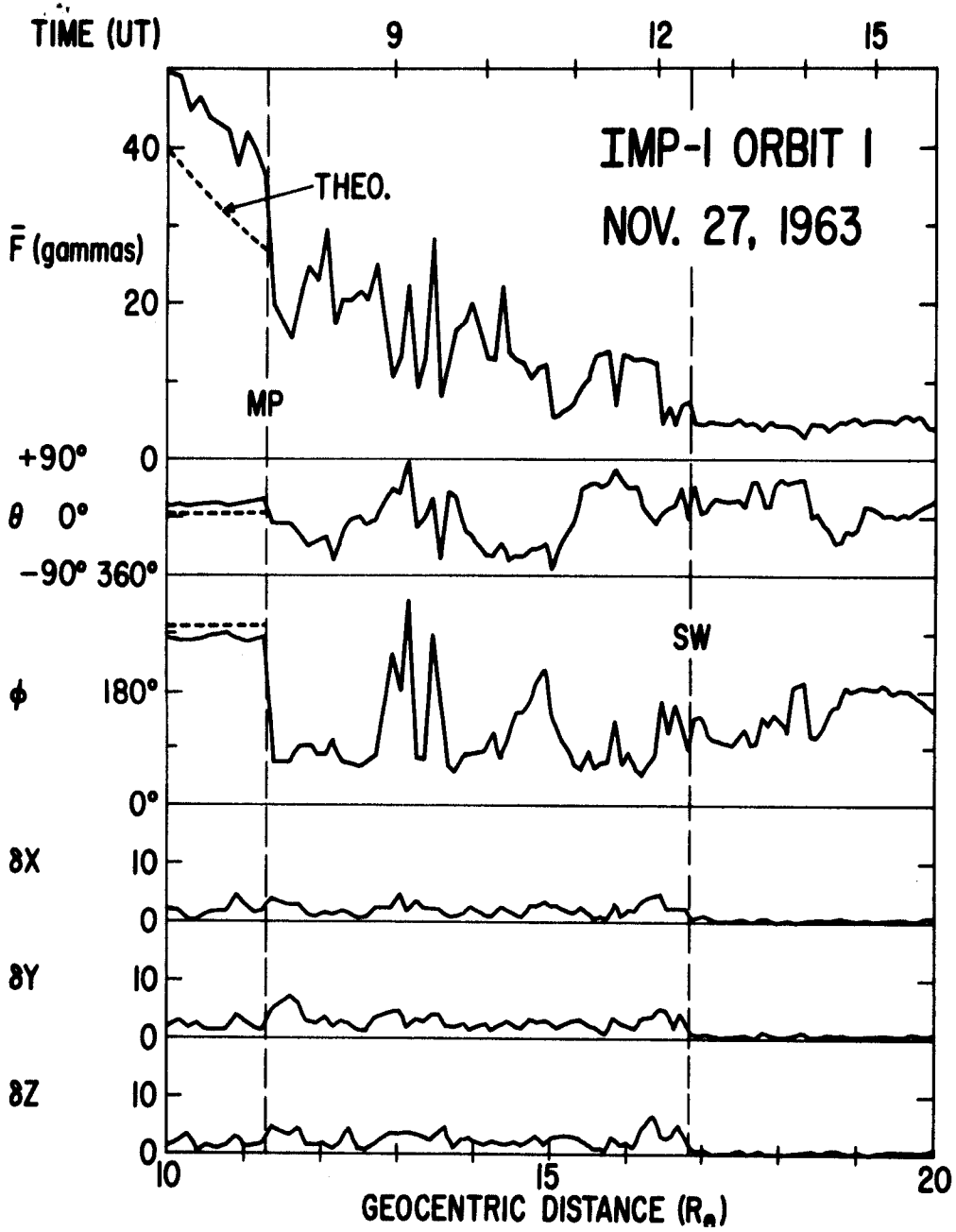

Figure 17. Observed magnetic field results on outbound orbit # 1 by the IMP-1 satellite, Nov. 27, 1963. Clearly evident are the magnetosphere boundary at 11.3 R_e and the collisionless shock wave at 16.8 R_e. For a definition of these boundaries see text.

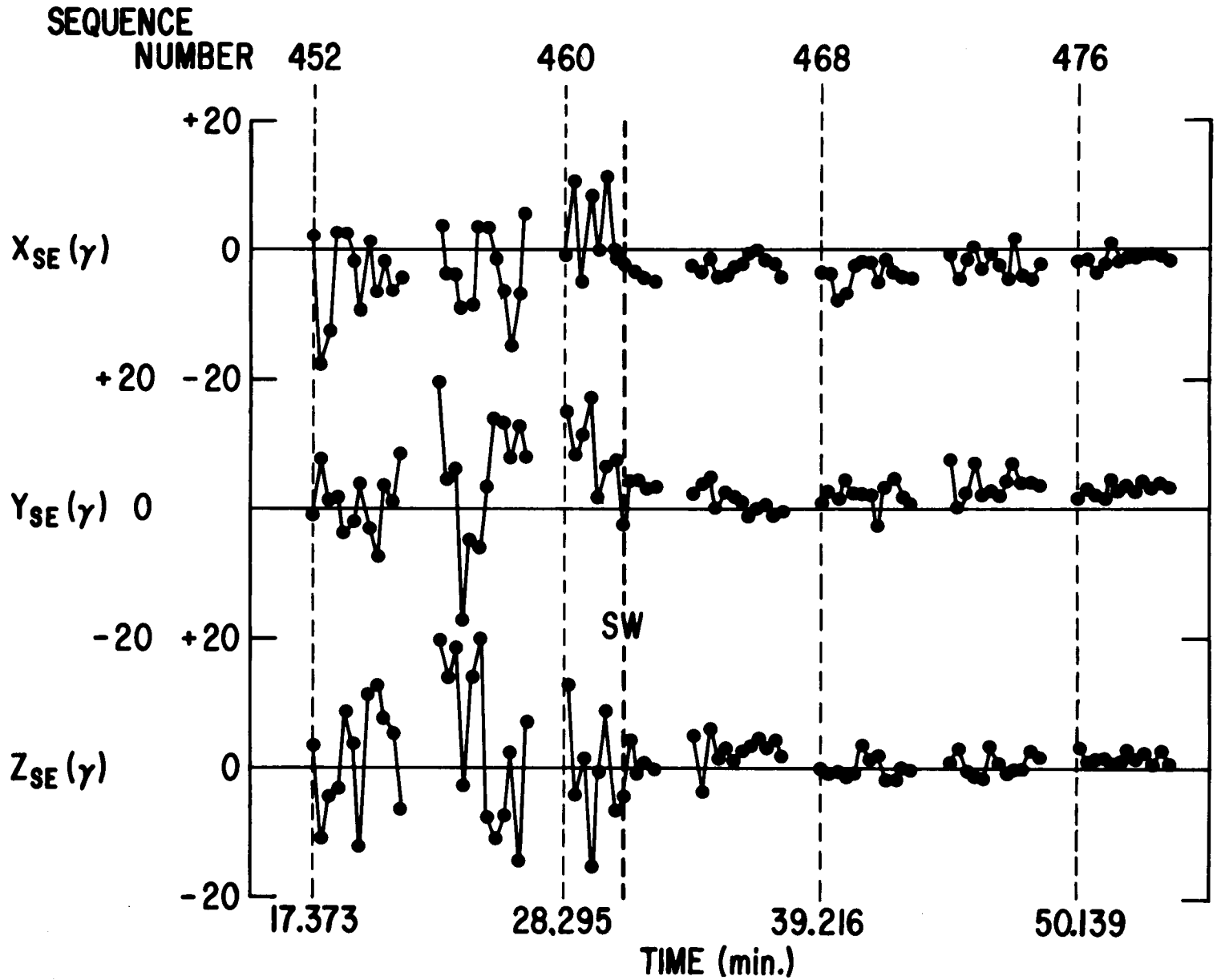

Figure 18. Detailed variation of the three orthogonal components of the magnetic field observed during the first outbound traversal of the shock wave by IMP-I. These data expand the time scale shown in Figure 17 to a distance scale corresponding to satellite motion of approximately 40 kilometers between successive sample points. The gaps in the data correspond to continuous transmission of the Rubidium vapor magnetometer data in the telemetry sequence.

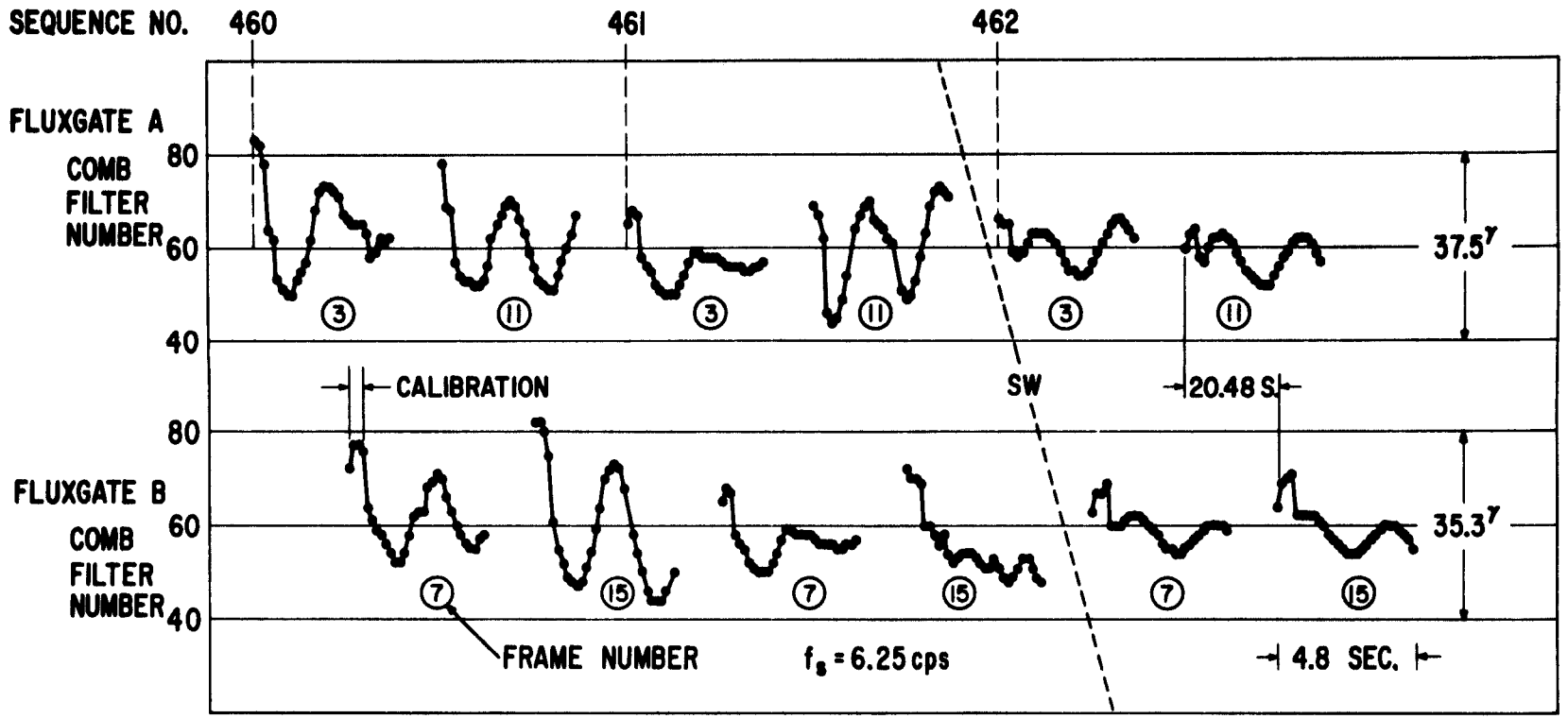

Figure 19. Fine detail of the collisionless shock wave thickness as observed on outbound orbit # 1 by IMP-I. Individual spin modulated signals observed for time intervals of 4.8 seconds are shown in time sequence. The position of the shock wave and the characteristic differences in the magnetic field modulation of the detected flux gate magnetometer signal are evident.

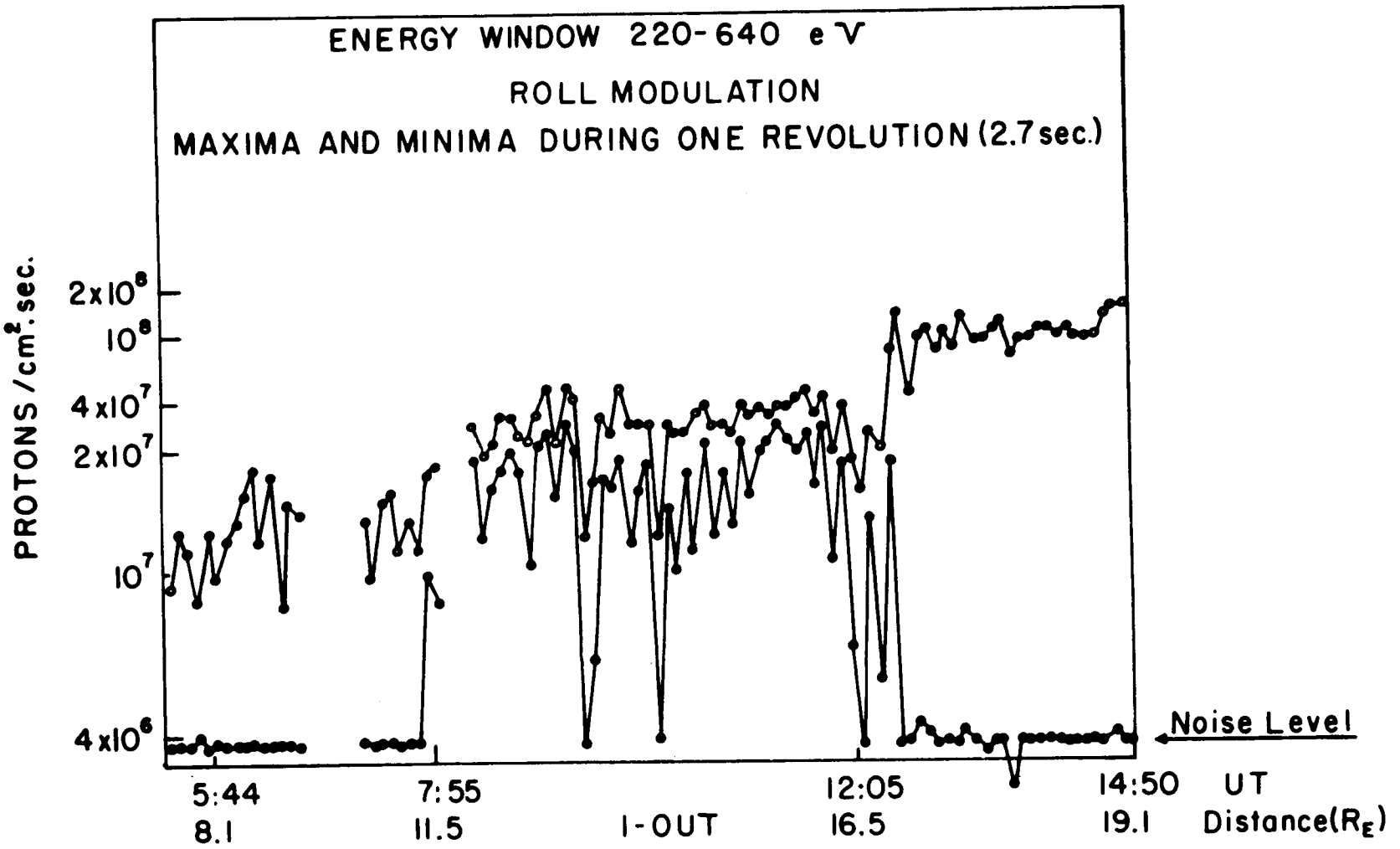

Figure 20. Representative results from the MIT plasma probe showing measurements of thermalized plasma by IMP-I during outbound orbit # 1. The positions of the boundaries are evidenced by the distinct change to small spin modulation of the observed flux between 11.3 and 16.8 R_e compared to measurements beyond these points (Bridge et. al., 1965).

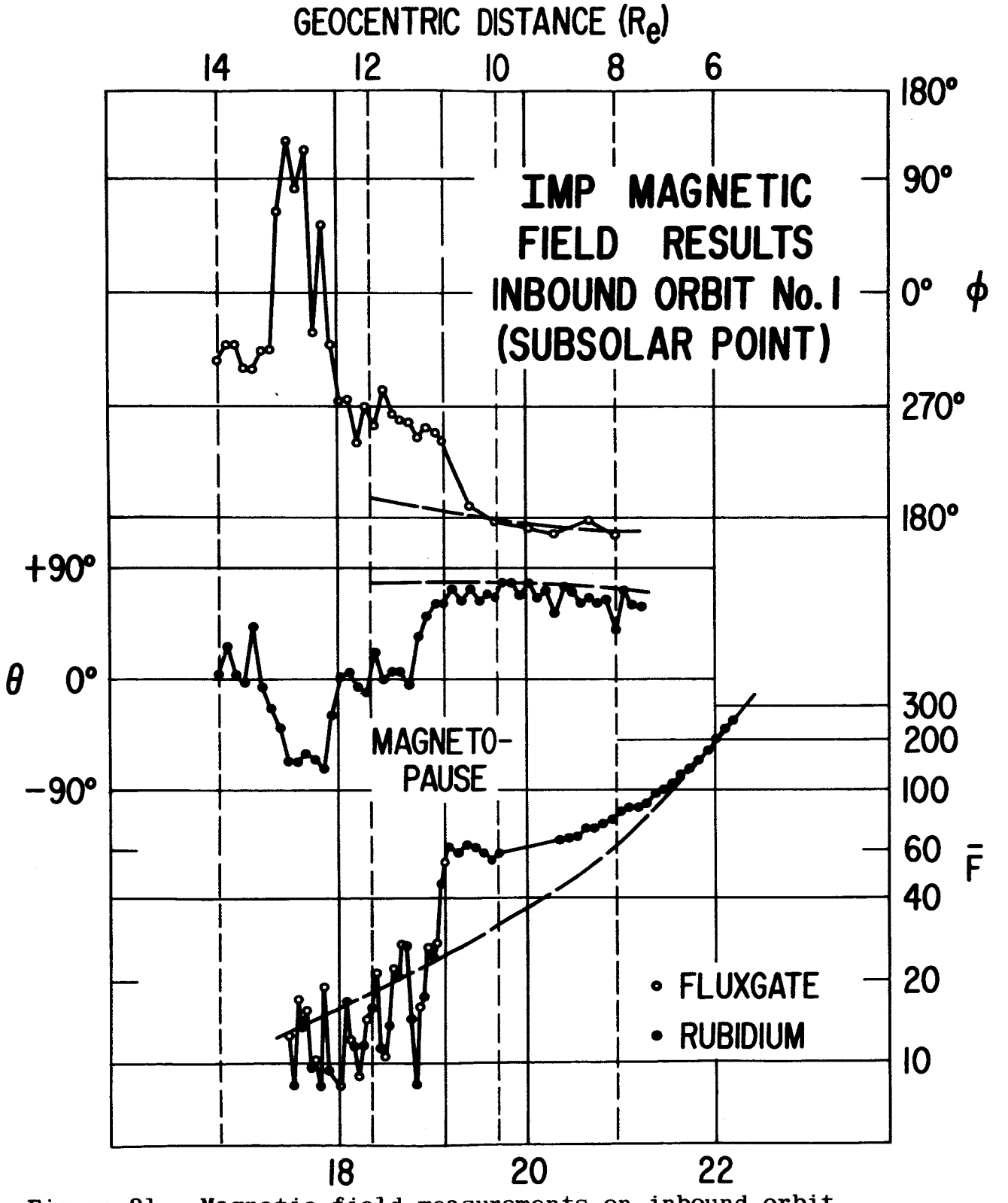

Figure 21. Magnetic field measurements on inbound orbit # 1 from the IMP-I satellite on Nov. 30, 1963. The magnetosphere boundary is observed distinctly as an abrupt magnitude and direction change at a geocentric distance of 10.8 R_e.

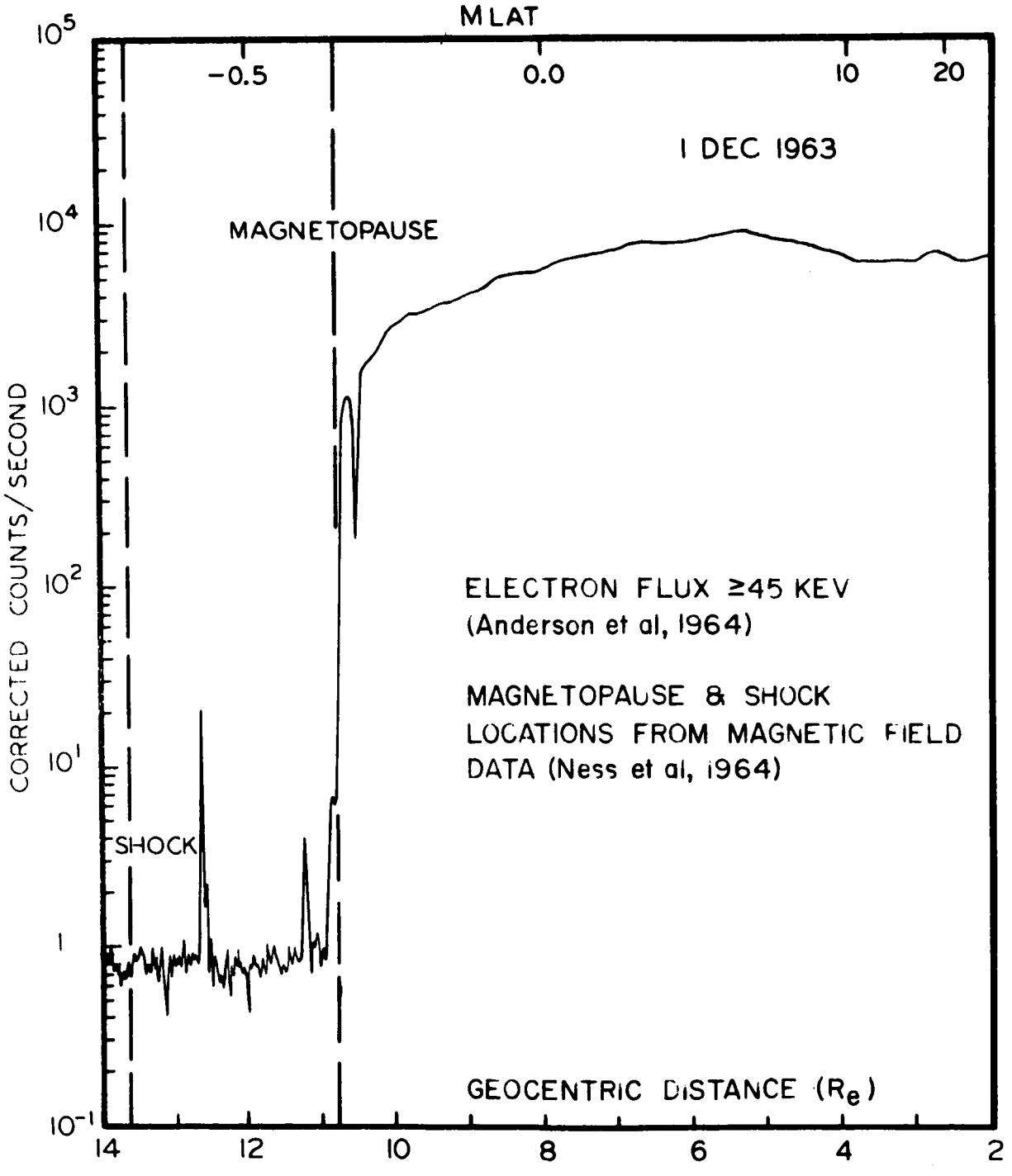

Figure 22. Measurements of flux of electrons with energy greater than 45 KeV on IMP-I inbound orbit # 1 showing coincidence of trapping region boundary with magnetopause at 10.8 R_e.

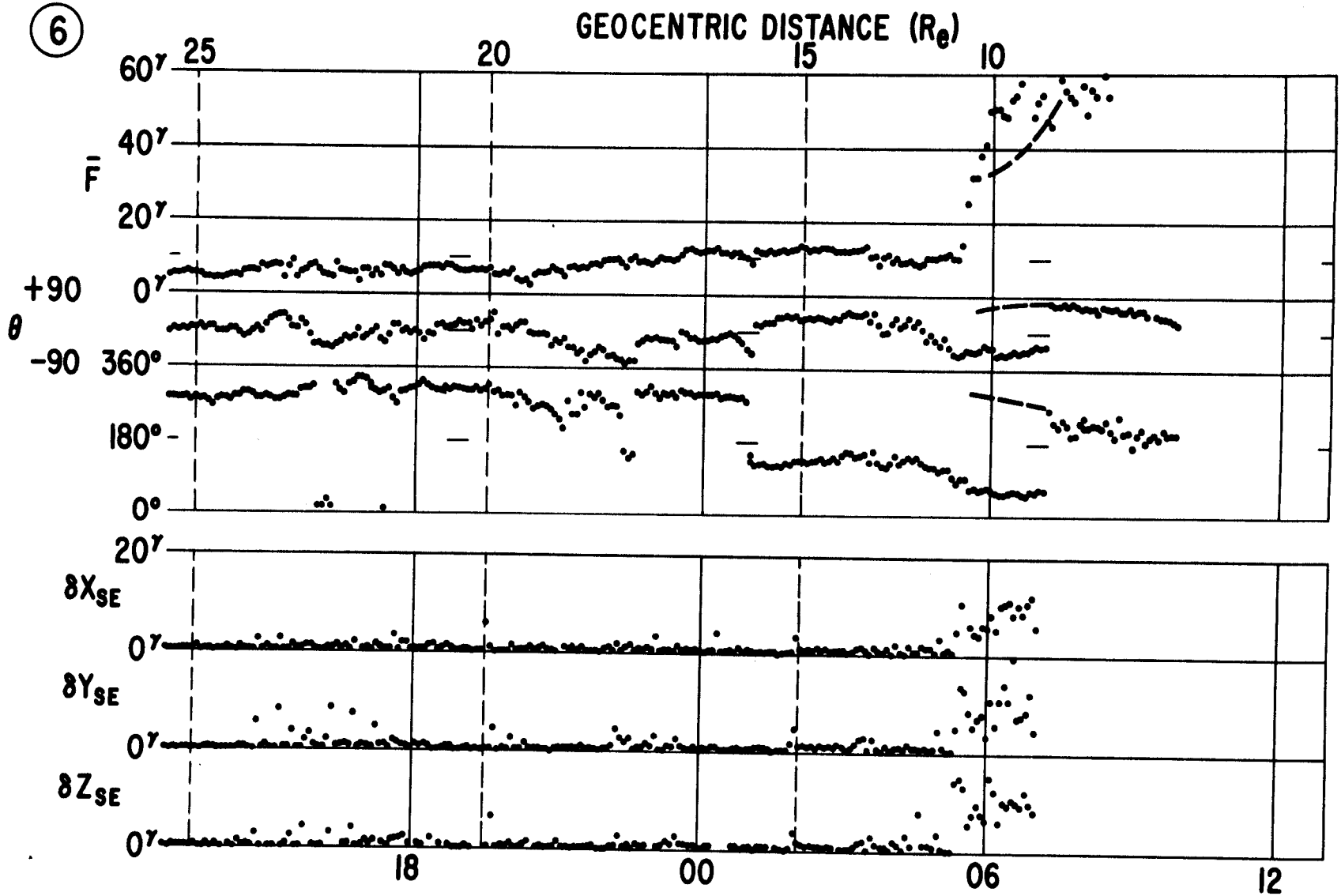

Figure 23. Magnetic field measurements on inbound orbit # 6 from the IMP-I satellite on Dec. 20, 1964 showing the interplanetary magnetic field beyond approximately 15 R_e and magnetosphere boundary at 8.1 R_e. This is determined by the abrupt change in direction of the field which is seen to be not coincident with the magnitude change. This particular orbit shows the magnetosphere boundary in considerably closer to the Earth than generally observed by IMP-I.

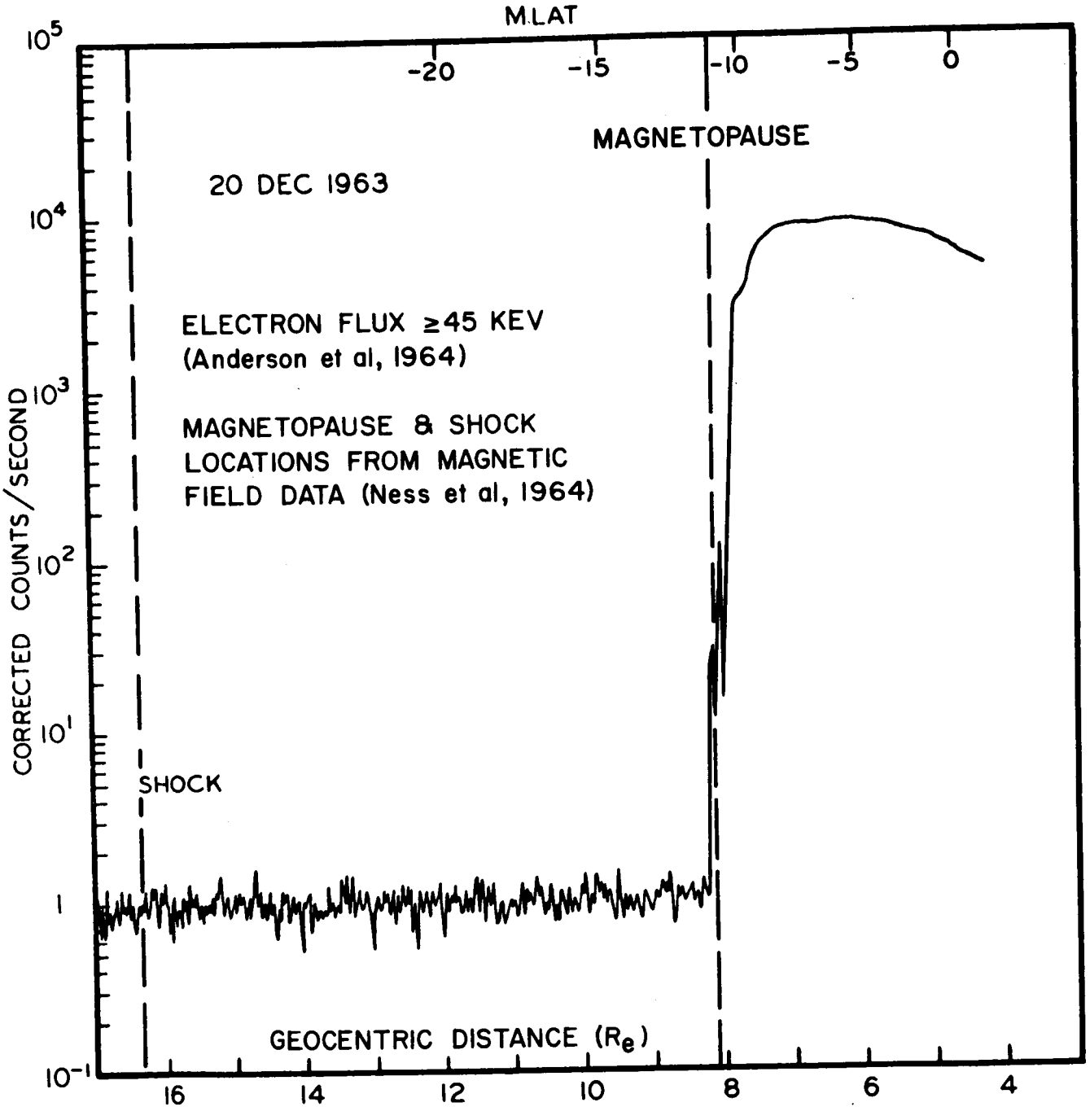

Figure 24. Measurements of the flux of electrons with energy greater than 45 KeV on inbound orbit # 6 by the IMP-I satellite. Coincidence of the magnetosphere boundary and the trapping region is again evidenced with small electron fluxes beyond the boundary.

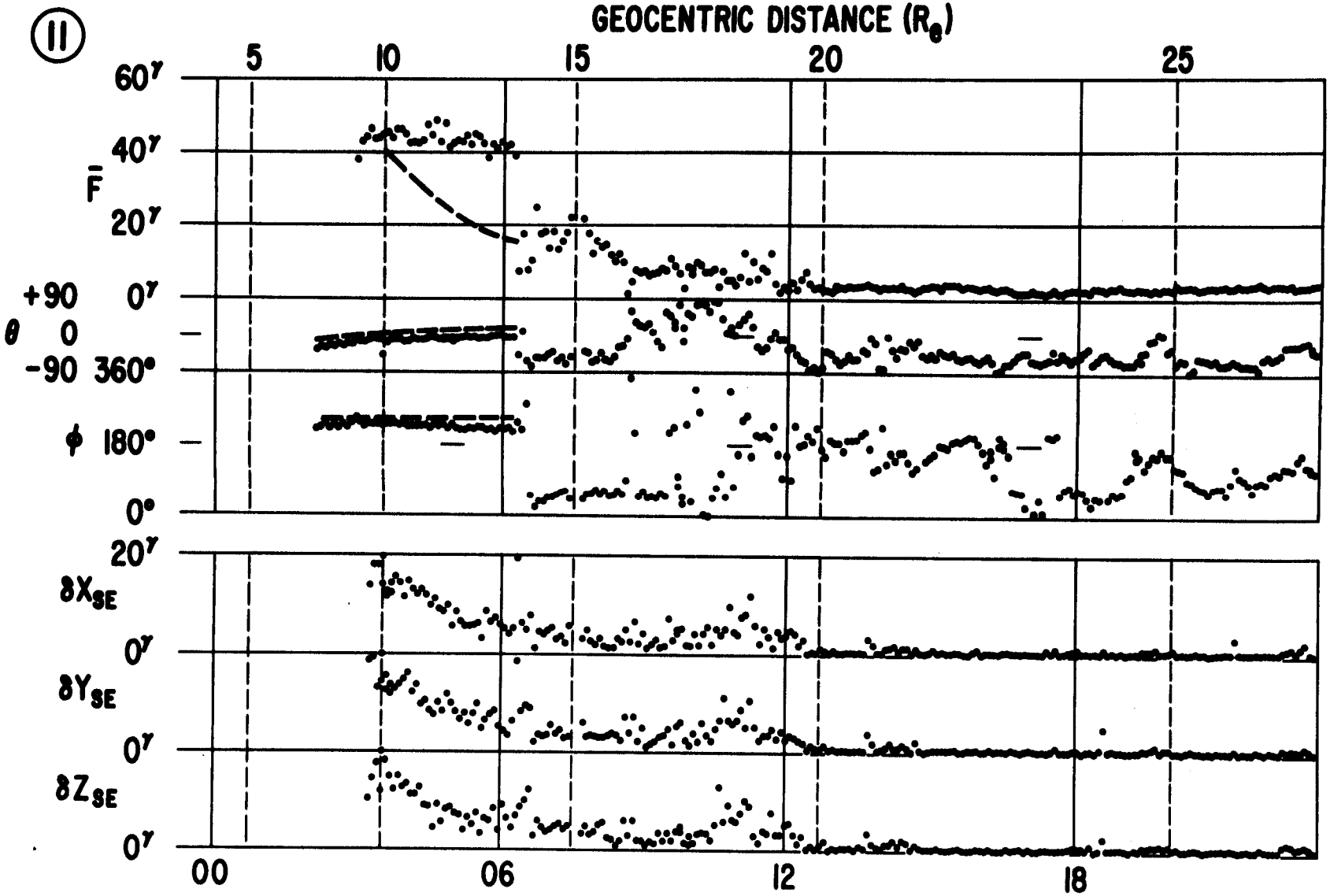

Figure 25. Magnetic field measurements on outbound orbit # 11 from the IMP-1 satellite on January 5, 1964. The magnetosphere boundary is observed at a distance of 13.6 R_e and the shock wave at a distance of 19.7 R_e. The satellite at this time was approximately on the sunrise terminator position with respect to the Sun-Earth line.

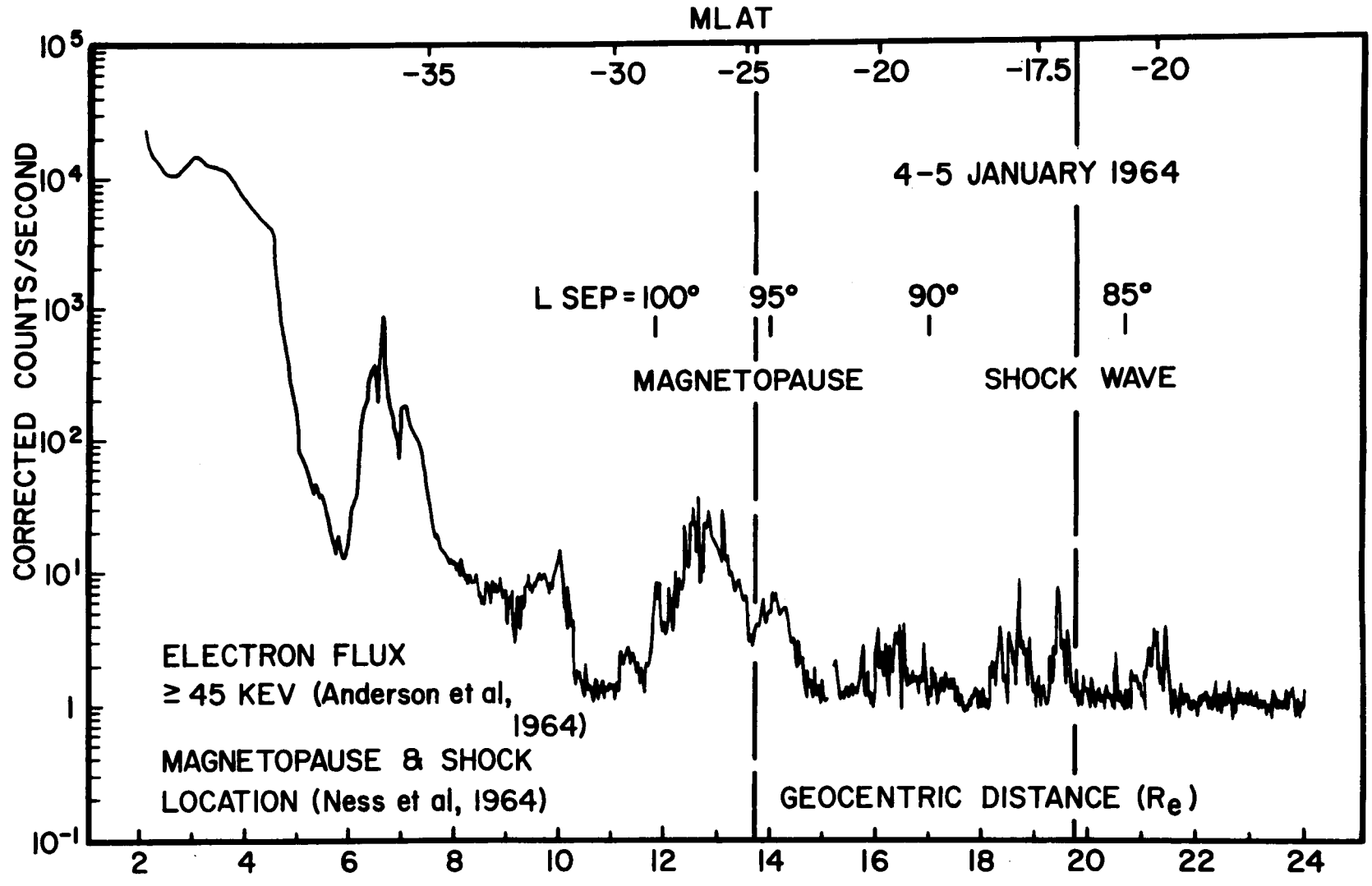

Figure 26. Outbound orbit # 11 from the IMP-I satellite on January 5, 1964 showing flux of electrons with energy greater than 45 KeV. The boundary of trapping is observed at approximately 5 R_e while the magnetopause is not observed until 13.6 R_e. The gap in these positions is associated with a change in the geomagnetic field topology surrounding the Earth and illustrates the strong day-night asymmetry in the characteristics of the magnetospheric cavity.

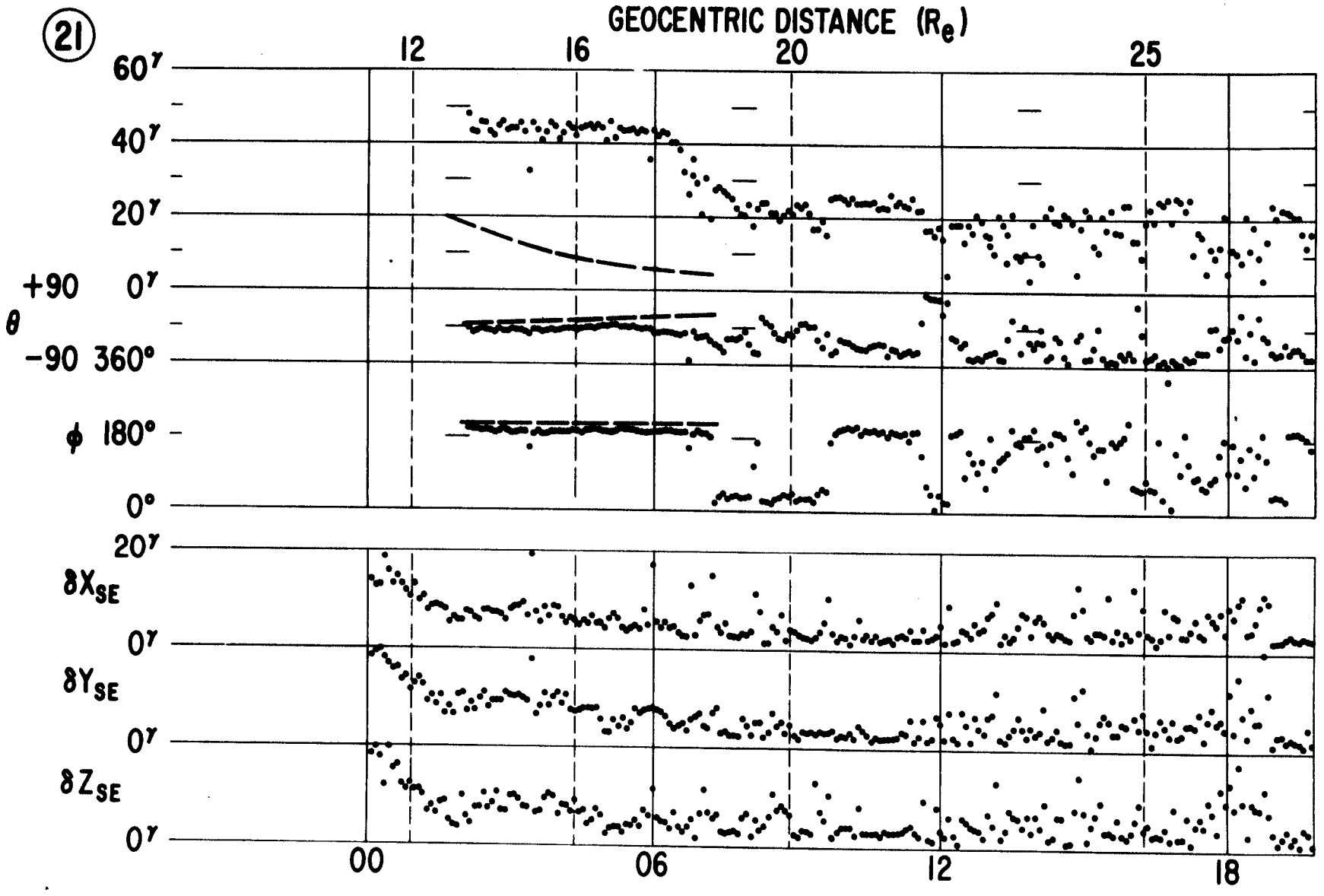

Figure 27. Magnetic field measurements on outbound orbit # 21 from the IMP-I satellite on February 13, 1964. The magnetosphere boundary is not observed until a radial distance of 18.7 R_e is reached. The boundary is evidenced by an abrupt directional change in the magnetic field corresponding to approximately anti-parallel fields across the boundary. Characteristic disturbed fields of the turbulent transition region are observed throughout the remainder of this data sample.

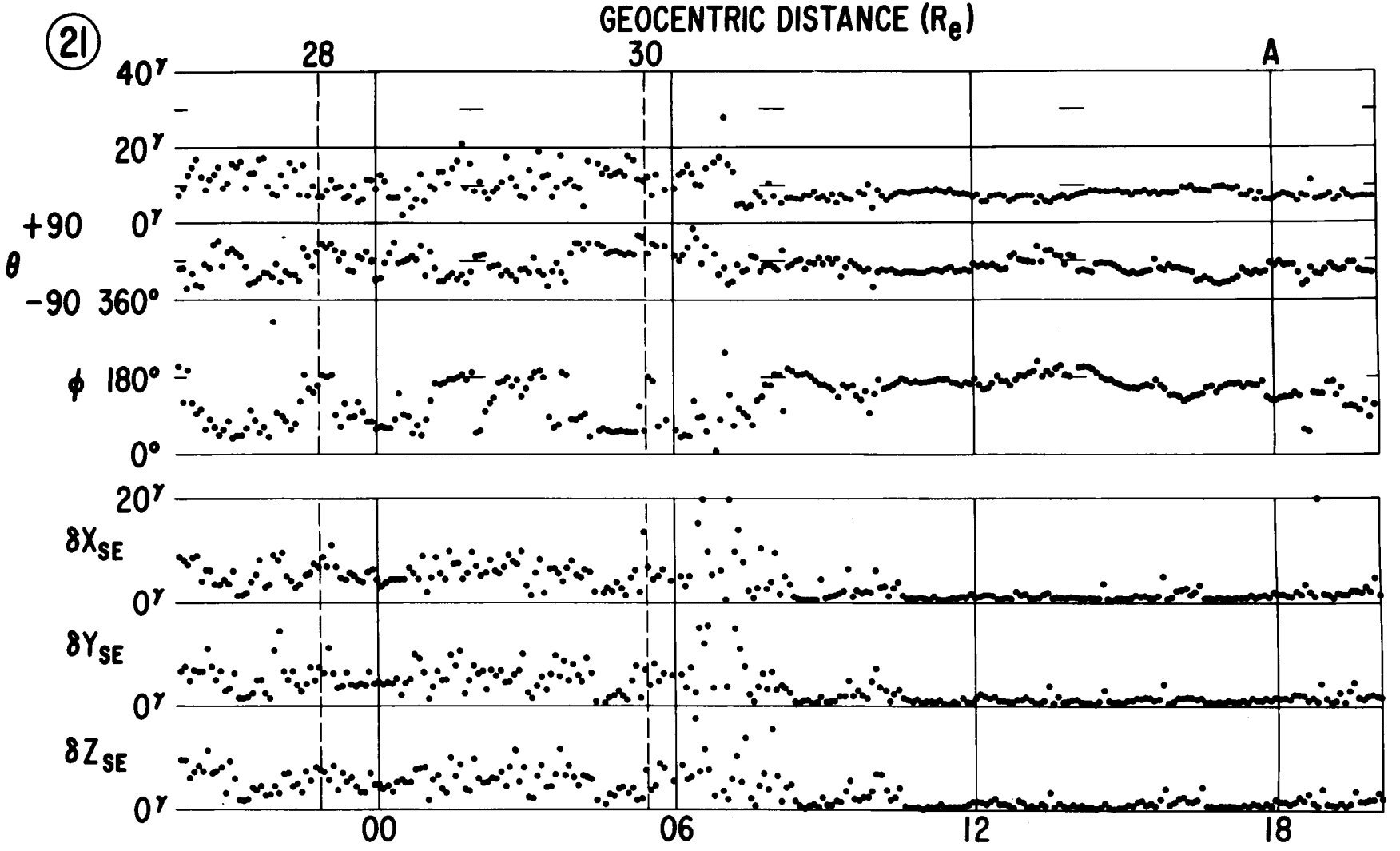

Figure 28. Continued measurements of the magnetic field on outbound orbit # 21 from the IMP-I satellite on February 14, 1964. The shock wave is not observed until a distance of 30.4 R_e is reached or approximately at satellite apogee. According to the magnetic field measurements this represents the last orbit on which the interplanetary medium was capable of being sampled by the IMP-I satellite.

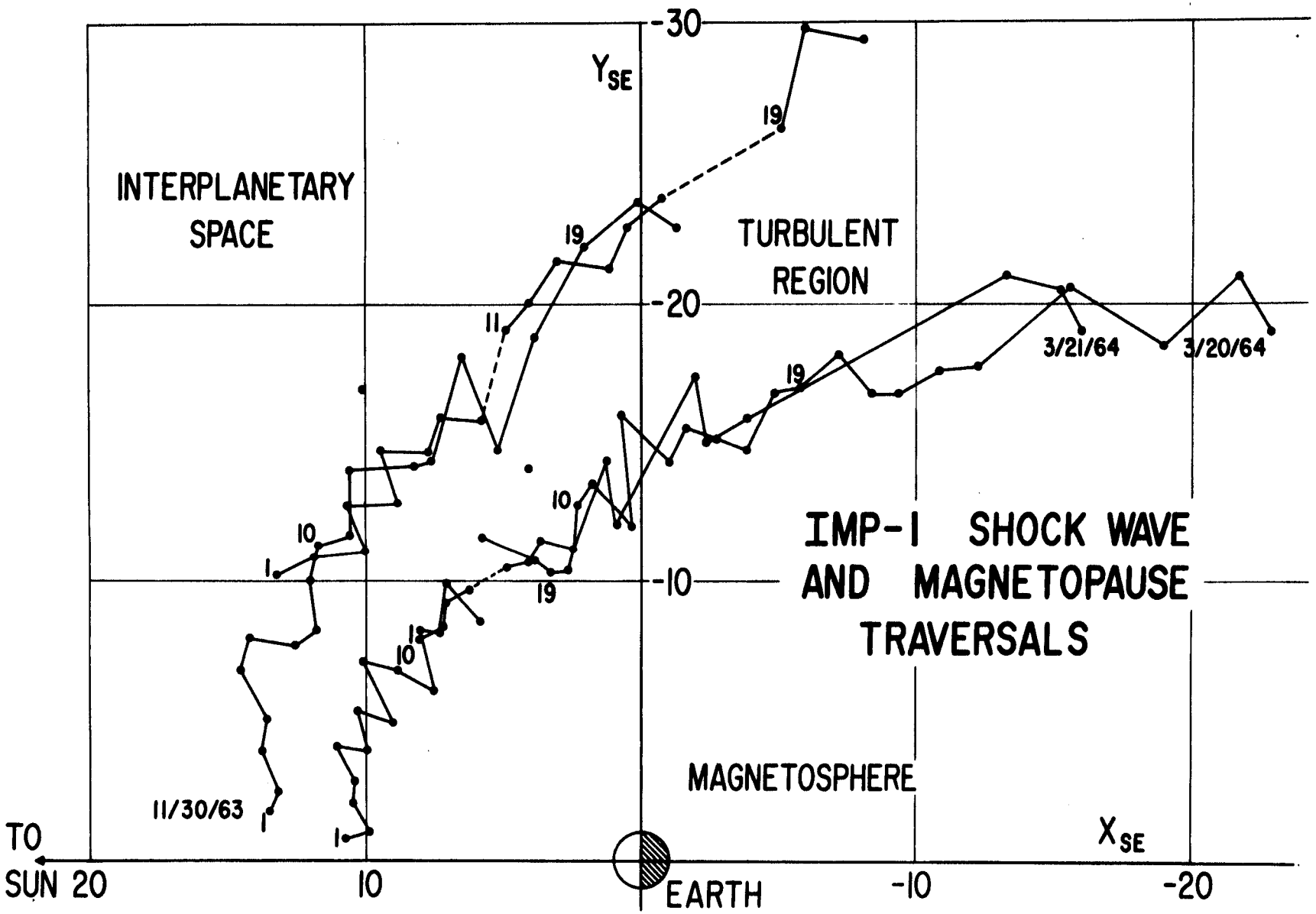

Figure 29. Summary of the magnetopause and shock wave boundary positions as observed by the IMP-I satellite. Individual observations have been rotated in a solar ecliptic meridian plane into the ecliptic plane. Successive traversals of the boundary are connected by straight lines if no gap exists in the data. Three regions of space are distinguished by these two boundaries: the interplanetary medium, the turbulent transition region and the magnetosphere or distorted geomagnetic field.

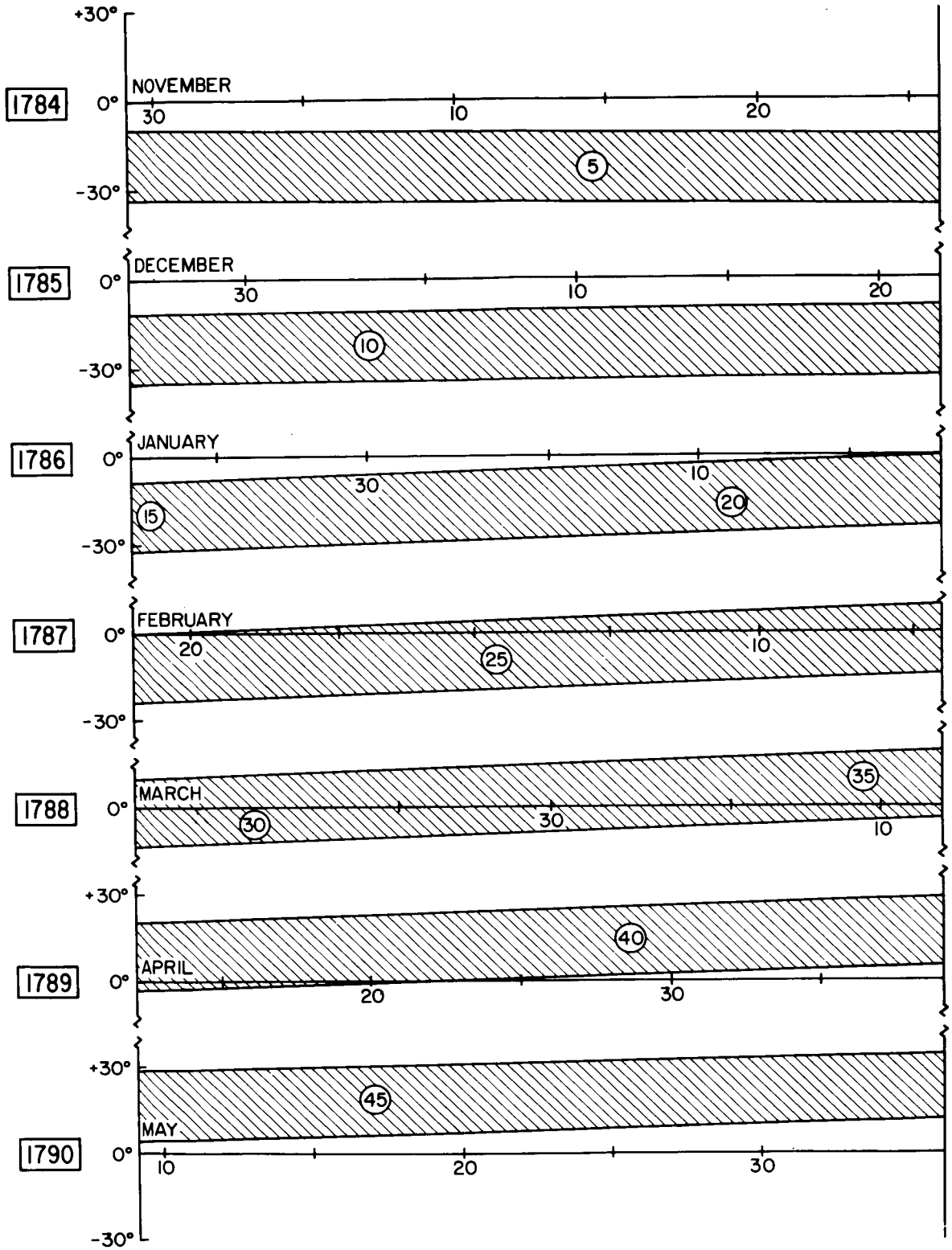

Figure 30. Variation of the geomagnetic latitude of the subsolar point during the life time of the IMP-I satellite. During the early portion of the satellite the "angle-of-attack" of the solar wind is seen to have been approximately-10 to-30 degrees.

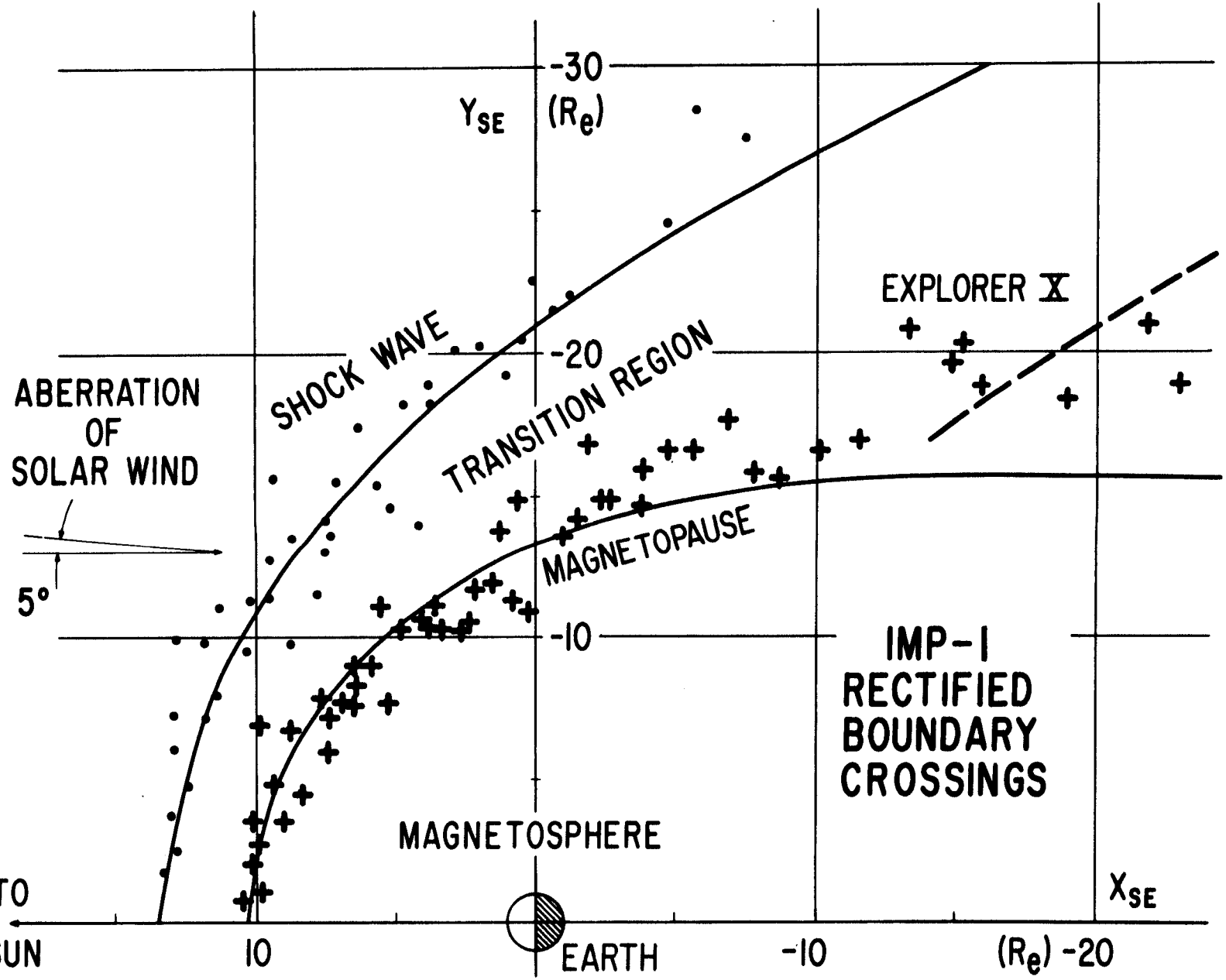

Figure 31. Comparison of the IMP-I rectified boundary crossings with the high speed gas dynamic shock model of Spreiter and Jones (1962). The standoff ratio has been adjusted to match the observed measurements. The predicted shape of the shock is seen to be rather closely matched by observations.

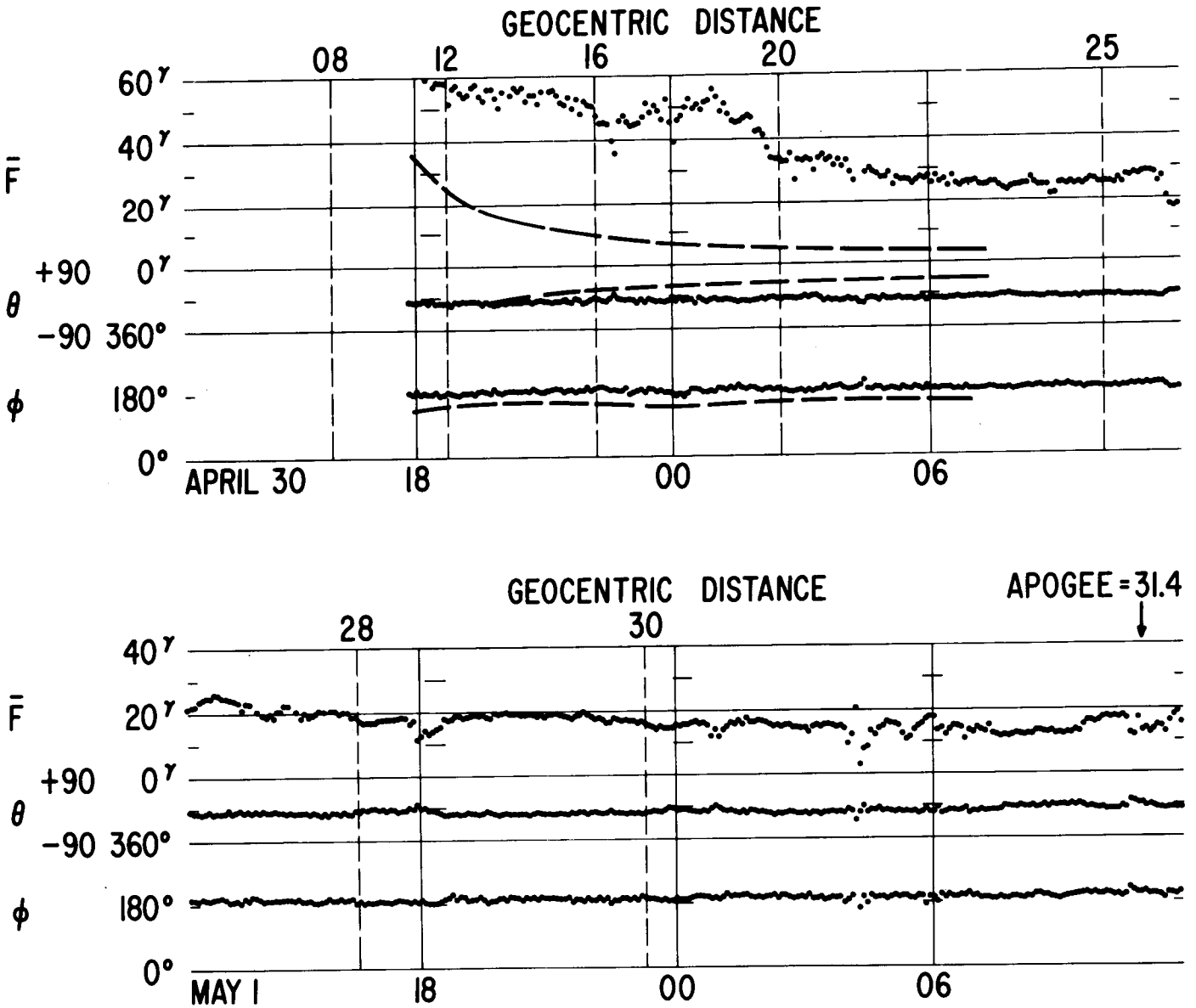

Figure 32. Magnetic field measurements of the Earth's magnetic tail by IMP-I on orbit # 41 outbound on April 30, May 1-2, 1964. The apogee of this orbit was approximately at a solar ecliptic longitude of 180°. Hence these results correspond to a noon-midnight meridian plane sample. Note the steady direction of the magnetic field parallel to the Earth - Sun line and pointed away from the Sun.

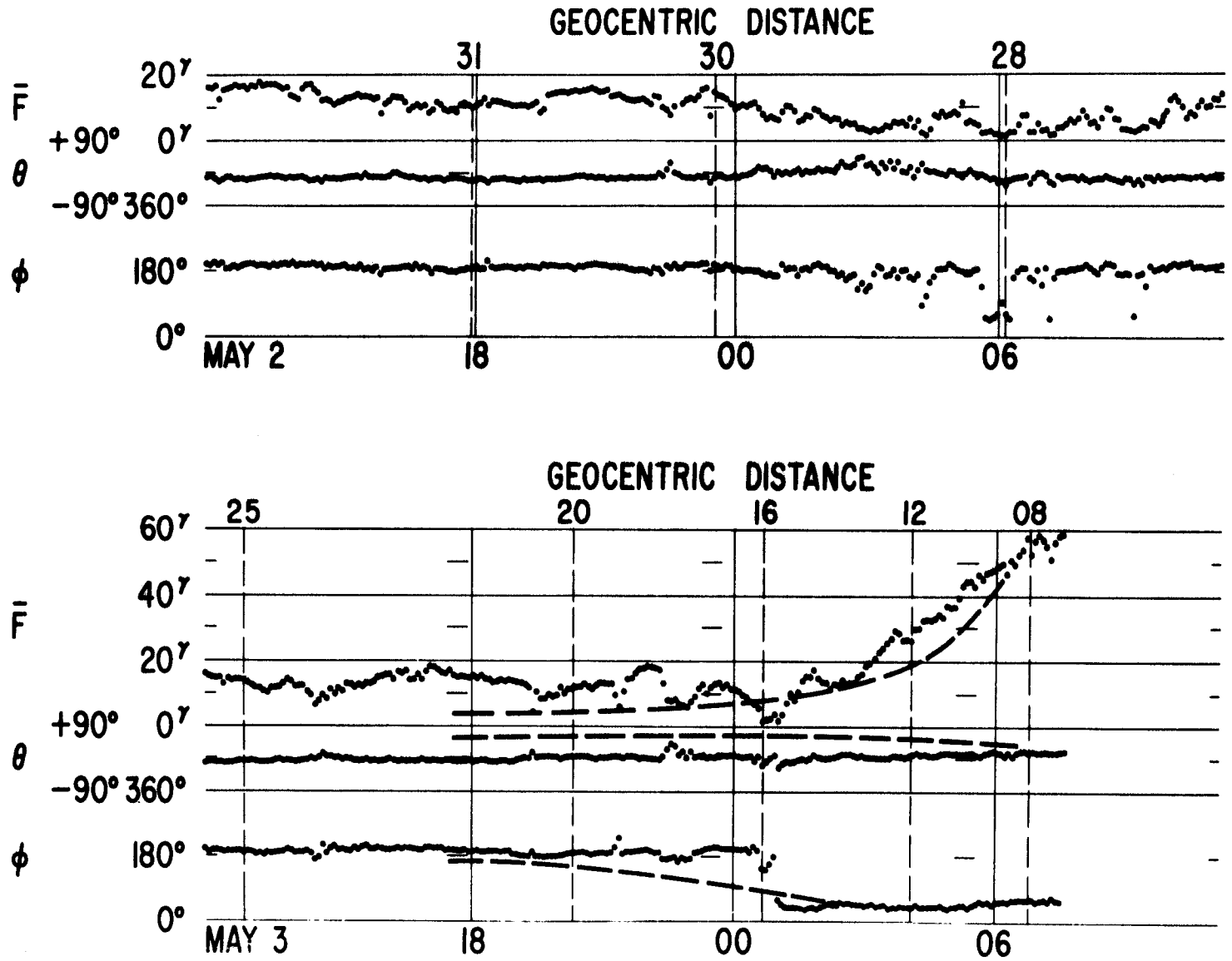

Figure 33. Magnetic field measurements of the Earth's magnetic tail by IMP-I on orbit # 41 inbound on May 2-4, 1964 corresponding to the remainder of the orbit shown in Figure 32. The direction of the field again closely parallels the Earth-Sun line with a rapid change in sense at a distance of 16 R_e. This is representative of the traversal of the magnetic neutral sheet in the Earth's magnetic tail by IMP-I.

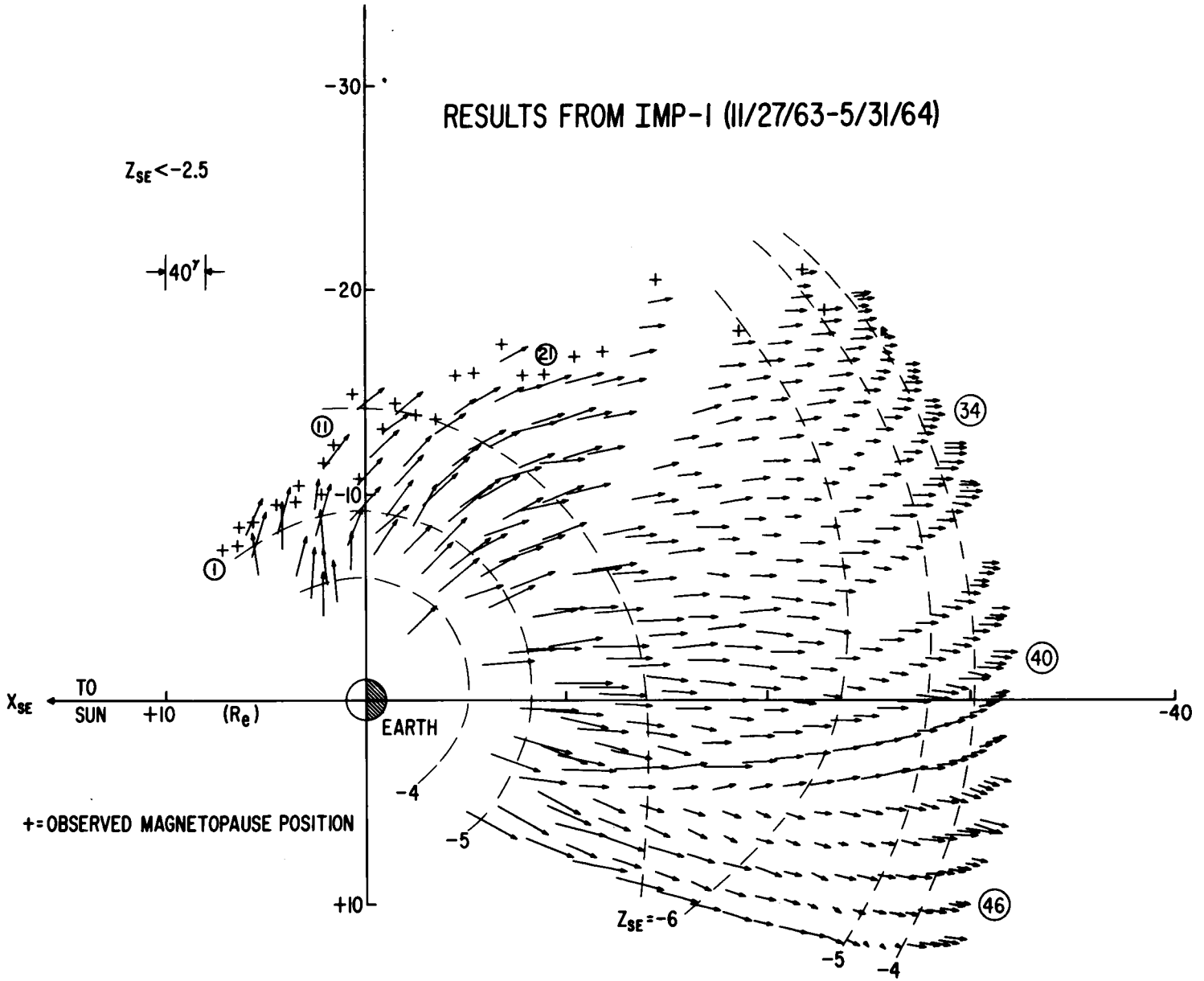

Figure 34. Summary of the X-Y hourly average component measurements by the IMP-I satellite for $Z_{sat} \leq -2.5\ R_e$ in the Earth's magnetic tail for orbits 1 through 47. Crosses indicate observed traversals of the magnetosphere boundary. Clearly evident is the distortion of the geomagnetic field forming an extended magnetic tail of the Earth.

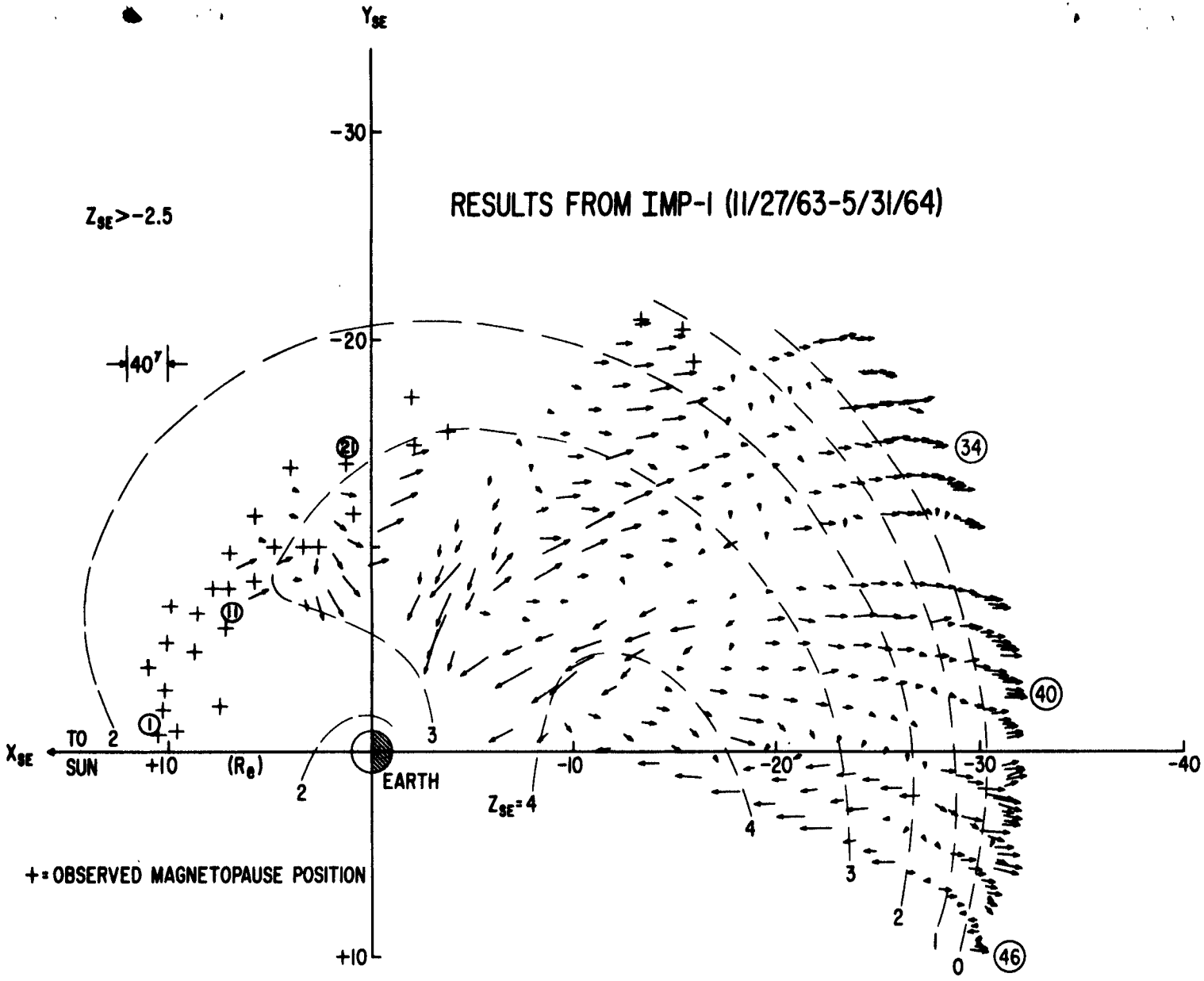

Figure 35. Summary of the X-Y hourly average component measurements by the IMP-I satellite for $Z_{sat} > -2.5\ R_e$ in the Earth's magnetic tail for orbits 1 through 47. Crosses indicate observed traversals of the magnetosphere boundary. Clearly evident is the distortion of the geomagnetic field forming an extended magnetic tail. Abrupt changes in the sense of direction of the tail field correspond to vertical traversals of the roughly horizontal neutral sheet.

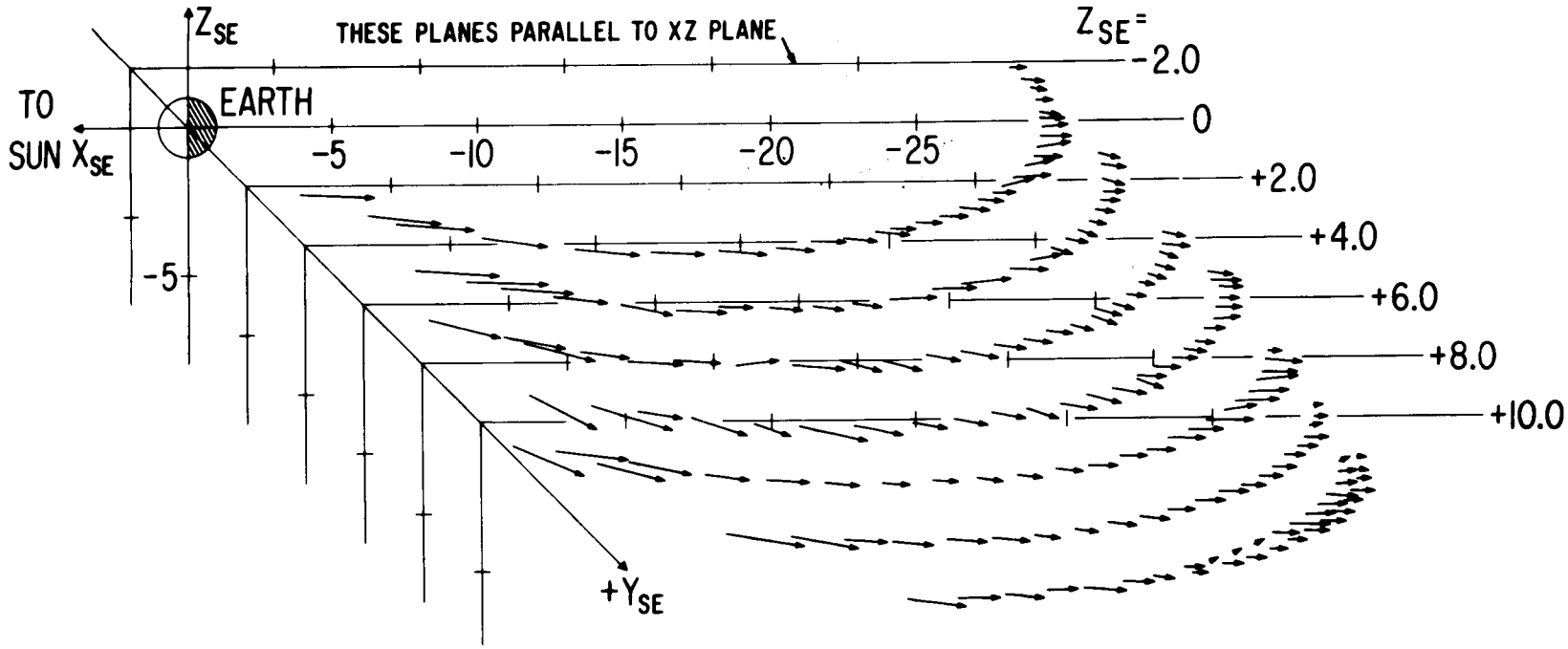

Figure 36. Summary of the X-Z hourly average component of the Earth's magnetic tail field for $Y_{sat} \geq -3.0\ R_e$ and $Z_{sat} < 0$. The field is seen to be parallel to the Earth-Sun line when compared with Figures 34 and 35.

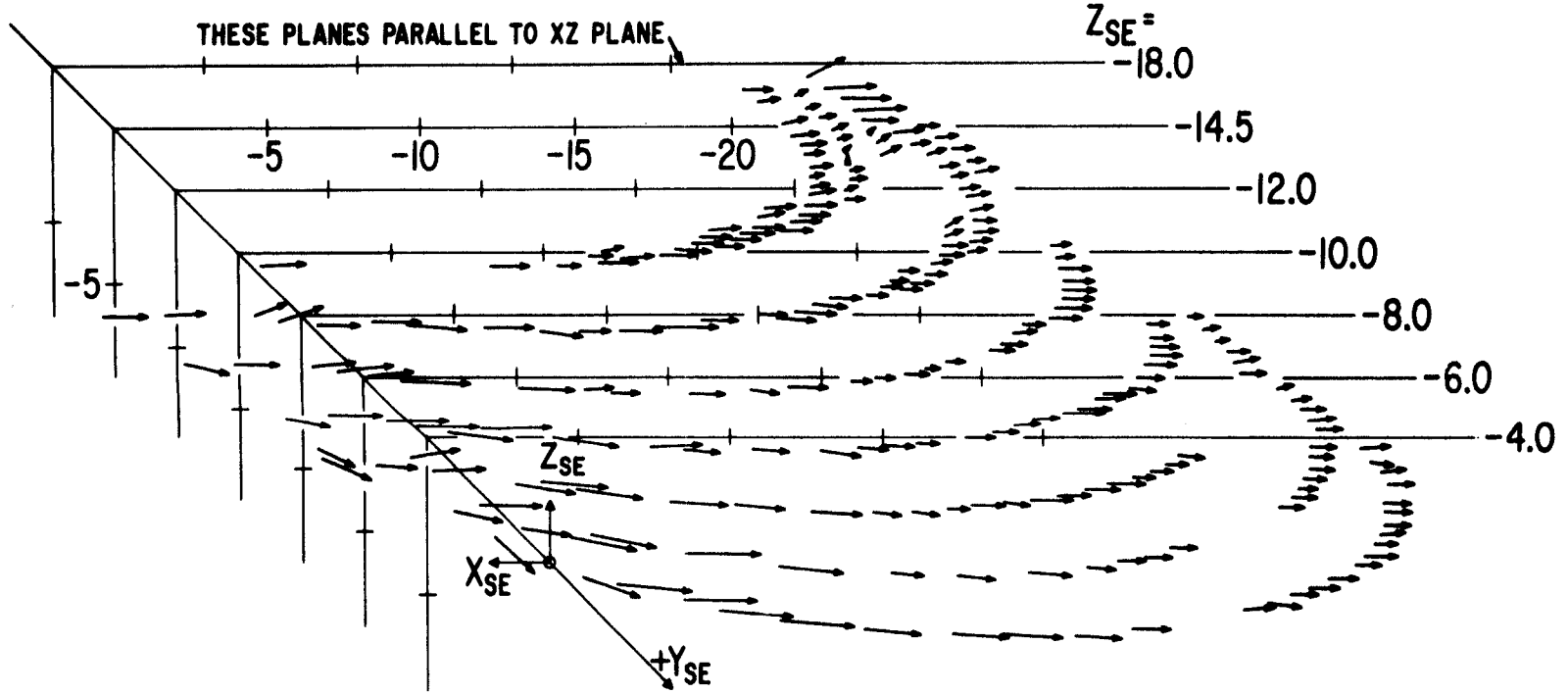

Figure 37. Summary of the X-Z hourly average component of the Earth's magnetic tail field for $Y_{sat} \leq -3.0\ R_e$ and $Z_{sat} < 0$. The field is seen to be parallel to the Earth-Sun line when compared with Figures 34 and 35.

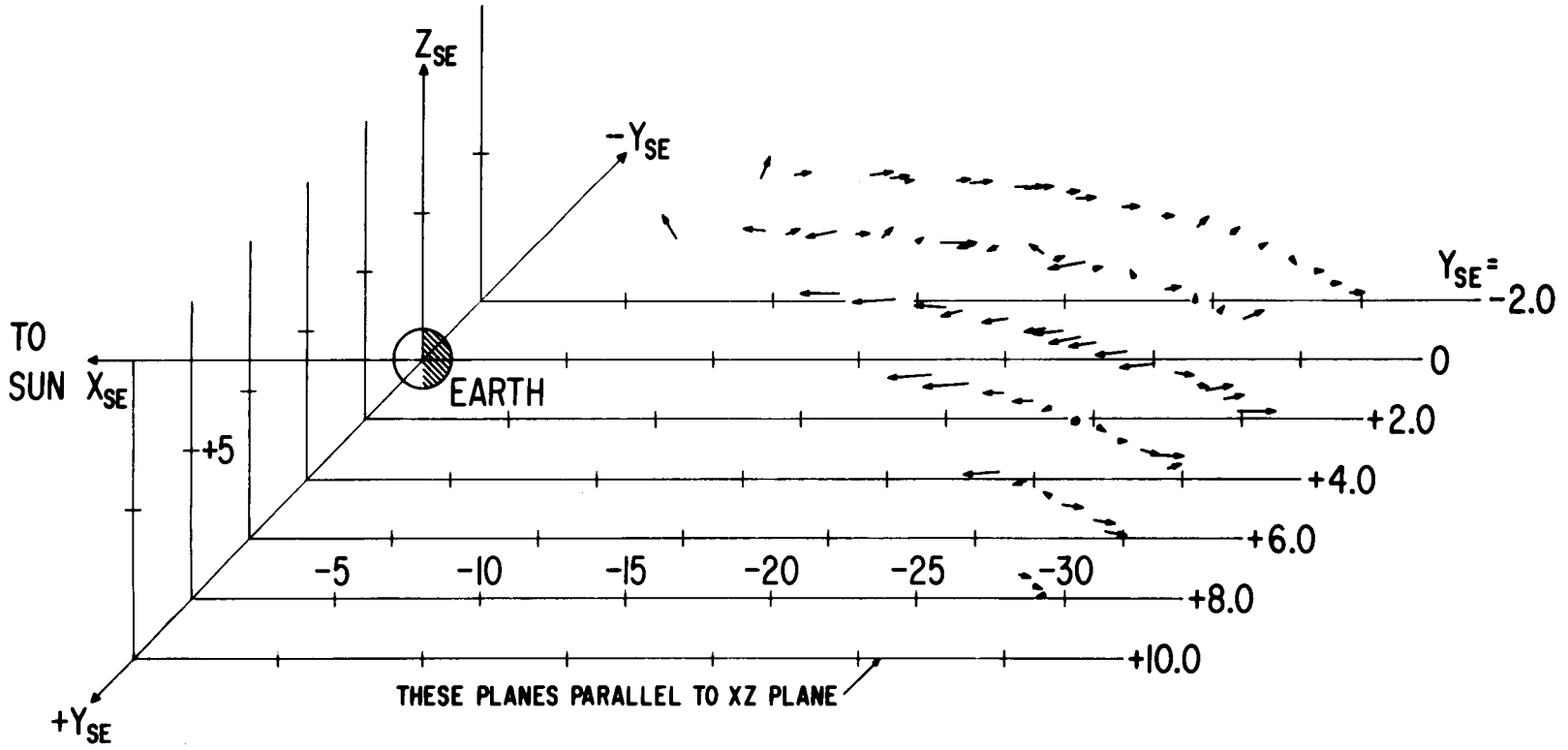

Figure 38. Summary of the X-Z hourly average component of the Earth's magnetic tail field for $Y_{sat} \geq -3.0\ R_e$ and $Z_{sat} \geq 0$. The field is seen to be parallel to the Earth Sun line when compared with Figures 34 and 35.

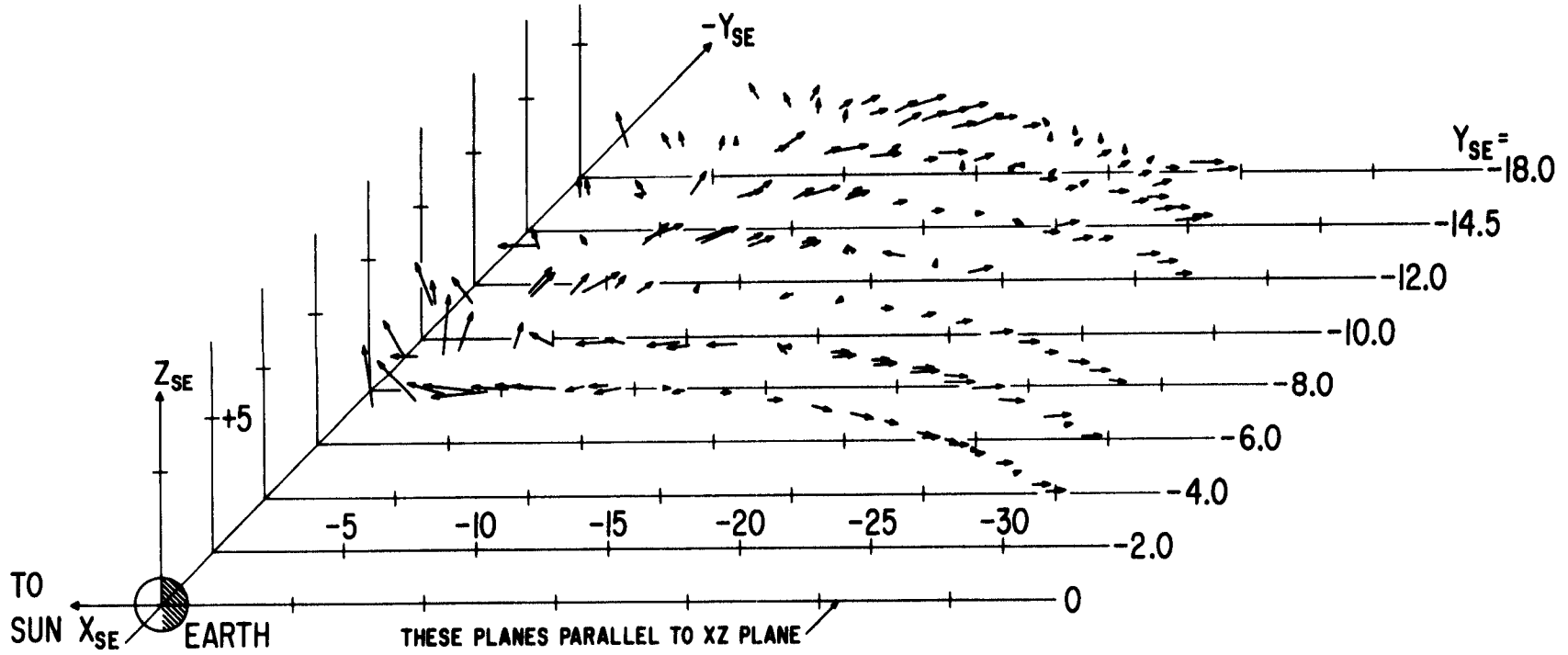

Figure 39. Summary of the X-Z hourly average component of the Earth's magnetic tail field for $Y_{sat} \leq -3.0\ R_e$ and $Z_{sat} \geq 0$. The field is seen to be parallel to the Earth-Sun line when compared with Figures 34 and 35.

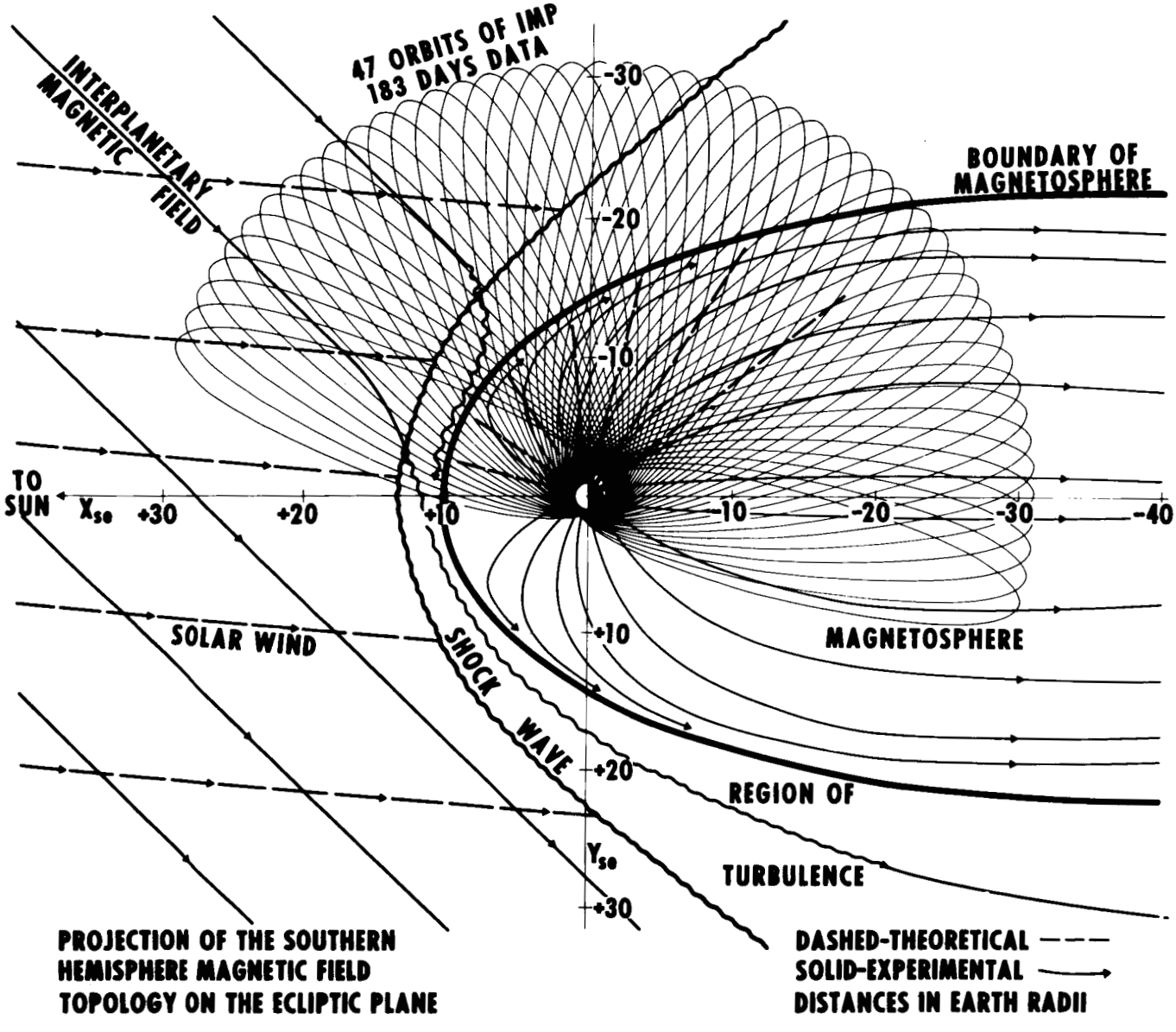

Figure 40.

Interpretation of the IMP-I magnetic field measurements of the cislunar environment. Illustrated are the directions of the interplanetary magnetic field, the positions of the magnetosphere boundary and the collisionless shock wave as observed by the magnetic field experiment. The extended magnetic tail is shown to be roughly cylindrical about the Earth-Sun line although IMP-I did not probe the sunset terminator portion of the boundary.

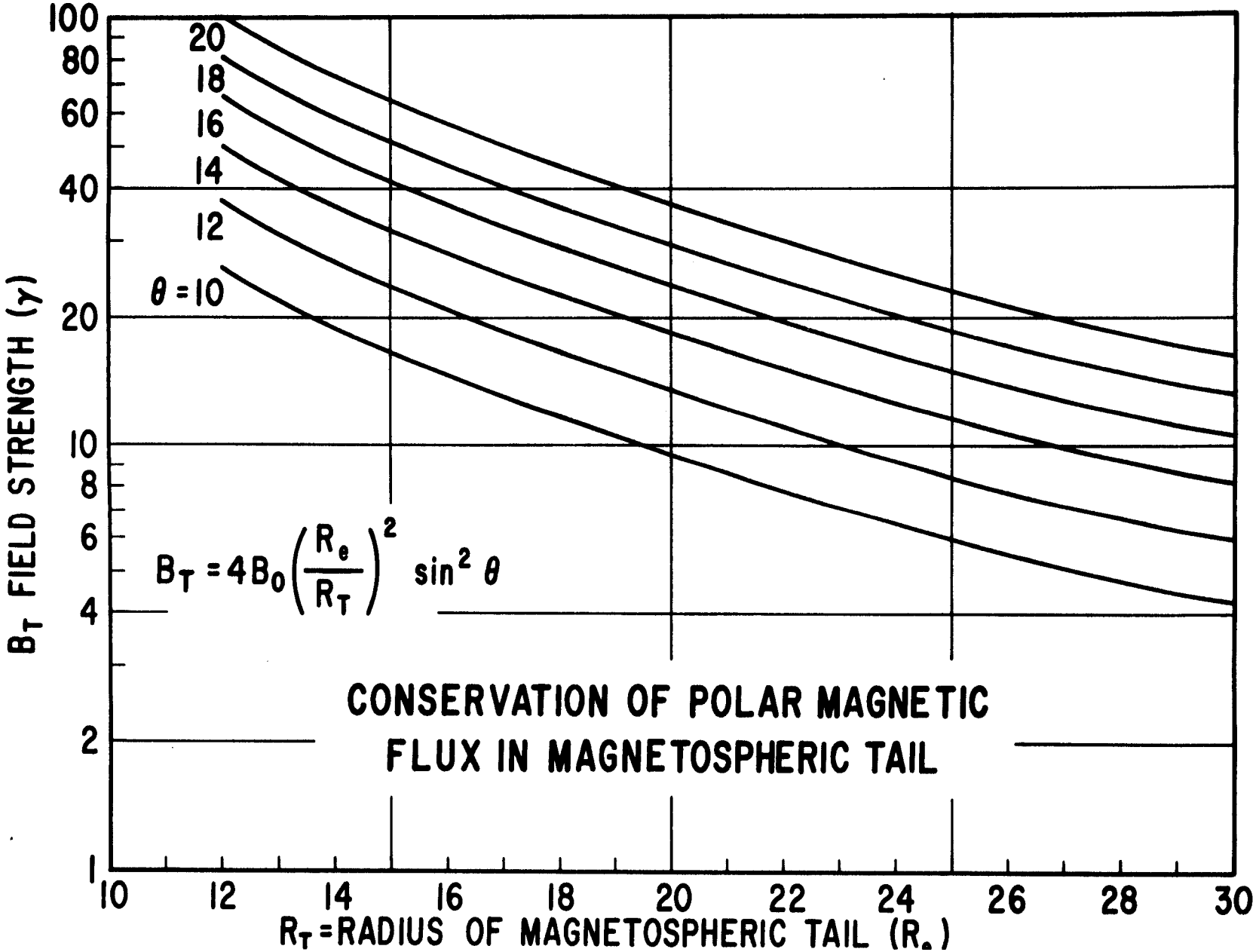

Figure 41. Chart for computing magnetic field strength in the Earth's magnetic tail assuming conservation of magnetic flux from polar cap regions. The variable parameters are the radius of the magnetospheric tail, R_T, and the colatitude of the polar cap region, θ.

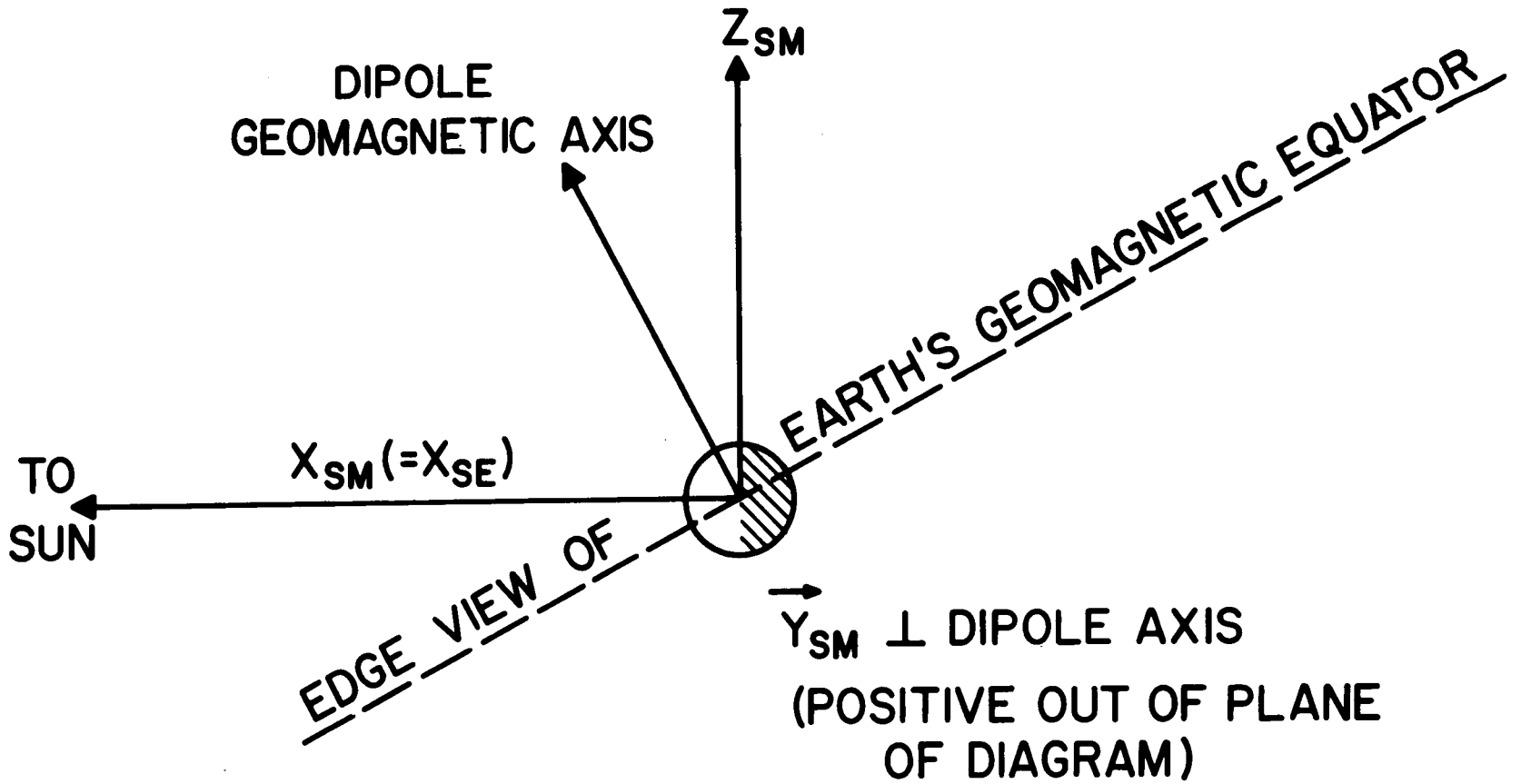

Figure 42. Definition of the solar magnetospheric coordinate system used in the interpretation of the position of the neutral sheet as observed in the magnetic tail of the Earth.

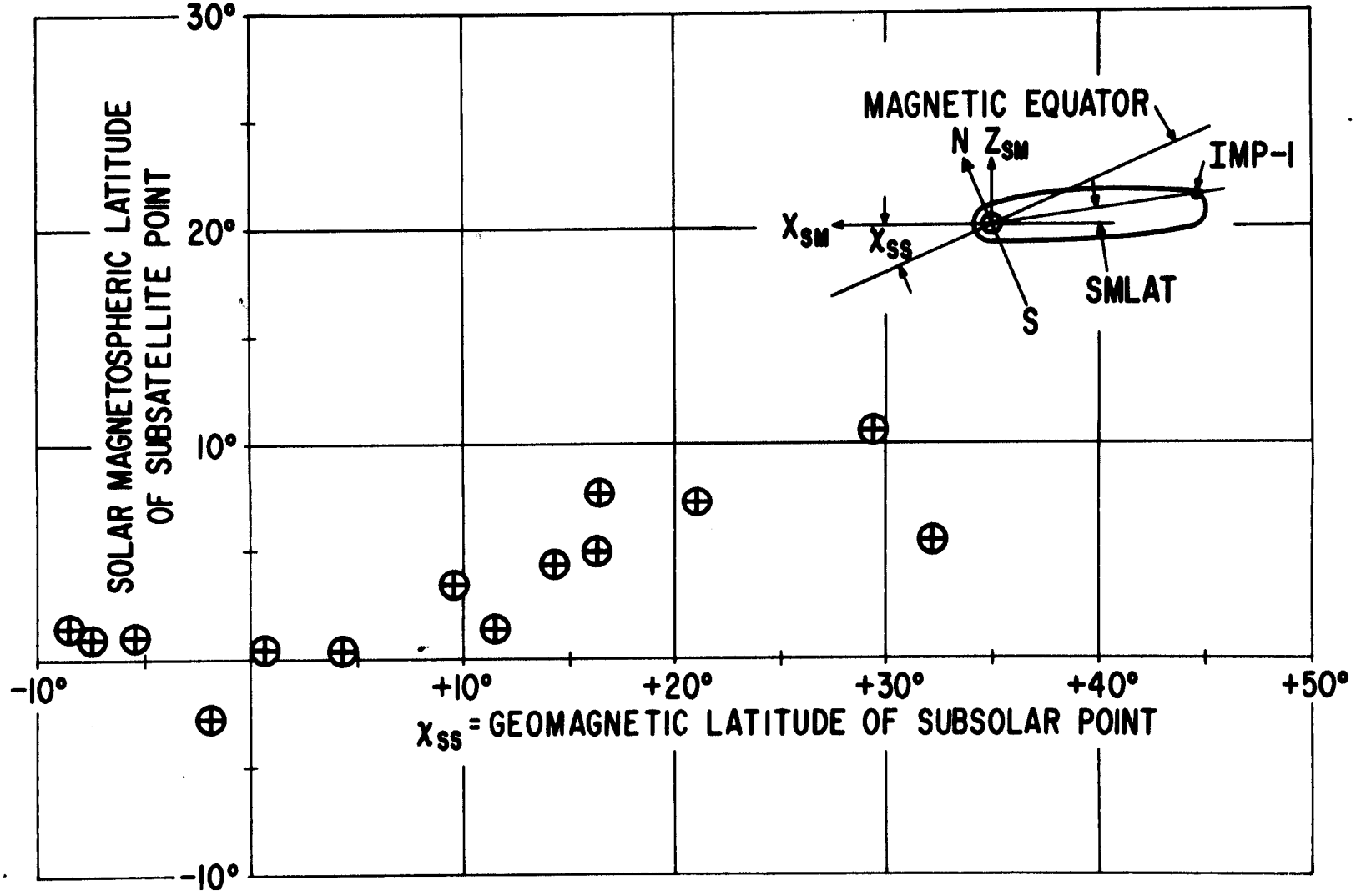

Figure 43. Position of the neutral sheet as observed by the IMP-I magnetic field experiment while in the magnetic tail of the Earth. The sheet is observed to be within 5^{o} or 10^{o} of the solar magnetospheric equatorial plane for the 14 observed crossings. The sheet is seen to be within 5^{o} or 10^{o} of the solar magnetospheric equatorial plane for the 14 available traversals.

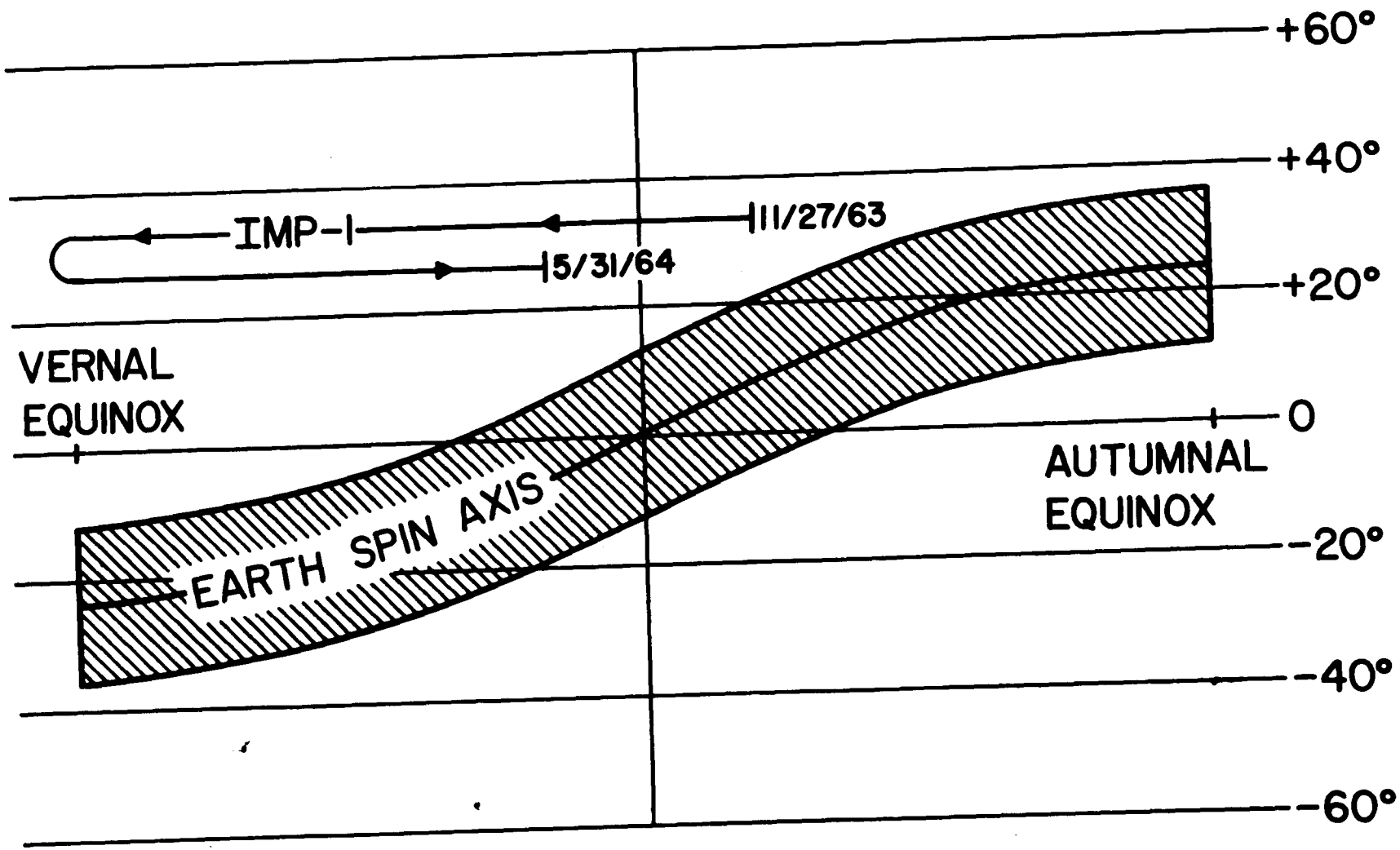

Figure 44. Illustration of the variation of the tilt of the equatorial plane of the solar magnetospheric coordinate system with respect to the ecliptic plane. Superimposed is the time interval covered by IMP-I.

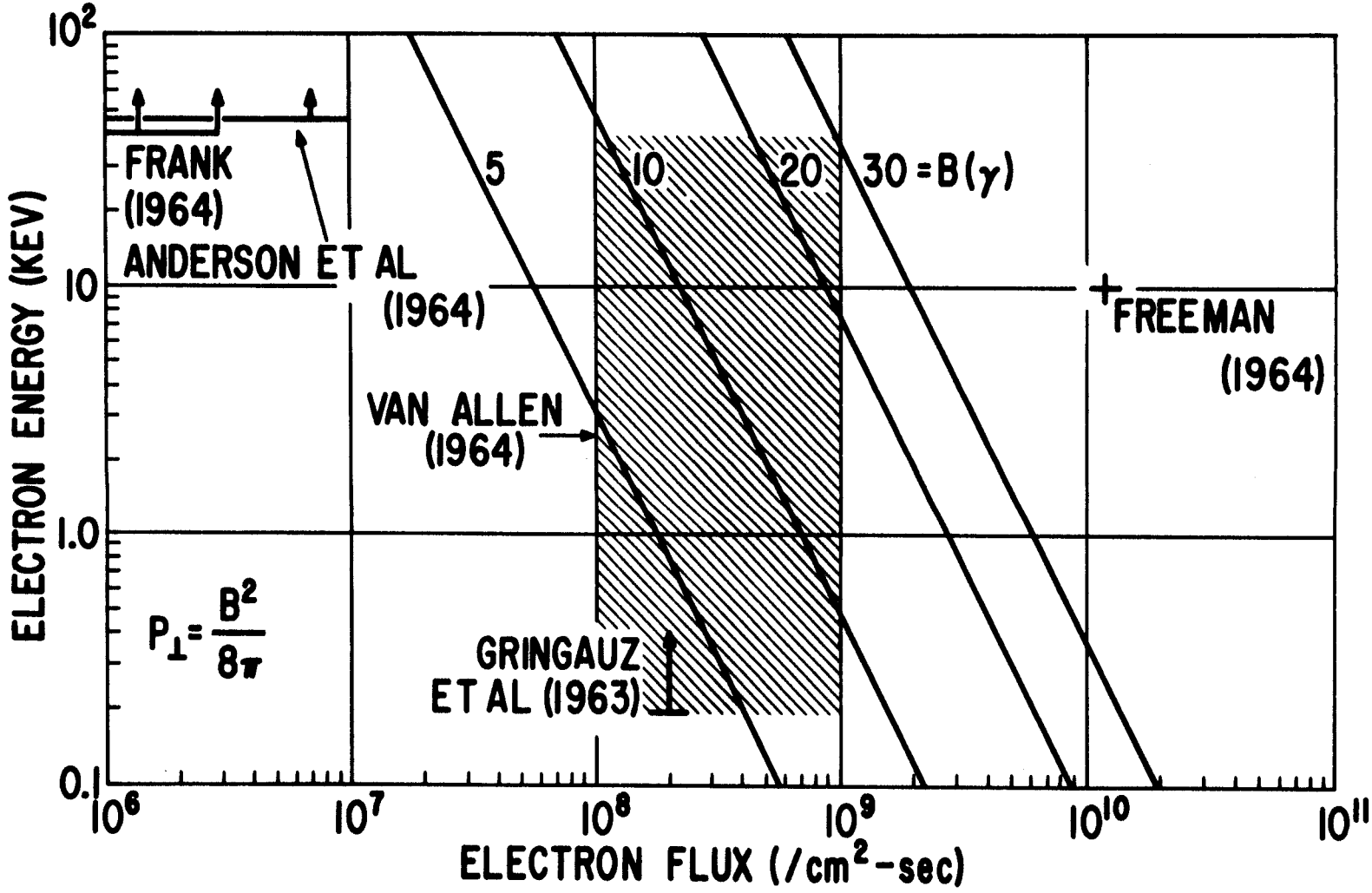

Figure 45. Assumed pressure balance between vacuum magnetic fields and nonmagnetized electron plasma corresponding to idealized model of neutral sheet. Superimposed are particle and plasma observations pertinent to the interpretation of the neutral sheet in the Earth's magnetic tail.

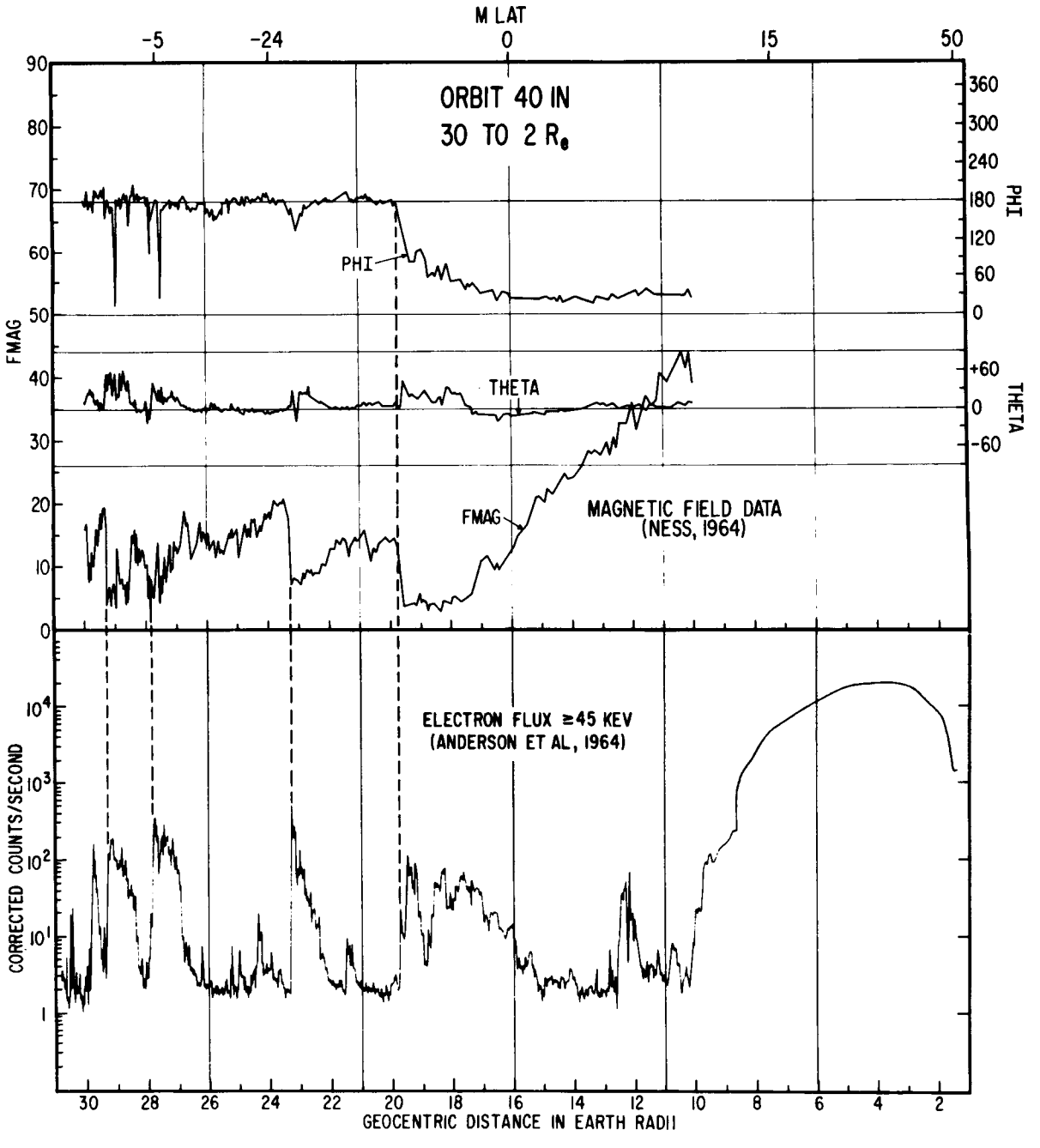

Figure 46. Correlated electron flux and magnetic field magnitude variations in the tail of the magnetosphere observed by IMP-I on orbit 40 inbound April 29, 1964. The sheet was observed during this orbit at a position of 19.8 R_e, coincident with an abrupt increase in the electron flux.

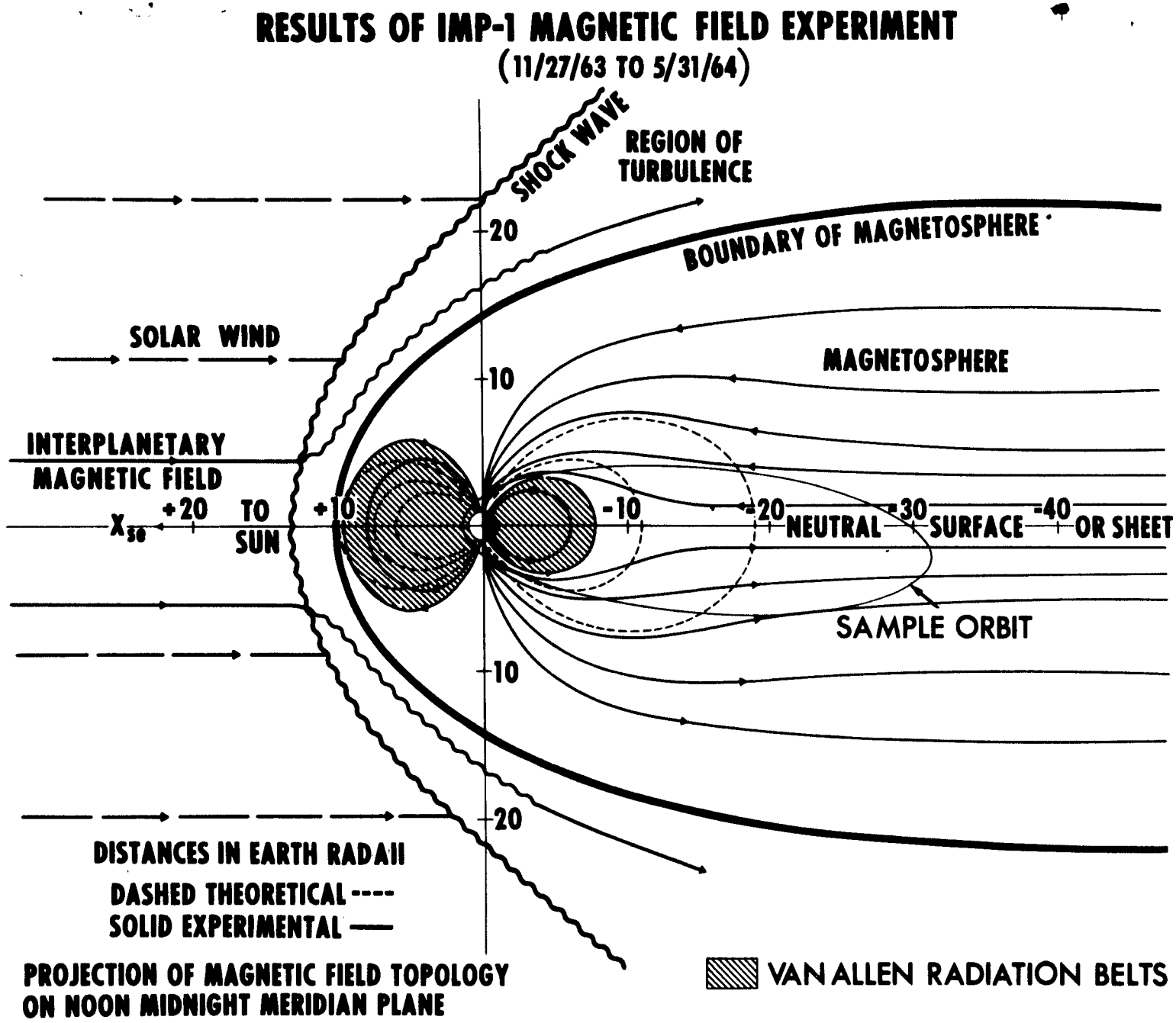

Figure 47. Summary illustration of the interpretation of the IMP-I data perpendicular to the plane of the ecliptic illustrating strong day-night asymmetry in the radiation belts and the development of the extended magnetic tail of the Earth.